annual progress

ENERGY STORAGE RESEARCH AND DEVELOPMENT

FreedomCAR and Vehicle Technologies Program

Less dependence on foreign oil today, and transition to a petroleum-free, emissions-free vehicle tomorrow.

U.S. Department of Energy
Energy Efficiency and Renewable Energy
Bringing you a prosperous future where energy is clean, abundant, reliable, and affordable

FreedomCAR & Fuel Partnership

21st CENTURY TRUCK PARTNERSHIP

U.S. Department of Energy
Office of FreedomCAR and Vehicle Technologies
1000 Independence Avenue S.W.
Washington, D.C. 20585-0121

FY 2006

Progress Report for Energy Storage Research and Development

Energy Efficiency and Renewable Energy
FreedomCAR and Vehicle Technologies

Approved by: David Howell
Manager, Energy Storage R&D

January 2007

TABLE OF CONTENTS

I. INTRODUCTION 1
I.A FreedomCAR and Vehicle Technologies Program Overview 1
I.B Energy Storage Research & Development Overview 1

II. BATTERY TECHNOLOGY DEVELOPMENT 3
II.A System Development 3
II.B Technology Assessment 14
II.C Benchmark Testing 14
II.D Small Business Innovative Research (SBIR) 14

III. APPLIED BATTERY RESEARCH 16
III.A. Introduction 16
III.B Understand Life-Limiting Mechanisms and Enhance Life 17
III.B.1 Introduction 19
III.B.2 TLVT Validation and Testing 19
III.B.3 SEI/Formation Study, DOEx, and Diagnostics 23
III.B.4 Gen 3 Cell Build Status, Testing, & Diagnostics 29
III.C Understand and Enhance Low-Temperature Performance 32
III.C.1 Introduction 32
III.C.2 Low-Temperature Performance Characterization 33
III.C.3 Low Temperature Electrolyte Modeling 35
III.C.4 Low Temperature Cell Performance Modeling 37
III.D Understand and Enhance Abuse Tolerance 40
III.D.1 Introduction 41
III.D.2 Thermal Abuse 41
III.D.3 Overcharge Abuse 52
III.E Cell-Level Cost Reduction 56
III.E.1 Introduction 56
III.E.2 Material Screening and Development 57
III.E.3 Evaluation of $Li_4Ti_5O_{12}$ Nano Materials 62

IV. FOCUSED LONG-TERM RESEARCH 69
IV.A New Cathode Materials 71
IV.A.1 $LiFePO_4$ and other Phosphate Systems: Performance and Limitations 71
IV.A.2 Spinel and Composite Systems: Performance and Limitations 81
IV.A.3 Nickelate Systems: Performance and Limitations 88
IV.B New Anode Materials 94
IV.C Novel Electrolytes and Their Characterization 101
IV.D Li-Ion Modeling, Diagnostics, and Cell Analysis 110

Appendix A – Contributors A-1

Appendix B – List of Acronyms B-1

INTRODUCTION

Our nation's energy security depends significantly on the efficiency of our transportation system and on which fuels we use. Transportation in the United States already consumes more oil (9 million [M] barrels per year) than we produce here at home (8M barrels),[1] and it is predicted that by 2025 about 70% of our oil will be imported. Reducing our dependence on fossil fuels could alleviate the currently tight supply as evidenced by the large fluctuations seen in gasoline prices in 2006, from over $3.gallon to just under $2 gallon in less than 6 months. Thus, the United States Department of Energy's (DOE) continuing research and development into alternative fuels, and the use of batteries for motive transportation offers the possibility of reducing our dependence on foreign oil and insulating the country from further rapid fluctuations in supply and price.

I.A FreedomCAR and Vehicle Technologies Program Overview

The DOE's FreedomCAR & Vehicle Technologies (FCVT) Program office[2] works with industry to develop advanced transportation technologies that reduce the nation's use of imported oil. Some of the technologies being supported by FCVT include hybrid drive system technologies, advanced energy storage devices (batteries and ultracapacitors), power electronics and motors, advanced structural materials, and advanced combustion engines and fuels.

Collaboration with automakers enhances the potential for success and the relevance of these programs. With this in mind, on January 9, 2002 the DOE and the United States Council for Automotive Research (USCAR)—representing DaimlerChrysler Corporation, Ford Motor Company, and General Motors Corporation—announced the creation of the FreedomCAR and Fuels Partnership[3].

This partnership is focused on funding high-reward/high-risk research that promises improvements in critical components needed for more fuel efficient, cleaner vehicles and provides ongoing guidance and expertise to FCVT activities.

I.B Energy Storage Research & Development Overview

Energy storage technologies, including batteries and ultracapacitors, have been identified as critical enabling technologies for advanced, fuel-efficient, light and heavy-duty vehicles. The Energy Storage Research and Development effort within the FCVT Program is responsible for researching and improving advanced batteries for a wide range of vehicle applications, including hybrid electric vehicles (HEVs), plug-in hybrid electric vehicles (PHEVs), battery electric vehicles (EVs), as well as fuel cell vehicles (FCVs). The office is working in close partnership with the automotive industry, represented by the United States Advanced Battery Consortium (USABC).

The current effort is comprised of three major activities, battery technology development, applied battery research, and long-term exploratory research. A summary of the work done in each of these areas is presented below:

---

[1] http://www.eia.doe.gov/neic/quickfacts/quickoil.html
[2] See http://www.eere.energy.gov/vehiclesandfuels/.
[3] For more information, please see http://www.uscar.org/guest/view_partnership.php?partnership_id=1.

Battery Technology Development is subdivided into three related sets of activities: full system development, technology assessment, and benchmark testing.

- *Benchmark Testing* - Benchmark testing of emerging technologies is important for remaining abreast of the latest industry developments. Working with the national laboratories, FCVT purchases and independently tests hardware against the manufacturer's specifications and the most applicable technical targets.

- *Technology Assessment* - Technology assessments are conducted on newly emerging technologies prior to full system development. These 12-month projects assess a developer's overall capabilities and validate technical claims through independent testing.

- *Full System Development* - In cooperation with industry, efforts are focused on developing and evaluating lithium-battery and ultracapacitor technologies and designs for advanced vehicles. Specifically, this work is focused on the development of batteries for HEVs, PHEVs (in 2007), and on the development of ultracapacitor technologies for the 42 Volt start/stop application.

Applied Battery Research is focused on addressing the cross-cutting barriers that face Li-ion systems which are closest to meeting all of the energy and power requirements for vehicle applications. Five national laboratories participate in this activity, each bringing its own expertise to the critical barrier areas of life, abuse tolerance, low-temperature performance, and cost.

Focused Long-term Battery Research addresses fundamental problems of chemical instabilities that impede the development of advanced batteries. This research provides a better understanding of why systems fail, develops models that predict system failure and permit system optimization, and investigates new and promising materials. The work presently concentrates on research into several promising systems, including $LiNi_{1/3}Co_{1/3}Mn_{1/3}O_2$, $LiFePO_4$, Mn spinel, and new higher energy materials such as composite cathodes and non-graphitic anodes.

Finally, contributors to the work described in each of these chapters are presented in Appendix A, and Appendix B provides a list of acronyms used throughout this report.

This report highlights the activities and progress achieved in the Energy Storage Research and Development Effort during FY 2006. We are pleased with the progress made during the year and look forward to continued work with our industrial, government, and scientific partners to overcome the challenges that remain to delivering advanced energy storage systems for vehicle applications.

David Howell
Manager, Energy Storage Research and Development
FreedomCAR and Vehicle Technologies Program

II. BATTERY TECHNOLOGY DEVELOPMENT

One of the primary objectives of the Energy Storage effort is the development of durable and affordable advanced batteries and ultracapacitors for use in a full range of vehicle applications, from start/stop to full-power hybrid-electric, electric, and beginning in 2007, plug in HEVs. This activity is subdivided into four mission areas: *system development*, focused on developing full battery systems; *technology assessment*, to evaluate developers' current capabilities and validate technical claims*; benchmark testing* of emerging technologies in order to remain abreast of the latest industry developments; and *Small Business Innovative Research (SBIR),* that provides funding for early-stage R&D to small technology companies or individual entrepreneurs.

II.A System Development

System Development is focused on the development of batteries and ultracapacitors for relatively high power applications such as HEVs, 42 Volt start/stop vehicle systems, and FCVs. All battery system development for light duty vehicles is conducted in collaboration with industry through the USABC. All of the USABC subcontracts to develop advanced batteries are awarded competitively and are cost-shared by the developer at a minimum of 50 percent.

Introduction

Historically, work on new battery technologies has been organized into High-Power Energy Storage and High-Energy Storage. Both of these efforts are part of a multifaceted effort within FCVT to develop the technologies needed to encourage the adoption of advanced, cleaner, more fuel-efficient light-duty vehicles in the commercial marketplace. High-power energy storage devices are among the critical technologies essential for the development and commercialization of HEVs, 42V vehicle systems, and FCVs.

This effort is focused on overcoming the technical barriers associated with commercialization of high-power batteries, namely:

- **Cost -** The current cost of Li-based batteries (the most promising high-power battery chemistry) is prohibitively high on a kW basis (a factor of two-three too high). The main cost drivers being addressed are the high cost of raw materials and materials processing, the cost of cell and module packaging, and manufacturing costs.

- **Performance -** The barriers related to battery performance are the reduced discharge pulse power that is available at low temperatures and the loss of available power over time due to use and aging.

- **Abuse Tolerance –** Many high-power batteries are not intrinsically tolerant to abusive conditions such as short circuits, overcharge, over-discharge, crush, or exposure to fire and/or other high temperature environments.

- **Life -** Hybrid systems with conventional engines have a life target of 15 years, and battery life goals have been set to meet these targets. The cycle life goal of 300,000 cycles has been attained in laboratory tests but the 15-year calendar life has not yet been demonstrated.

The high-power energy storage activity was created to develop solutions to these challenges. Battery requirements for HEVs and draft goals for FCVs were developed in close coordination with industry through the USABC technical teams and the former are shown in Table II-1. (See http://www.uscar.org/guest/view_team.php?teams_id=11 for more details.)

Table II-1. Energy Storage Targets for Power Assist Hybrid Electric Vehicles

Characteristics	Minimum value	Maximum value
Pulse discharge power (kW)	25 (for 10 seconds)	40 (for 10 seconds)
Maximum regenerating pulse (10 s; kW)	20 (50 Wh pulse)	35 (97 Wh pulse)
Total available energy (kWh)	0.3	0.5
Round trip efficiency (%)	>90–25 Wh cycle	>90–50 Wh cycle
Cycle life for specified SOC increments (cycles)	300k 25-Wh cycle (7.5 MWh)	300k 50-Wh cycle (15 MWh)
Cold-cranking power at −30ºC (three 2-sec pulses, 10-s rests between; kW)	5	7
Calendar life (years)	15	15
Maximum weight (kg)	40	60
Maximum volume (liters)	32	45
Production price @ 100k units/year ($)	500	800
Maximum operating voltage (Vdc)	<400 maximum	<400 maximum
Minimum operating voltage (Vdc)	$>0.55 \times V_{max}$	$>0.55 \times V_{max}$
Maximum self-discharge (Wh/d)	50	50
Operating temperature (ºC)	−30 to +52	−30 to +52
Survival temperature (ºC)	−46 to +66	−46 to +66

Specific objectives of this activity include:

- By 2010, develop an electric drive train energy storage device with a 15-year life at 300Wh with a discharge power of 25 kW for 18 seconds and a cost of $20/kW.
- Reduce the projected production cost of a high-power 25-kW battery (for light-duty vehicle) from $3000 to $750 in 2006 and to $500 in 2010 (priority FCVT goal).
- Develop hardware for specific applications that can be tested against respective performance targets and used for subsystem benchmarking.

In the past, two candidate battery chemistries were identified as the most likely to meet the performance and cost targets: NiMH and lithium-based technology. NiMH batteries offer relatively good power capability as a result of the good ionic conductivity of the electrolyte. Lithium-based batteries offer excellent energy density that can be traded for higher power.

The USABC has supported development of these two technologies since the early 1990s by awarding subcontracts to a number of developers. Significant progress has been made as summarized in the graph shown in Figure II-1. The USABC is continuing to support the development of Li-ion technology through contracts with Johnson Controls-Saft (Li-ion), CPI/LG Chem (Li-ion polymer), EnerDel (Mn spinel/Lithium titanate), and A123Systems (iron phosphate). Details on these contracts and on development work on ultracapacitors follows.

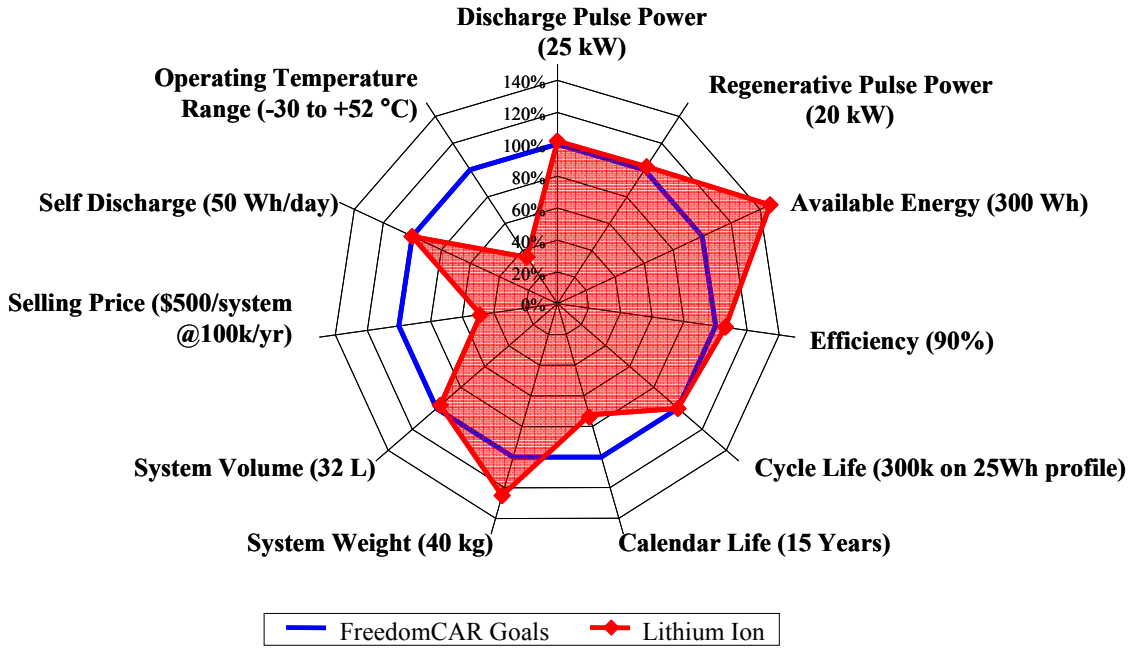

Figure II-1. Lithium ion Status versus Goals for Power Assist HEV

Li-ion Battery Development (40kW HEV)

In May of 2006, the USABC awarded a contract to the newly created joint venture Johnson Controls-Saft (JCS), for development of a 40 kW Li-ion battery with significantly reduced cost and improved abuse tolerance. Johnson Controls Inc. and Saft Batteries created this joint venture to complement the two companies' strengths in high-volume manufacturing (specifically for the auto industry) and Li-ion electrochemistry respectively. The effort is being led by the advanced battery systems team at in Milwaukee, WI.

The contract is 24 months in duration, and will concentrate on establishing state of the art cell making capability at the Milwaukee location, and on leveraging JCI's high-volume manufacturing expertise to enable the best possible system cost. Initial development in Milwaukee has yielded electrodes that are nearly identical to those produced at Saft's facility in Bordeaux, France.

Li-ion Polymer Battery Development (25kW HEV)

In September 2006, Compact Power/LG Chem was awarded an 18-month contract to continue development of Li-ion polymer cell technology for HEV applications using a $LiMn_2O_4$ spinel-based cathode. $LiMn_2O_4$ spinel is an attractive cathode for HEV batteries due to the fact that Mn is abundant, environmentally benign, potentially abuse-tolerant, and capable of high-rates of discharge. Major problems to be overcome in this effort are the relatively poor calendar life, particularly at elevated temperatures, and the comparatively poor cold cranking and low-temperature charging characteristics.

CPI will also evaluate a new separator that promises to improve the abuse tolerance of this system. In addition, they will further evaluate the ability of pouch packaging to attain 15-year calendar life.

High Rate Low Cost Li-Ion Battery Development (25kW HEV)

In late 2006, EnerDel was awarded a 12-month contract to scale up a nano-phase lithium titanate (LiTO)/Mn spinel cell that promises extremely high rate capability along with low cost, good abuse tolerance as well as good low-temperature performance. The nano-phase LiTO is characterized by extremely small primary particles (10 to 20 nm) agglomerated into 1 to 2 μm secondary particles that can be more easily processed into electrodes and can provide higher electrode density.

A proof of concept of this chemistry has been provided by Argonne National Laboratory, who has been included as a subcontractor to work on the scale up of the nano-scale LiTO material. However, EnerDel will continue to evaluate other materials companies to determine the optimum LiTO material.

Low-cost Separator Development

Studies at the national laboratories have shown that the cost of the separator dominates the cost of the non-active materials in a high-power Li-ion battery. To reduce this cost research and development is taking place into lower-cost materials and improved processing techniques. The goal is to develop a replacement separator (which costs $\$1/m^2$ or less) for current materials (which cost more than $\$2/m^2$) having the following properties:

- Thickness: < 25 μm
- Wettability: Complete Wet Out in Electrolytes
- Puncture Strength: > 300g/25.4 μm
- Permeability: MacMullin Number of < 11
- Pore Size: < 1 μm
- Moisture Content: < 50 ppm
- Chemical Stability: Stable in Battery for 10 Years

Contractors engaged in this activity during 2006 include Celgard, Inc. and Ultimate Membrane Technologies (UMT). Some highlights of the FY 2006 activities are presented below.

- **Celgard, Inc.** reported progress in developing a low-cost separator material that provides high-temperature melt integrity, an important quality for improved abuse tolerance. Studies of low-temperature shut-down using alternative resins and hand-stretch samples were also undertaken but it was determined that high-temperature melt integrity would be a more achievable goal for this contract.

- **UMT** was focused initially on demonstrating process uniformity and reproducibility of 135°C shut-down/165°C melt integrity material and then on exploration of lowering the shutdown temperature further, down below 135°C. The developmental work on this contract was completed in August 2006.

Ultracapacitor Research and Development

Ultracapacitors (symmetric carbon-carbon double layer type) have been extensively tested at the Idaho National Laboratory (INL) and appear capable of attaining about 50% of the energy density requirements for HEVs in power-assist mode. Full requirements are shown in Table II-2.

However, their very high-power capability makes them a candidate technology for the 42V start-stop applications. To this end, the USABC has contracted with two developers, Maxwell Technologies and NESSCAP, to develop ultracapacitors for the 42-volt start-stop architecture. The primary barriers being addressed by both of these developers are the relatively low energy density and high cost of the systems. Highlights of the FY 2006 activities are presented below.

Table II-2. Ultracapacitor Requirements

FreedomCAR Energy Storage Goals		Ultracapacitors[4]		
Characteristics	**Unit**	**12V Start-Stop**	**42V Start-Stop**	**42V Transient Power Assist**
Discharge Pulse Power	kW	4.2 for 2 sec	6 for 2 sec	13 for 2 sec
Regen Pulse Power	kW			8 for 2 sec
Recharge Rate	kW	0.4	2.4	2.6
Cold cranking power @ -30°C (3 pulses)	kW	4.2 @ ≥7V for 2 sec	8 @ ≥21V for 2 sec	
Available Energy	Wh	15 @ 1 kW	30 @ 1 kW	60 @ 1 kW
Calendar Life	year	15		
Cycle Life	cycle	750k cycles for 150k miles		
Energy Efficiency (on Cycle-Life/Load Profile)	%	95 for UC10		
Maximum Self-discharge	var.	4% (72 hours from V_{max})		
Max Operating Voltage	Vdc	17	48	
Min Operating Voltage	Vdc	9	27	
Maximum System Weight	kg	5	10	20
Max System Volume	liter	4	8	16
Operating Temp Range	°C	-30 to +52		
Survival Temp Range	°C	-46 to +66		
Selling Price @ 100,000 units/year	$	40	80	130

- **Maxwell Technologies, Inc.** whose contract ended in September 2006, successfully completed design validation and delivery of 2.85V, 3600F cells and delivered cells to INL for evaluation. The cells appear to meet all performance requirements set for their contract (which are slightly relaxed from those shown above). Specifically, Maxwell more than doubled the energy density of their cells, increased the cold cranking power by approximately 50%, and reduced the system cost by approximately 50%. However, the proposed system fell short of both program and USABC cost goals.

- **NESSCAP Co., Ltd**. is developing ultracapacitors for 42V start-stop applications by improving fundamentals. The tasks include materials and electrode formulation, production verification, and module design. In 2006, despite significant performance gains during the 1st year, NESSCAP determined that a PC based electrolyte was unlikely to meet all performance and cost goals (particularly low temperature operation), and therefore

changed their focus to acetonitrile (ACN). Nesscap is focusing on producing a larger cell, with high-performance electrodes using advanced carbons and binders.

High Energy Battery R&D

The current EV activity is focused on benchmarking studies of advanced batteries from the U.S. and abroad to determine whether any can meet the technical requirements for the application, as defined in Table II-3.

Table II-3. U.S. Advanced Battery Consortium Goals for Electric Vehicle Batteries

Primary Criterion	Long-term goals[4] (2005-2008)
Power Density, W/L	460
Specific Power, W/kg (80% DOD/30 sec)	300
Energy Density, Wh/L (C/3 discharge rate)	230
Specific Energy, Wh/kg (C/3 discharge rate)	150
Life, years	10
Cycle life (cycles)	1000 (80% DOD) 1,600 (50% DOD) 2670 (30% DOD)
Power and capacity degradation[5] (% of rated spec)	20%
Ultimate price[6], $/kWh (10,000 units @ 40 kWh)	<$150 (desired to 75)
Operating environment	-30C to 65 C
Recharge time	< 6 hours
Continuous discharge in 1 hour (no failure)	75% (of rated energy capacity)
Secondary Criteria	**Long-term goals (2005-2008)**
Efficiency (C/3 discharge and C/6 charge[7])	80%
Self-discharge	<20% in 12 days
Abuse resistance	Tolerant. Minimized by on-board controls.

Thermal Management and Simulation

In support of the Battery Technology Development element of the DOE Program, the National Renewable Energy Laboratory (NREL) performs research and analysis in two areas: 1. Thermal analysis and characterization, and 2. Simulation and requirements analysis of energy storage systems. Nearly all of this work is performed in direct support of USABC contractors' efforts to design and build safe, thermally stable, battery cells, modules and packs.

1. ***Thermal analysis and characterization*** – Proper thermal control is critical to achieving the life, performance, and safety goals of an energy storage system. Poor thermal control could lead to a reduction in battery performance, reduced cycle and calendar life, and increased chance of poor abuse response, and thus substantial increase in cost. This activity is aimed at

[4] For interim commercialization (reflects USABC revisions of September 1996).
[5] Specifics on criteria can be found in *USABC Electric Vehicle Battery Test Procedures Manual, Rev. 2,* DOE/ID 10479, January 1996.
[6] Cost to the original equipment manufacturer.
[7] Roundtrip charge/discharge efficiency.

addressing issues related to thermal control and improving the thermal performance through thermal characterization and testing, measuring thermal properties, and control strategies.

2. ***Simulation and requirements analysis*** – These activities are aimed at developing models and tools for simulating behavior of batteries and using them in existing vehicle simulation tools to support the development of requirements for energy storage systems (batteries and ultracapacitors or combinations) to make advanced vehicles such as micro and mild hybrids, fuel cell hybrids, and plug-in hybrid vehicles most efficient and affordable.

Thermal Analysis and Characterization

Thermal Characterization of Saft Cells – Thermal properties and characteristics of 18 Ah Li-ion cells (VL20P) developed by Saft for the 42V M-HEV FreedomCAR targets were measured. Thermal characterization included thermal images and heat generation of single cells and three cells connected in series under constant current and continuous charge/discharge pulses. Comparing the thermal images from a single cell with the middle cell in a three-cell string, Figure II-2, it was found that the electrical cables connected to the terminals act as a heat sink in taking away heat from the single cell and the two side cells in the three-cell string. The single cell's temperature was about 6°C to 8°C lower than the middle cell's temperature after 1 hour of continuous 112 A charge and 110 A discharge pulses. This confirms that, in a 42 V M-HEV module consisting of 12 VL20P cells, the end cells connected to power cables would be cooler than the other cells and thermal module design should consider this. The heat generation from cells at constant current rates of 18A, 36A, 72A, and 90A at 0ºC, 30ºC, and 45ºC was also measured. At the 2C rate (36A), the heat generation rate was 3.5 W at 30ºC to 45ºC, but was about 7 W at 0ºC. The efficiency of the cells was >95% at room temperature and ~90% at 0ºC.

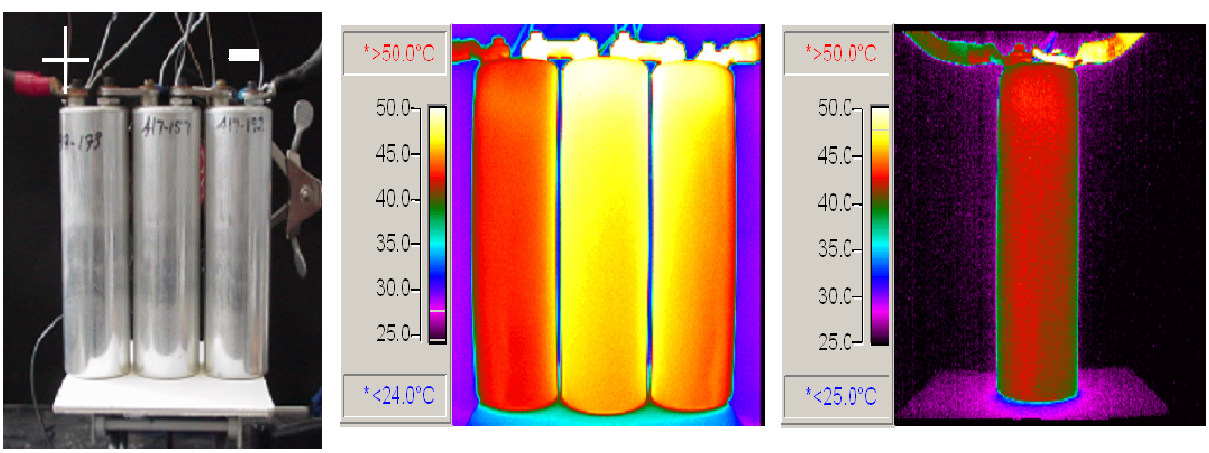

Figure II-2. Three Li-ion cells connected in series (left), thermal image of three-cell string (center), and thermal image of single cell (right) after 1 hour of continuous 112A charge – 110A discharge 2-second pulses.

Thermal Analysis and Testing Improve Design of HEV Modules - Researchers performed analysis of a Saft 42V Li-ion liquid-cooled module using computational fluid dynamics and heat transfer analysis to explore improved thermal design. The developer incorporated the recommendations in their final design and provided a prototype module for testing and evaluation. The module contained 12 VL20P cells connected in a series in two rows as shown in Figure II-3. Researchers assessed the thermal performance of the module under several continuous charge/discharge pulse cycles and found that the cell temperatures rose less than 7°C for moderate

current pulses (75 A) and less than 10°C for high current (250 A), acceptable for most driving conditions. Furthermore, the temperature variation between cells within the module was less than 2°C, an excellent result considering the aggressive power profile applied to the module.

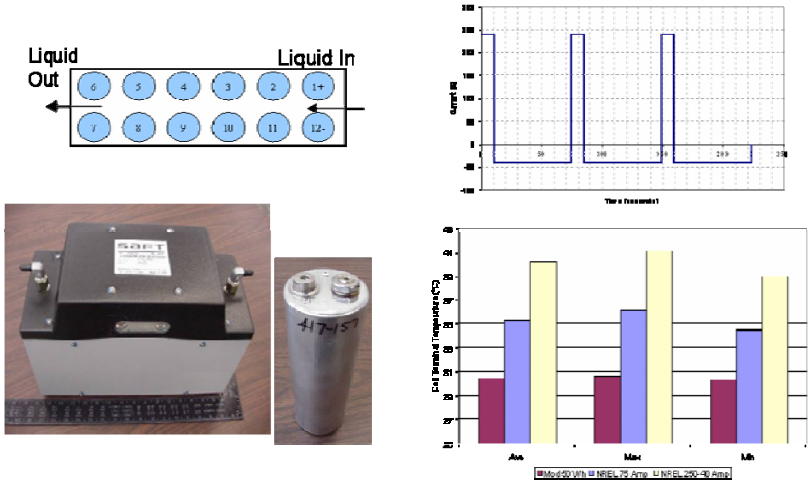

Figure II-3. Saft 12-cell Module (bottom left), one of VL20P cells in the module (bottom center), Configuration of cells in the module (top left), Aggressive discharge/charge pulse cycles (top right), and Results for three charge/discharge cycles (bottom right).

Development of a 3-D Model of Thermal Runaway – A 3-dimensional model that predicts thermal runaway of Li-ion batteries when the cells are exposed to high temperatures has been developed in collaboration with Dr. Bob Spotnitz. The model was applied to oven heating simulations and also localized heating (internal short circuit) for cylindrical cells with cobalt oxide cathodes. Simulations indicated that cell size greatly affects thermal behavior. Smaller cells such as 18650 may cool down faster than large format cells such as 50900, Figure II-4.

Fabrication of an Advanced Calorimeter – Construction of a newly designed advanced calorimeter was started. This newly designed and constructed calorimeter will be used in the second half of FY2007 to measure heat generation from large liquid-cooled energy storage devices (similar to PHEV batteries) to improve their thermal designs. It is imperative to the vehicle operation to understand how an energy storage system generates heat. This includes interconnects between cells/modules and the efficiency differences between individual cells/modules within a battery pack. Furthermore, understanding how much heat is generated from the battery electronics and battery management system will aid in the design of a thermally efficient pack. NREL presently has a calorimeter capable of measuring heat generation from "air-cooled" cells and small mono-blocks. To enhance current capabilities, the new advanced calorimeter was designed to measure heat from large, "liquid-cooled" modules and sub-packs. The large calorimeter is intended to be flexible enough to test various sizes of energy storage devices as well as other electronic equipment.

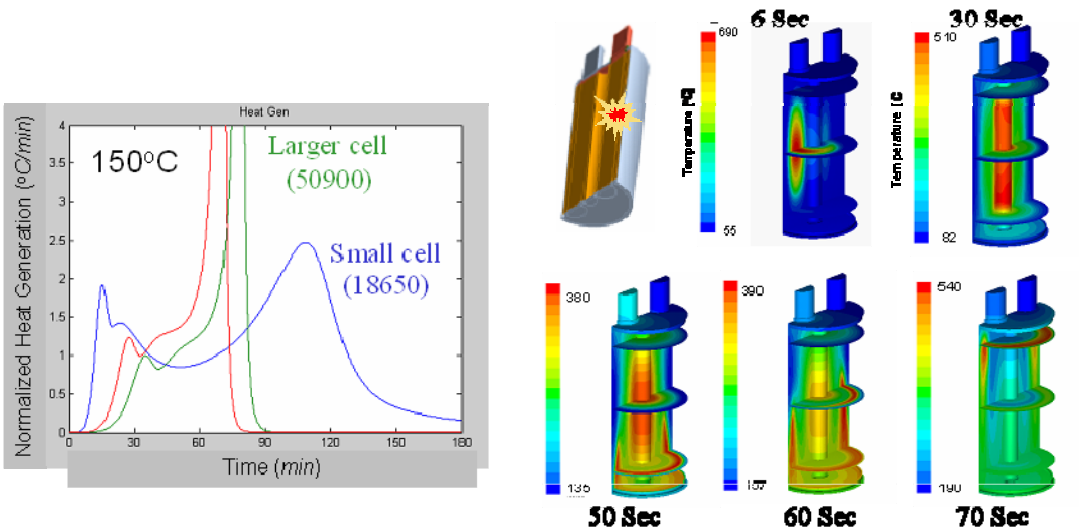

Figure II-4. Smaller cells such as 18650 may cool down faster than large format cells such as 50900, providing the opportunity for the small cell to not go into thermal runaway under the same abuse.

As shown in Figure II-5, the advanced calorimeter consists of four chambers; an internal chamber that holds the battery and accommodates wiring; an inner chamber that holds the heat flux sensors for measuring heat coming from the batteries; an external chamber that holds isothermal fluid around the inner chamber; and an outer chamber that covers the external chamber with insulation and a skin. Additional external isothermal baths are needed for keeping fluid at a constant temperature around the batteries. The internal chamber and isothermal baths have been fabricated. The rest of chambers and components will be fabricated in FY07. Testing of the FreedomCAR batteries will commence after initial validation and calibration.

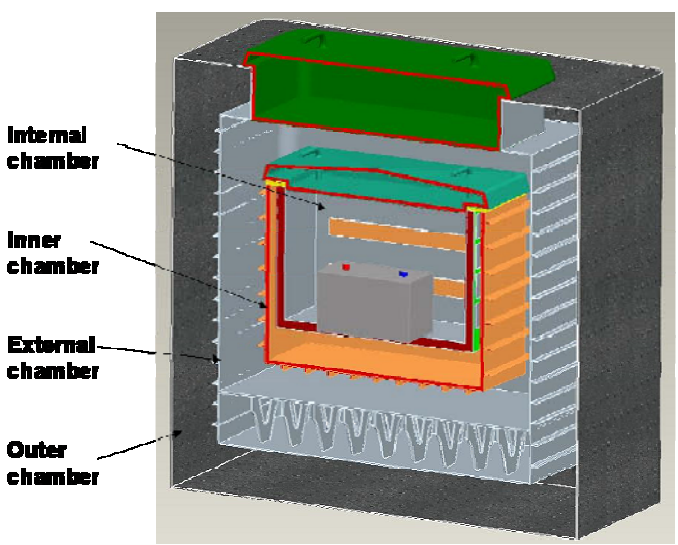

Figure II-5. Schematic of the new advanced calorimeter with multiple chambers.

Simulation and Requirements Analysis

DOE-EPRI Project Produces PHEV Cycling Data – Electric Power Research Institute (EPRI), in collaboration with DOE/NREL, has developed a PHEV battery test procedure. Based on the

Sprinter van PHEV operation and simulations, EPRI developed a cycle consisting of three parts: charge-depleting; HEV-like charge-sustaining; and recharge, Figure II-6. Each of the charge depleting and charge sustaining sections consists of many sub-cycles simulating typical driving.

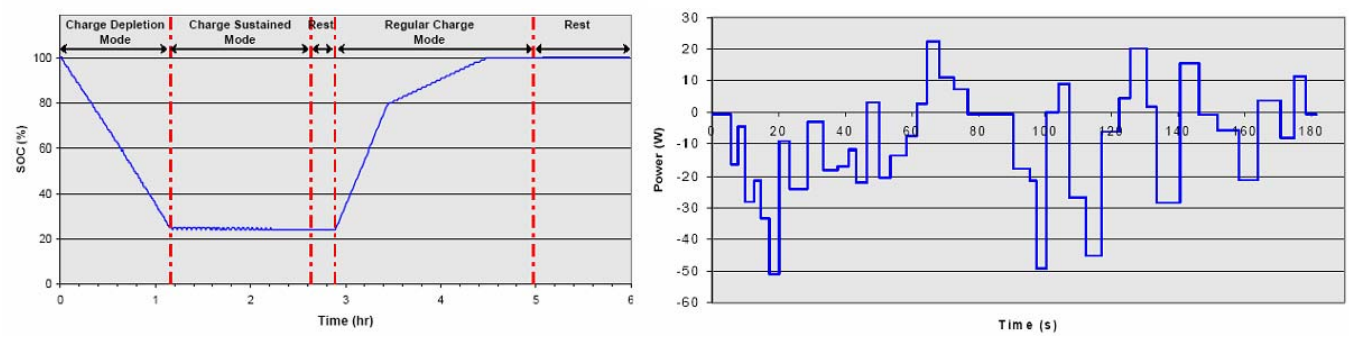

Figure II-6. PHEV cycling profile (top left); subcycle for charge sustaining profile (top right).

This cycle profile was used by EPRI's testing partner (Southern California Edison) to evaluate the capacity and power fade of a 14.4 kWh NiMH pack (Varta) and a 15.5 kWh Li-Ion pack (Saft). This is the first time such data has been produced for battery cycling under PHEV operation. Initial results indicate that the battery power and capacity fade is relatively modest, although some reviewers maintain that the magnitude of the current/power should be higher for passenger vehicles (SUVs and cars). After 21.5 months of testing, the NiMH battery has completed 2280 cycles with only 10% power fade and 1% capacity fade. After 18.5 months of testing, the Li-Ion battery has gone through 1790 cycles with only 6% power and 5% capacity fade, Figure II-7. NREL is evaluating the thermal results of the tests.

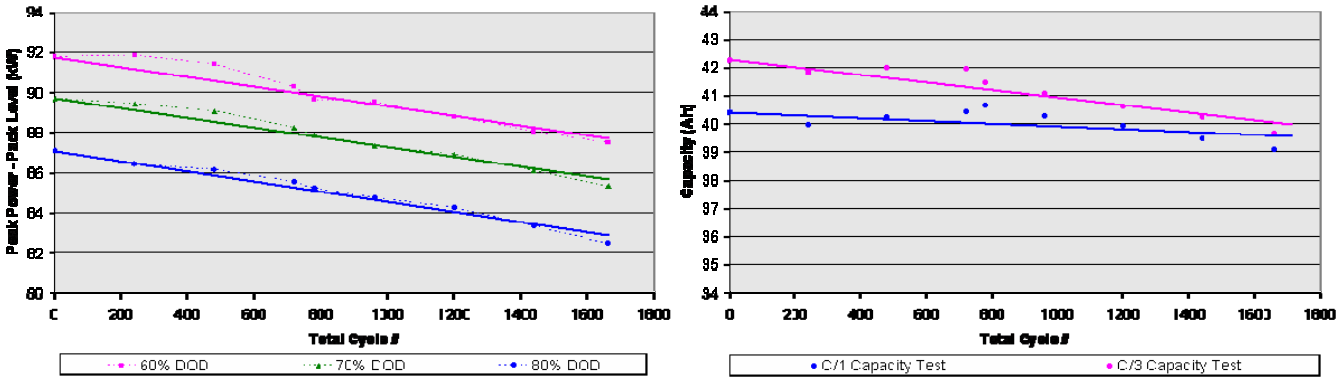

Figure II-7. Pulse power fade vs. cycle number (left); Capacity fade vs. cycle (right); (source: EPRI and Southern California Edison).

Fuel Cell Hybrid Vehicles Energy Storage Requirements – In support of the USABC, NREL performed energy storage simulations and analysis for hybrid fuel cell vehicles to further refine the energy storage requirements proposed in FY05. The impacts of vehicle mass and acceleration on the energy storage requirements were investigated. For a lightweight midsize car with a large fuel cell, the discharge power requirement was about 20 kW (for 10 seconds) and the usable energy requirement was about 230 Whr. For the same midsize car but with smaller fuel cell, the discharge power requirement was about 37 kW for 10 seconds) and the energy requirement was about 280 Whr. These battery requirements are similar to the existing FreedomCAR targets for HEVs.

Analyses of Mild HEVs with Ultracapacitors and Batteries – NREL analyzed and compared the fuel economy of mild HEVs with no engine downsizing using ultracapacitors and batteries. This work was performed was in response to analyses presented by UC Davis at two recent Advanced Automotive Battery Conferences (AABC) which claimed that a "mild" hybrid system using a relatively small ultracapacitor could provide significant fuel economy gains (~60%) on the urban dynamometer driving schedule cycle. Analysis of the simulation details revealed that the author allowed the engine in the ultracapacitor hybrid to cycle on and off very quickly (5-10 seconds) throughout the drive cycle while ignoring drivability issues and driveline/friction losses associated with such engine operation. The Energy Storage Tech Team, in collaboration with the Vehicle Systems & Analysis Tech Team, determined that this was an impractical approach and that the high fuel economies predicted were not attainable.

After modifying the model to simulate a more realistic control strategy (engine off with the idealized zero friction assumption only during low-speed electric launch/deceleration and stop), vehicle simulations at ANL and NREL predicted more modest fuel economy improvements in the range of ~12-20% over a conventional vehicle with no engine downsizing, similar to other start/stop applications. A small Li-ion battery in this mild hybrid configuration achieved comparable fuel economies, Figure II-8.

Configuration	ESS	ESS kg	Unadjusted Fuel Economy mpg (mpg increase over conven. %)		
			UDDS	US06	HWFET
Conven 5-spd 120 kW	N/A	N/A	26.0	27.8	38.4
HEV 5-spd (120 + 15/27) kW	Advanced NiMH	20	31.8 (22.3%)	31.3 (12.6%)	39.6 (3.1%)
HEV 5-spd (120 + 15/27) kW	Current Li-Ion	20	32.1 (23.5%)	31.7 (14.0%)	39.8 (3.6%)
HEV 5-spd (120 + 15/27) kW	Ultracap	7	32.2 (23.8%)	31.3 (12.6%)	39.7 (3.4%)

Figure II-8. Results of analysis (fuel economy over various drive cycles) when hybridizing a conventional midsize car with various energy storage systems (ESS) without any engine downsizing using practical engine Off/On and regen capture.

The question still remained regarding the benefit of using ultracapacitors in mild hybrids. Even if an ultracapacitor hybrid provides only equivalent performance to a comparable Li-ion battery, there may be reason to consider the technology based on, e.g., cold temperature performance and longer life if the long-term costs are comparable. Any future comparison of battery and ultracapacitor hybrid technologies should include a larger range of configurations and control strategies encompassing moderate and full hybrid approaches. In this way, a performance- or cost-optimized ultracapacitor hybrid could be compared to a similarly optimized battery hybrid (rather than constraining each to use the same arbitrary engine/motor sizing and controls). NREL presented this work in a paper titled "Recent Analysis of Ultracapacitors in Mild Hybrids," at the 6th AABC in Baltimore, Maryland, in May 2006.

Future Directions

In support of the President's Advanced Energy Initiative, work on higher energy applications such as commercially competitive, full-function Plug-In Hybrid Electric Vehicles (PHEVs) is expected to begin in 2007 (see http://www.whitehouse.gov/news/releases/2006/01/20060131-6.html). Draft PHEV energy storage requirements are being developed by the Electrochemistry Energy Storage Technical Team in collaboration with the Vehicle Systems & Analysis Technical Team. These requirements are expected to be published on the USABC web site in early 2007.

II.B Technology Assessment

Technology assessments are conducted in order to validate a developer's technical claims by means of independent testing and to gauge the developer's ability to deliver a full-scale, fully packaged battery. The tests are performed both at the developer's facilities and at the DOE national laboratories in order to familiarize the developer with vehicular requirements and USABC testing procedures. The companies also share in the cost of the testing.

II.C Benchmark Testing

Benchmark testing of emerging technologies is important for remaining abreast of the latest industry developments. FCVT, working through ANL and INL, regularly purchases advanced battery hardware (cells and modules) and independently tests these battery systems against the most applicable USABC technical targets. Some products that were tested in 2006 include:

- Lithium Tech/GAIA (42V)
- Hitachi (25kW HEV)
- SK Corporation (40kW HEV)
- A123Systems (25kW HEV)
- GSY (40kW HEV).

II.D Small Business Innovative Research (SBIR)

The SBIR program was created by the Small Business Innovation Development Act of 1982 (P.L. 97-219) and has been reauthorized again until September 30, 2008. The SBIR program was designed to stimulate technological innovation, strengthen the technological competitiveness of small businesses, and use small businesses to meet Federal research and development needs. Phase I awards of up to $100,000 each for about 9 months are used to explore the feasibility of innovative concepts. Phase II is the principal research or R&D effort, with awards up to $750,000 over a two-year period.

Over the past several years, SBIR/STTR contracts have provided valuable support to EV and HEV battery development efforts. Phase II contracts active in FY 2006 are listed below:

- ***Physical Sciences Inc.:*** Electroactive Polymer Separator to Protect from Overcharging in Lithium Ion Batteries

- ***TIAX, LLC:*** Technology to Improve the Performance of Lithium-Ion Cells at Low Temperatures

- ***TOXCO Inc.:*** Improved Electrolytes For Electrochemical Capacitors

- ***Farasis Energy, Inc.,*** High Energy Density Intermetallic Anode Material for Li-Ion Batteries

- ***Phoenix Innovation, Inc.,*** Polythiophosphonate Electrolytes for Rechargeable Magnesium Batteries

- ***TDA Research,*** Lithium Ion-Channel Polymer Electrolyte for Lithium Metal Anode Rechargeable Batteries

One STTR Project was funded in 2006:

- ***MER Corporation (Materials and Electrochemical Research) and Brookhaven National Laboratory,*** Improved Performance of Li-ion Cells at Low Temperature

The following Phase I Proposals were funded in FY 2006:

- ***EIC Laboratories, Inc:*** Improving the Performance of Lithium Ion Batteries at Low Temperature

- ***Farasis Energy, Inc:*** Novel, Redox-Stabilized Li-Ion Cell

- ***Ionix Power Systems, LLC***: Improved Electrode Materials for Electrochemical Capacitors Based on Non-synthetic Precursor Materials

- ***NEI Corporation:*** High Power Density Li-Ion Batteries with Good Low Temperature Performance

- ***TDA Research, Inc.:*** Low-Cost Porous Carbons for Ultracapacitors

- ***TIAX, LLC:*** Nano-Structured Carbon/Silicon Composite for High Energy, Long Cycle Life Lithium-Ion Batteries

III. APPLIED BATTERY RESEARCH

III.A Introduction

The applied battery research program is being conducted in support of the FreedomCAR and Fuel Partnership, which is targeting more fuel-efficient light duty vehicles that can reduce U.S. dependence on foreign petroleum, without sacrificing performance. There is an emphasis on developing and improving critical component technologies; and energy storage technologies are one of these critical components. Energy storage devices enhance the efficiency of the prime power source in HEVs by leveling the load, and they capture regenerative braking energy to produce more fuel efficient and cleaner vehicles. Better energy storage systems are needed to help expand the commercial markets for HEVs. The energy storage requirements for various vehicles are presented in Section II. This program focuses on assisting developers of high-power Li-ion batteries to overcome key barriers to the commercialization of this promising technology for use in light-duty HEV applications. The key barriers are:

- 15-year calendar life,
- Operation between -30ºC and +52ºC,
- Selling price of $20/kW and,
- Adequate abuse tolerance for use in light-duty vehicles.

This applied battery research program, denoted the Advanced Technology Development (ATD) program, focuses on these barriers for high-power Li-ion batteries. It was initiated to understand the factors that limit calendar life, abuse tolerance, and performance over the desired temperature range, so that improvements can be made in these key areas. Also, it addresses the cost barrier at the cell level through the identification and development of lower-cost and more-stable cell materials and components.

The program seeks to advance the development of more optimal cell chemistries through the identification and development of cell materials that are more chemically, structurally, electrochemically, and thermally stable in the cell environment, as well as possessing a cost advantage over current materials. Conventional high-energy Li-ion batteries, of the type used in consumer electronics, employ rather sophisticated electronic control systems that limit their exposure to abusive conditions. This program focuses on enhancing the inherent abuse tolerance of the cell chemistry, which will help reduce the level of sophistication of the electronic control system and thereby realize additional cost savings.

This year the program focused on the four cell-level areas listed below, each addressing one of the key barriers:

- Understand life-limiting mechanisms and enhance life,
- Understand and enhance low-temperature performance,
- Understand and enhance inherent abuse tolerance, and
- Realize lower cell-level costs via lower cost materials, components, and technologies.

In recent years, the program has thoroughly studied and characterized its own Gen 2 cell chemistry and assessed two variations on it. These cell chemistries were defined in the 2005 report. Development of cells employing a new Gen 3 chemistry, employing a lithium-rich $LiNi_{1/3}Mn_{1/3}Co_{1/3}O_2$ (called NMC or 1/3) layered cathode material and a synthetic graphite anode (MCMB 10-28), has been delayed due to a number of issues at the cell and material level. General specifications of this chemistry are shown in Table III-1. Partly as a result of these issues, and at the recommendation of the 2005 merit review panel, the program has expanded its investigation into the fundamental limitations associated with low T performance, and into the characteristics of the solid electrolyte interphase (SEI) and how it is impacted by formation conditions. In particular, a new capability to create binder and carbon free electrodes has enabled detailed *in-situ* diagnostics of the new Gen 3 cathode material and for work to be done on correlating this with formation approaches.

Table III-1. General specifications for Gen 3 cells.

Positive Electrode	8 wt % PVDF binder 8 wt % carbon black 84 wt % $Li_{1.05}(Ni_{1/3}Co_{1/3}Mn_{1/3})_{0.95}O_2$
Negative Electrode	8 wt % PVDF binder 2 wt % graphite fiber 90 wt % MCMB 10-28
Electrolyte	1.2 M $LiPF_6$ in EC:EMC (3:7)
Separator	25 μm PE

Five DOE national laboratories collaborate in the program. Argonne National Laboratory (ANL) is the lead laboratory and provides coordination of the program activities for DOE. The other four participating DOE laboratories are Brookhaven National Laboratory (BNL), Idaho National Laboratory (INL), Lawrence Berkeley National Laboratory (LBNL), and Sandia National Laboratories (SNL). Also, the U.S. Army Research Laboratory (ARL) contributes in identifying and developing more optimal electrolyte systems, including for low-temperature operation. As part of this program, ANL researchers maintain close communications (and in some cases collaborations) with a large number of international material supply companies, through which they gain access to the latest advanced electrode and electrolyte materials for evaluation.

The following subsections provide technical highlights and progress on the Applied Battery Research program for FY 2006. The information provided is representative only and detailed information is available in the publications sited at the end of this section.

III.B Understand Life-Limiting Mechanisms and Enhance Life

OBJECTIVES

- Develop aging protocols and explore new tests, analyses, and modeling methodologies related to calendar and cycle life and provide results to battery developers and other researchers.
- Conduct diagnostic studies on cells with the Gen 3 chemistry, including cells containing binder- and carbon-free oxide electrodes, to develop an understanding of life-limiting mechanisms.
- Understand the impact of various formation protocols on cell life and performance

  - Gain an understanding of the underlying mechanisms that govern the formation of passivation films on the positive and negative electrodes, and
  - Quantify conditions that promote favorable SEI layer formation, as well as conditions that lead to poor (less stable and/or high impedance) SEI layers.
- Develop life models and correlations to gain understanding of fade mechanisms.
- Validate Technology Life Verification Test (TLVT) methodologies as described in the TLVT manual.

APPROACH

- Conduct electrochemical studies on cells with the Gen 3 chemistry to examine the role of each electrode in the aging process.
- Apply advanced microscopy, spectroscopy and diffraction diagnostic techniques, such as SEM, x-ray photoelectron spectroscopy (XPS), and XRD, to understand the impact of electrode microstructure on cell life and performance.
- Apply statistical design of experiments approach to investigate the most significant formation cycle independent parameters (and their interactions).
- Correlate the morphology and composition of electrode surface films with formation cycle protocols to determine the role of the passivation films on cell performance and life.
- Refine and apply cell model to correlate diagnostic findings to performance degradation.
- Perform validation tests on the TLVT methodology and use the results to improve and update the TLVT manual.

ACCOMPLISHMENTS/FINDINGS

- Ordered Gen 3 high power cells for evaluation and are engaged with manufacturers in determining causes of early-life cell failure.
- Updated the Gen 3 cell chemistry based on initial cell screening.
- Examined the effect of temperature and upper cutoff voltage in the formation process on cell performance and determined that cells formed a $0^{o}C$ have relatively higher ASI, higher interfacial impedance, and lower capacity than cells formed at higher temperature.
- Studied electrodes from cells subjected to various formation cycle protocols and determined that the major differences are associated with the films that form on the negative electrode; the positive electrode surface films were similar in all cases.
- Determined that the negative electrode graphite particles from higher impedance cells have an SEI layer that is thicker, denser, and contains more LiF.
- Published TLVT manual and began testing cells to validate the manual.

FUTURE STUDIES

- Investigate capability to produce and use laboratory pouch cells to perform aging and diagnostic studies on advanced chemistries.
- Begin accelerated aging, data analyses, and diagnostics, on Gen 3 cells.
- Continue modeling of Gen 3 cells.
- Continue Phase I cell formation/SEI study to determine the key parameters of the formation process that produce more stable SEI layers.
- Complete TLVT validation by performing life testing on developer cells.

III.B.1 Introduction

This subsection provides highlights and progress on work to understand the life-limiting mechanisms in high-power Li-ion cell chemistries and to relate that information to developing more stable and lower cost cell chemistries. Since the beginning of this program, it has been studying the aging characteristics of different cell materials and chemistries. New diagnostics into the Gen 3 electrodes have begun using binder and carbon free electrodes and laboratory made pouch cells (~100mAh). A new investigation into the impact of formation on cell performance and life has begun, and researchers are currently working with manufacturers to understand the issues that have led to early Gen 3 (18650 sized) cell failure. Finally, the TLVT team has nearly completed its initial testing to validate the TLVT methodology. Table III-2 summarizes how the five DOE laboratories contribute to the work.

Table III-2. Summary of how DOE laboratories contribute to the "Life Enhancement" focus are.

	ANL	BNL	INL	LBNL	SNL
Accelerated Cell Aging and Data Analysis	X		X	X	
Cell Transport Modeling	X				
Advanced Chemistry Cell Build	X				
SEI Investigation	X	X		X	
Formation Study	X		X		
TLVT Validation Testing and Data Analysis	X		X	X	X

III.B.2 TLVT Validation and Testing[8]

The purpose of this effort is to develop a method for accurately predicting battery life with an acceptable lower confidence limit (LCL) for any prescribed driving condition based on a limited amount of accelerated cell testing data. The Technology Life Verification Test (TLVT) manual is complete with a Monte Carlo Simulation package that can be used to estimate the expected cell life and the 90% LCL. The package is based on a model of cell aging developed by the supplier. If the supplier does not have such a model, the manual describes a means for establishing such a model and then using it to create a larger test matrix for acquiring a set of data from which the most accurate projection can be made for a given set of cells and conditions.

The first draft of the manual was completed in June of 2004. The focus since then has been the validation of the methodology. In 2006, the cell testing methodologies were evaluated including the use of a new characterization test, the minimum pulse power characterization test (MPPC). This effort was performed through the acquisition of 55, 7 Ah, high power, Li-ion cells of a similar chemistry to the Gen 2 chemistry, upon which the methodology was developed. Cells arrived in November of 2005 and calendar life testing initiated in February 2006 according to a test matrix designed previously. Preliminary analysis of the cell test data pointed to problems with the way in which the measurement error should be calculated, inconsistencies with the model of rate of change of cell variability when compared to the data, limitations of the default model in fitting resistance rise of a cell if it does not level off, and limitations of using the MPPC for predicting available power. Each of these issues required the development of either new methodologies or the reinstitution of older ones. Following is a summary of the improved means of measuring

[8] Most projects in the ATD program involve multiple collaborations, often at multiple national laboratories. POCs for, and contributors to, each task are provided in Appendix A.

uncertainty, the results of the calendar aging of cells, and a summary of the data analysis using a global model developed as an alternative to the manual default model.

Measurement Uncertainty – A proper understanding of noise characterization, including both manufacturing variability and measurement noise, is critical for accurate life estimation. Measurement error is directly estimable using the process defined in the INL Uncertainty Manuals.[9] After calibration, a series of accuracy checks are performed at various current and voltage levels over the full-scale range of the test channel. These data, along with the calibration error of the accuracy check equipment (shunt and digital volt meter), are used to calculate the total channel error. The uncertainty expressions for derived parameters such as resistance are arrived at by applying these error terms to the voltage and current measurements taken during testing to determine the total parameter error as a percent of reading. The resulting expression for resistance uncertainty is shown in Equation 1,

$$\%R_S = \left[2\left(\frac{\%errV_{STD}}{V(t_1)-V(t_2)} V_{FS} \right)^2 + 2\left(\frac{\%errI_{STD}}{I(t_1)-I(t_2)} I_{FS} \right)^2 + (\%errV_{CAL})^2 + (\%errI_{CAL})^2 \right]^{1/2} \quad (1)$$

where $\%errV_{STD}$ and $\%errI_{STD}$ are the standard deviations for voltage and current, respectively (as determined from the accuracy check), $\%errV_{CAL}$ and $\%errI_{CAL}$ are the equipment calibration errors, V_{FS} and I_{FS} are the full scale voltage and current levels for the test channel, and $V(t)$ and $I(t)$ are the voltage and current measurements taken during a discharge or regen pulse.

This methodology was applied to the resistance calculated from the MPPC test for the TLVT calendar-life cells. The resulting measurement uncertainties per channel at both SOC_{MAX} and SOC_{MIN} at beginning of life are shown in Table III-3. The uncertainties range from 0.9 to 0.09% of reading (all below the suggested maximum of 1% in the TLVT Manual). However, different testers yield different channel uncertainties, and this may be due to several factors such as equipment age, amount of leakage current in the channel, or oscillations in the power supplies.

Table III-3. MPPC discharge resistance uncertainty at beginning of life

Test		High	Average	Low
Maccor 8	SOC_{MAX}	0.90%	0.58%	0.29%
	SOC_{MIN}	0.80%	0.53%	0.27%
Maccor 9	SOC_{MAX}	0.61%	0.43%	0.28%
	SOC_{MIN}	0.55%	0.39%	0.27%
Maccor 10	SOC_{MAX}	0.23%	0.17%	0.10%
	SOC_{MIN}	0.21%	0.15%	0.09%

Calendar-Life Aging – The TLVT calendar-life testing consists of resting at OCV with a daily taper charge back to the target SOC. Every 31.5 days, aging is interrupted for a reference performance test (RPT), which consists of the MPPC test at both the life-test temperature and reference temperature (30°C). At beginning of life, and at RPT6, a low-current HPPC test was also performed to determine loss in available power using the FreedomCAR procedures.

[9] *Uncertainty Study of INEEL EST Laboratory Battery Testing Systems Volume 1: Background and Derivation of Uncertainty Relationships*, INEEL/EXT-01-00505. December 2001, *Uncertainty Study of INEEL EST Laboratory Battery Testing Systems Volume 2: Application of Results to INEEL Testers*, INEEL/EXT-01-00505. March 2003.

Figure III-1 shows the average temperature-compensated discharge resistance growth from the MPPC test at SOC_{MAX} for each temperature group (closed symbols), with data for 30, 40 47.5, and 50ºC shown from bottom to top. The 30°C group only consists of three cells aged at SOC_{MAX}. Each of the other groups consists of nine cells, three each aged at SOC_{MAX}+10%, SOC_{MAX}, and SOC_{MAX}-10%, respectively. However, the effect of SOC appears to be minimal (less than 3%), so all nine cells were included in the average. These data show that temperature is a significant stress factor for these cells.

Figure III-1 also shows the average temperature-compensated discharge resistance growth between RPT0 and RPT6 interpolated from the HPPC test at SOC_{MAX} for each temperature group (open symbols). The HPPC test yields lower resistance growth after six months of aging than the corresponding MPPC test. Additional RPTs are needed to confirm trends, but this indicates that life estimations based on resistance measurements from the MPPC test will be more conservative.

Modeling – To fully evaluate the TLVT process one needs a model that accurately reflects cell performance (aging) over time. Such a model was not provided by the manufacturer for the cells being tested here. Thus, data from the TLVT validation experiments are being used to develop an aging model. Since the cycle life experiment is just now beginning, only calendar life data is available. Thus, the modeling reported here is reflective only of calendar-life aging through approximately six months of testing.

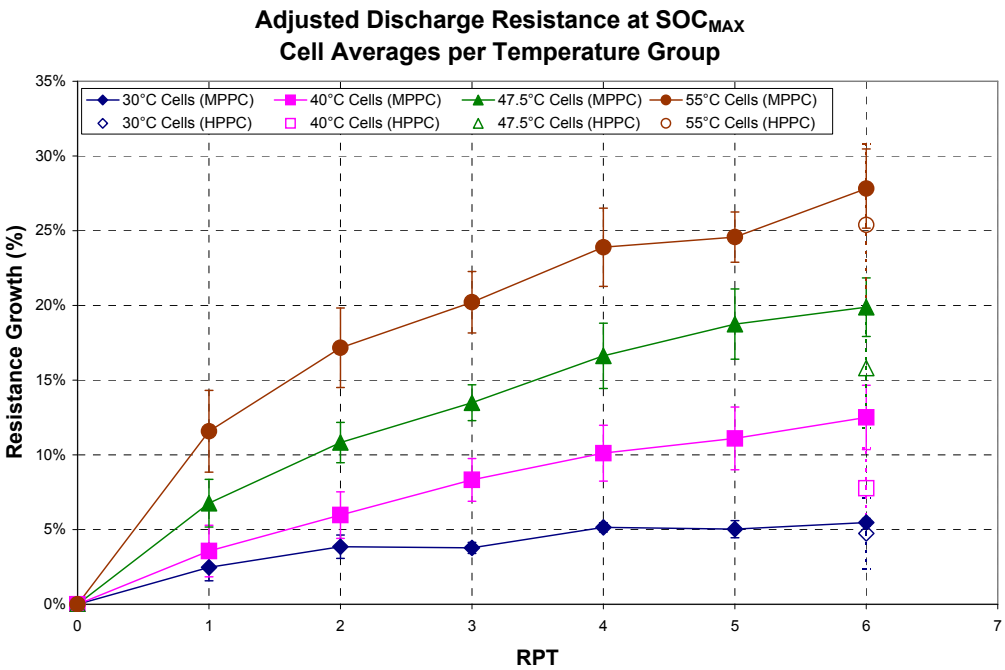

Figure III-1. Temperature-compensated discharge resistance growth at SOC_{MAX}

As currently written, the TLVT manual considers each accelerated aging condition separately. This model did not apply to the current situation. In other situations where there is a sufficient amount of experimental data (more cells per condition over a longer length of time), it may succeed. An alternative modeling methodology (to be described in more detail in a revised version of the TLVT manual), integrating all accelerated aging conditions, was developed and applied here.

The alternative model is based on the discharge resistance at SOC_{MAX}. Overall, the measured resistance of the jth cell (assigned to the ith experimental condition) at time t is represented by $R(i,j;t) = \mu(i;t) + e(i,j;t)$, where $\mu(i;t)$ is the average resistance of the cell population and $e(i,j;t)$ is the deviation of the observed resistance from the average resistance (a combination of measurement error and cell-specific effects) at the indicated conditions. Based on the experimental data, separate models were developed for μ and e. Assuming that these models are accurate, they can be used to evaluate the efficacy of hypothetical experiments specified by test duration, RPT frequency, experimental conditions, and number(s) of cells per condition.

A useful fitted model for the average relative resistance of cells in the ith experimental group at time=t versus time t=0, $\hat{Y} = \frac{\mu(i;t)}{\mu(i;0)}$, is: $\hat{Y} = \exp\left(\hat{\lambda} \cdot t^{0.5}\right)$, where $\hat{\lambda} = \exp\left(\hat{\beta}_0 + \hat{\beta}_1 \cdot \frac{1}{T}\right)$, $\hat{\beta}_0 = 16.86, \hat{\beta}_1 = -5850$, and t and T are in terms of years and degrees (K). Note that the SOC-level did not have a discernable effect on aging. Figure III-2 illustrates the model prediction versus the observed experimental values. Note that the data at 30°C were not used to estimate the model parameters and thus provide some level of model validation.

A simple model of the deviations from the average relative resistance model was also developed based on the TLVT validation data. The variance of the observed deviations for cells in the ith experimental group at time t was approximated well by: $V\hat{a}r(e) = \hat{a} + \hat{b} \cdot \frac{\hat{\mu}^2(i;t)}{\hat{\mu}^2(i;0)} + \hat{c}$ with $\hat{a} = -.087$, $\hat{b} = .11$, and $\hat{c} = .0009$, where $\hat{c}$ is due to measurement error, $\hat{a} + \hat{b}$ reflects the intrinsic cell-to-cell variation at t=0, and $\hat{b} \cdot \frac{\hat{\mu}^2(i;t)}{\hat{\mu}^2(i;0)}$ indicates how the intrinsic cell-to-cell variation increases as cells age (*i.e.* the mean resistance increases). The value for $\hat{c}$ (a relative measurement error of about 1%) is based on the measurement uncertainty work at INL. Values for the other parameters were estimated via analysis of the experimental data.

Simulations based on these models were used to explore how well cell life could be estimated for a variety of hypothetical experiments. Cell life is the average time required to increase cell resistance by 30% when cells are aged at 30ºC. Figure III-3 summarizes the results of one set of 1000 simulation trials where 30 cells (10 each at 40ºC, 47.5ºC, 55ºC) were hypothetically tested for one year with an RPT every 4 weeks. On average, the simulations produced an "estimated life" of about 9.5 years (which is what is expected if the underlying model, given by $\hat{Y}$, is accurate). Ten percent of the simulations produced an "estimated life" of less than 8.9 years. In this case, the implication is that in order to have 90% confidence that an experiment will yield an estimated life at or above some target life, the true life will need to exceed the target life by as margin of about 0.6 years.

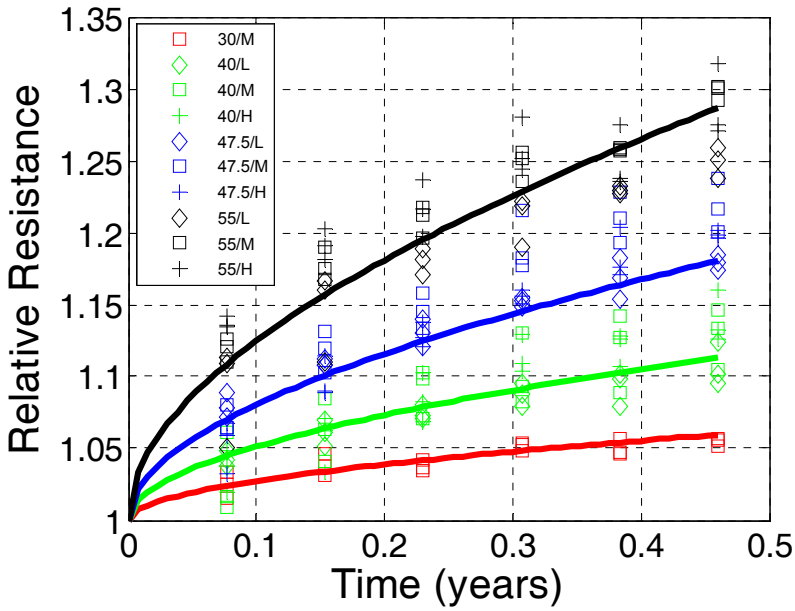

Figure III-2. Relative resistance: model prediction (lines), observed (symbols)

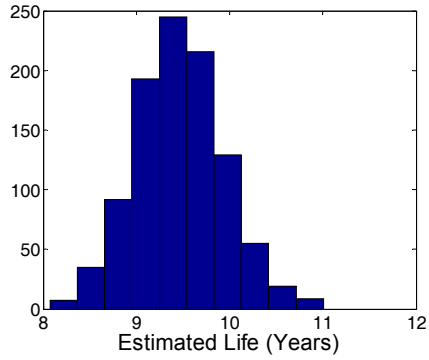

Figure III-3. Distribution of estimated cell life (from simulation)

III.B.3 SEI/Formation Study, DOEx, and Diagnostics

The formation process is a very important first step in producing stable cells that will exhibit good power and energy characteristics over long life. Formation cycling is defined as the initial cycling, under a controlled set of conditions, conducted on every Li-ion cell before it is given to the end-user. The formation cycling goals include: (a) limited cell capacity fade and impedance rise, (b) similar performance of identical cells when subjected to similar test conditions, and (c) "desirable" passivation films on the electrode active materials. These passivation films are known to protect electrode active materials from further reactions with electrolyte components; the nature of these films affects both initial and long-term cell performance, and has a significant influence on cell calendar life and safety characteristics. Desirable properties of passivation films include: (a) low resistance to Li-ion transport, (b) low solubility in the electrolyte, and (c) stability under oxidizing and reducing conditions. The passivation films on the negative electrode, known as the SEI layer, are critical to extending the life of high-energy cells for which end-of-life is defined by capacity fade. Appropriate passivation films on the positive electrode may be key to extending the life of high-power cells for which end-of-life is (normally) defined by power fade.

The objective of this study is to gain an understanding of the underlying mechanisms that govern the formation process. The study also aims to quantify conditions that promote favorable SEI films, as well as conditions that lead to poor formation and subsequent poor cell performance. A complementary goal is to produce a protocol that achieves satisfactory formation in a fraction of the time required by conventional (C/24-based) methods. Another goal is to correlate favorable and unfavorable formation conditions, such as temperature and time, with the nature and composition of electrode surface films.

A two-path approach is being followed: (1) the most significant formation cycling parameters (and their interactions) are being studied based on a statistical design of experiments using 2032-type coin cells containing 1.6 cm^2 electrodes, and (2) diagnostic testing to correlate the morphology and composition of electrode surface films with formation cycling protocols, which includes examination of electrodes harvested from pouch cells containing 5 x 5 cm^2 electrodes. The experiments are being conducted in cells containing a positive electrode based on $Li_{1.05}(Ni_{1/3}Co_{1/3}Mn_{1/3})_{0.95}O_2$, a negative electrode based on MCMB 10-28 graphite, an EC-EMC (3:7 by wt.) + 1.2M $LiPF_6$ electrolyte, and Celgard 2325 separator. It should be noted that the formation experiments and data described in this report are for one battery chemistry. Because SEI attributes and performance are related to battery chemistry, care should be taken when making inferences between the results from this study and other cell chemistries.

Statistical DOEx and Data from Stage 1 Tests – This work is an initial study to determine which factors have the most influence on SEI formation. Foremost test parameters for this study include temperature (T) and the upper cutoff voltage (UCV). Other parameters include the cycling rates on charge (C_{ch}) and discharge (C_{dis}), open circuit rest periods (t_{ocv}), and the net number of complete formation cycles per cell (n_{cyc}). To accommodate both the large overall matrix and a finite number of test channels, the study was divided into three stages, where each stage has one or more distinct set of test parameters in sub-matrices. A statistical fractional factorial approach was employed in setting up the matrix. Considering the variability among button cells, the size of the test matrix, and the limited number of available test channels, at least six cells were tested at each condition. Formation parameters are shown in Table III-4, and fixed conditions are shown in Table III-5. The relative effect of parameters on SEI formation and subsequent performance was assumed to be of the order: $T > UCV > C_{ch} > C_{dis} > t_{OCV} > n_{cyc.}$

Table III-4. Summary of relevant formation parameters, * = default values

Parameter	Values		
Formation Temperature (T), °C	0	30*	50
Upper Cutoff Voltage (UCV), Volts	3.7	4.0*	4.2
Charge Cycling Rate (C_{ch})	$C_1/24$	$C_1/10$*	
Discharge Cycling Rate (C_{dis})	$C_1/24$	$C_1/10$*	
OCV rest after each UCV and LCV taper time (t_{OCV})	None*	4 hours	
Total number of complete formation cycles (n_{cyc})	2*	3	

Table III-5. Summary of fixed formation conditions.

Condition	***Value***
Lower Cutoff Voltage (LCV)	3.0V
Time at taper charge upon reaching UCV	End taper charge when $I \leq I_{ch}/10$.
Time at discharge condition upon reaching LCV	None. Taper discharging might damage cells under formation by causing SEI dissolution.
Soak Time Limit	Terminate taper time after 2 hours if above condition not met.

Immediately following formation cycling, the cells are characterized by various techniques that include: (a) electrochemical impedance spectroscopy (EIS) measurements at 80% SOC (~3.9V), (b) C/1 and C/24 capacity measurements, and (c) self-discharge tests, in which cells charged to 4.0V are left at OCV for two days. The cells are then cycle-life aged at 50°C using a continuous cycling profile at a $C_1/1$ rate around 80% SOC. Periodic characterization yields information on the degradation of cell performance.

In Stage 1, the effects of T (0, 30, and 50°C) and UCV (3.7, 4.0, and 4.2V) were examined using 60 cells. A full statistical analysis of the results is in progress. The observations from Stage 1 are: (a) Formation at 0°C yields cells with relatively higher area specific impedances (ASIs), higher interfacial impedances, and lower capacities. (b) In some cases the 50°C formation condition produces data with more scatter, which indicates that a higher temperature can cause inconsistent SEI formation. (c) In most cases, a higher UCV produces cells with higher capacities and lower ASIs. (d) While under cycle life testing at 50°C, the increase in ohmic impedance over aging is about 2 to 3% per day, and the trend is roughly linear. (e) At the end of 30,000 cycles at 50°C, all cells exhibited significant capacity fade and high self-discharge. (f) For the Gen 3 chemistry, an overall favorable formation condition is (T=30°C, UCV=4.0-4.2V).

Results from the tests are shown in Figure III-4, which compares the mid-frequency arc width in the EIS data before cycle-life testing and after 30,000 cycles at 50°C. In general, the data indicate that the mid-frequency arc width, which is believed to result from electrode-electrolyte interfacial processes, is approaching a relatively consistent level by end of test. Furthermore, this final interfacial impedance appears to be somewhat independent of formation conditions.

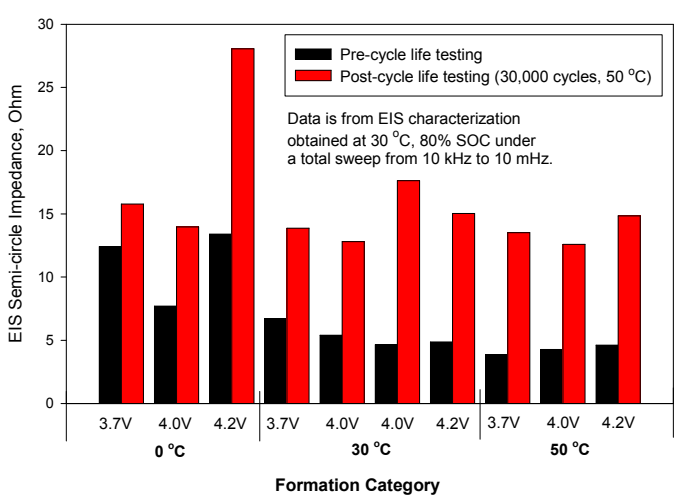

Figure III-4. Representative EIS data from Nyquist semi-circle analysis of Stage 1 cells

Diagnostic Examination and Formation Cycling Mechanisms

S*tudies in cells with Li counter electrodes* – Cells containing Gen 3(-) electrode vs. Li and Gen 3(+) electrode vs. Li were prepared to study electrochemical processes during the 1st few cycles, which are of interest from a formation cycling perspective. The dQ/dV data on the Gen 3(-) electrode cell (Figure III-5a) show that electrolyte reduction to form the anode SEI layer (a) occurs mainly during the 1st Li-intercalation cycle into the graphite, and (b) starts at ~0.8V vs. Li. Other experiments have shown that solvent reduction starts at ~0.8V vs. Li, followed by LiF formation that starts at <0.2V vs. Li. When cycled at a very slow rate, the anode SEI layer consists of an inner organic layer containing solvent reduction species and an outer layer, which is a heterogeneous mix of organic (solvent reduction) and inorganic (LiF, $LiPF_y$, salt decomposition) compounds.

The data on the Gen 3(+) electrode cell (Figure III-5b) show that the cathode displays a 1st cycle capacity loss that results from the inability of Li ions to fully intercalate into the oxide in the 3.0-4.3V range. A study of this phenomenon has shown that all the Li may be reinserted into the oxide by lowering cell voltage to ~1.5V vs. Li, *i.e.*, the 1st cycle capacity loss in the nominal cycling range is a kinetic effect that results from a decrease in Li-ion mobility as the oxide Li occupancy rises above a threshold value. The dQ/dV data on the Gen 3(+) electrode (Figure III-5b) show two prominent peaks (at ~3.7V and ~3.8V vs. Li) in the 1st Li-extraction cycle that are apparently related to Ni oxidation in the closely related H1 and H2 polymorphs present in $Li_{1.05}(Ni_{1/3}Co_{1/3}Mn_{1/3})_{0.95}O_2$. The significant decrease in the 3.7V peak height observed in the 2nd cycle is related to the 1st cycle capacity loss because the peak is observed in cell cycling data obtained after full Li reinsertion into the oxide.

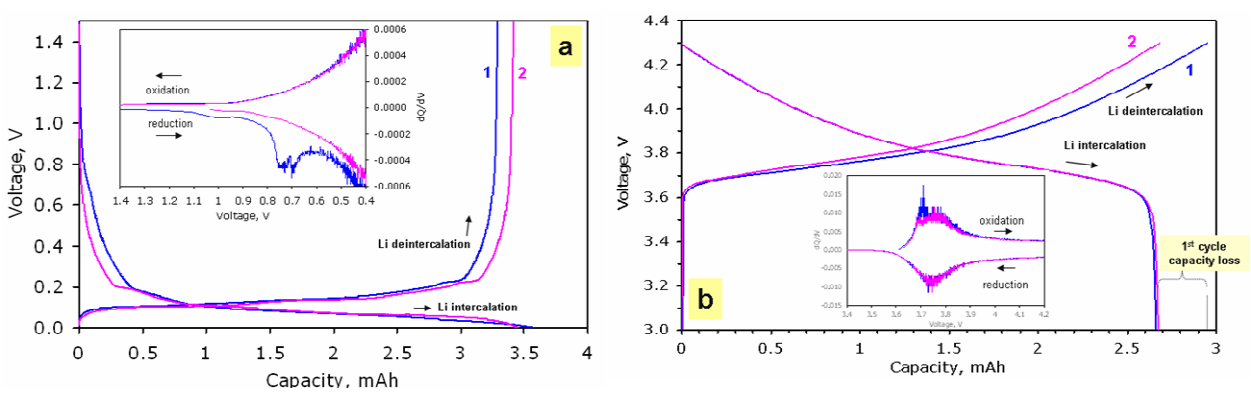

Figure III-5. Voltage vs. capacity and dQ/dV plots from (a) Gen 3(-) vs. Li and (b) Gen 3(+) vs. Li cells. Data from the 1st two cycles are shown; these data were acquired at 30°C with a 0.064 mA (~C/50).

Pouch Cell and Other Studies – A limited number of pouch cells with the Gen 3 chemistry were prepared, formation-cycled, and aged to correlate cell performance with (a) formation cycling protocols, and (b) nature and composition of electrode surface films. The four formation protocols studied are shown in Table III-6; three cells were prepared for each protocol to ensure data reproducibility.

EIS measurements were conducted on the cells immediately following formation cycling. The data (Figure III-6) show that little difference in the mid-frequency arc width (interfacial impedance) between cells cycled slowly (~C/25 rate) at 0°, 30°, and 50°C. However, the cell cycled relatively rapidly (~C/5 rate) at 0°C shows a higher interfacial impedance.

Table III-6. Pouch cell tests – formation cycling protocols

Voltage Range	Number of Cycles	Temperature	Cycling rate
3.0-4.0 V	3	50 °C	~C/25
3.0-4.0 V	3	30 °C	~C/25
3.0-4.0 V	3	0 °C	~C/25
3.0-4.0 V	2	0 °C	~C/5

To determine individual electrode contributions, impedance data were acquired in cells containing a Li-Sn reference electrode (RE) that were formed under conditions similar to those in the pouch cell studies. Data showed that the interfacial impedance is higher for a cell formed rapidly at 0°C than for a cell formed slowly at 30°C, which is consistent with the pouch cell data and the coin cell data. Furthermore, the higher impedance for the rapidly formed 0°C cell mainly arises from the negative electrode.

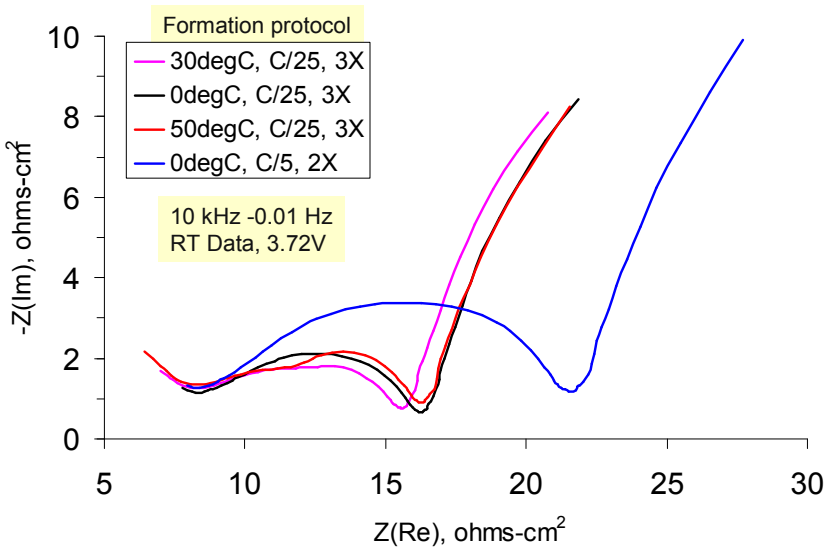

Figure III-6. EIS data from pouch cells cycled under various formation protocols.

Scanning electron microscope (SEM), XPS and Time-of-flight (TOF) secondary ion mass spectrometry (SIMS) studies were conducted on samples harvested from pouch cells after formation cycling to shed light on the impedance behavior differences. The SEM images showed clear morphology differences between anode samples harvested from the pouch cells that were rapidly formed at 0°C and anode samples harvested from the other cells. The SEI layer on the former samples appeared thicker and denser (Figure III-7a) and showed distinct crystallite presence on the carbon fibers (Figure III-7b), which have a smooth morphology in fresh electrode samples.

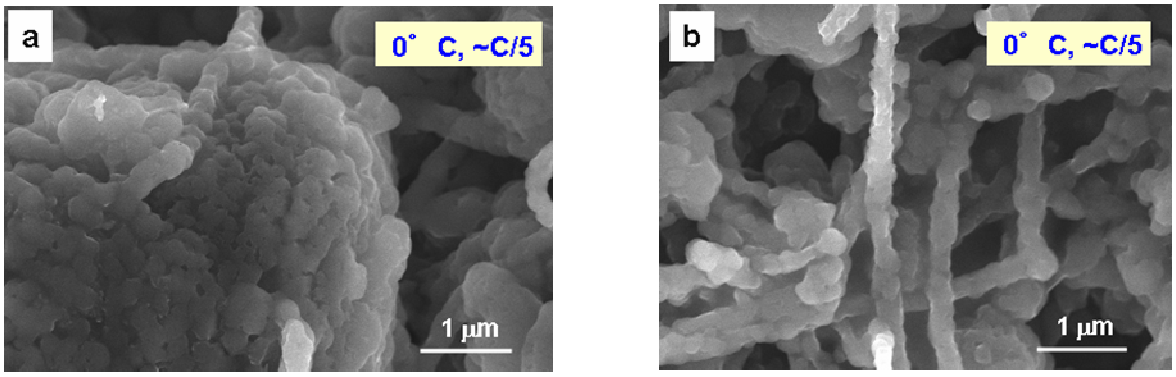

Figure III-7. SEM images of a Gen 3(-) electrode sample harvested from a pouch cell that was rapidly formed at 0 °C. The MCMB graphite and carbon fibers are prominent in (a) and (b), respectively.

The C1s XPS spectra (Figure III-8a) of the fresh anode showed distinct graphite and PVdF peaks, as expected. However, these peaks were mostly obscured by the SEI layer after formation cycling. In addition, the graphite peak intensity was lower for the rapidly formed 0°C sample, which suggests that the graphite is covered by a thicker, and probably denser, SEI layer.

This observation was confirmed by TOF-SIMS experiments, wherein longer sputtering times were required to expose the graphite on the 0°C sample. The F1s XPS spectra (Figure III-8b) showed a significantly higher proportion of LiF on the rapidly formed 0°C sample, which is the crystallite species observed in the SEM images. In general, the XPS data showed that (a) solvent reduction products are dominant in the anode SEI of cells formed at slow rates, (b) a heterogeneous mixture of LiF and solvent reduction species is present in the anode SEI of samples from the rapidly formed 0°C cells, and (c) small differences are observed in the cathode surface films of the variously formed cells, *i.e.*, the main influence of formation cycling is on the negative electrodes of the cells. The data also suggests that the higher impedance of the rapidly formed 0°C cells may result from LiF crystallites that are adjacent to the graphite edge planes. Further diagnostic and aging experiments are underway to confirm these mechanistic scenarios.

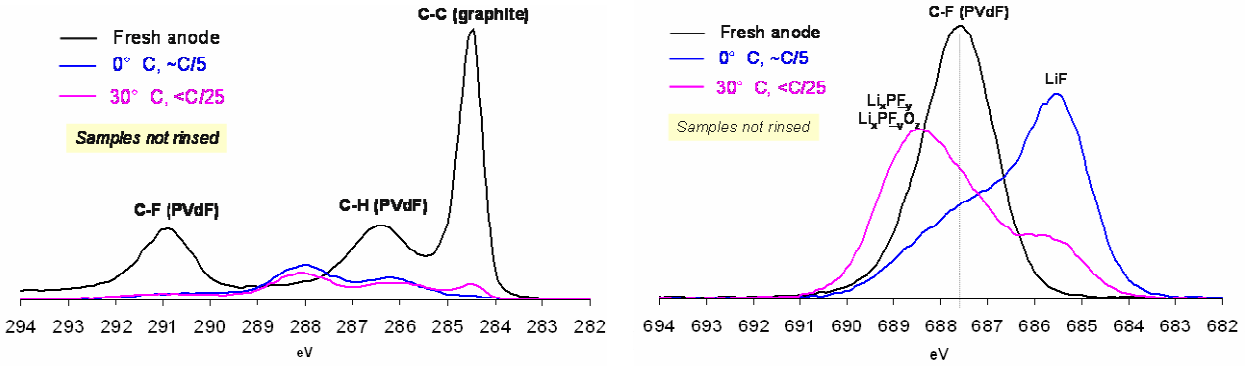

Figure III-8. (a) C1s and (b) F1s XPS spectra from Gen 3(-) electrode samples.

III.B.4 Gen 3 Cell Build Status, Testing, & Diagnostics

In 2005, a Gen 3 cell chemistry was selected for implementation in high-power 18650 cells. The main objective with the new chemistry is to make a major change in the positive electrode used in the cell, because studies on Gen 1 and Gen 2 cells showed that the positive electrode played a dominant role in both the life and inherent abuse tolerance limitations of these two cell chemistries. The Gen 1 and Gen 2 cells employed lithiated nickel-cobalt oxide positive electrodes, where the Gen 2 positive electrode was stabilized by the use of 5% aluminum. In Gen 3 cells, a lithium-rich nickel-cobalt-manganese oxide ($Li_{1.05}(Ni_{1/3}Co_{1/3}Mn_{1/3})_{0.95}O_2$) positive electrode will be used. To avoid potential complications associated with the use of advanced graphite in the negative electrode, MCMB was selected. The enhanced stability of this type of positive electrode has been discussed previously and it is anticipated that the cells will exhibit longer calendar life and enhanced inherent abuse tolerance.

Based on lab-scale studies with these electrode materials, electrode and cell specifications were developed and provided to a developer for fabrication of 18650 trial cells in 2005. An unusually high rate of early-life failures occurred with those cells. So, in 2006 work focused on resolving this issue through a series of trial cell builds. Two different cell builders were used along with a company that specializes in coating electrodes for the Li-ion battery industry. With the help of one of the cell builders, localized metal deposits on the negative electrode side of the separator were identified as the most probable cause of early cell failures, via the creation of soft shorts at these localized areas. These metal deposits are comprised of iron and copper. Efforts are currently underway to determine the source(s) of these metal impurities.

The latest electrode and cell specifications for the Gen 3 cells are shown in Table III-1. In the latest trial cells, ~ 50 μm thick electrode coatings are being used. Internally fabricated pouch cells that employ these specifications perform very well (especially when electrolyte additives are employed that stabilize the electrode passivation films) which provides promise that once metal impurity issues are resolved, the high-power Gen 3 18650 cells will perform well also. Figure III-9 shows improved aging characteristics in a Gen 3 trial cell that was aged at 55ºC and 60% SOC.

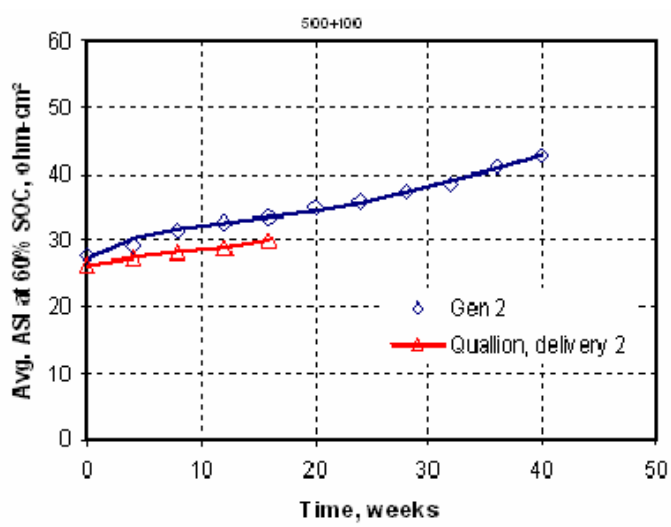

Figure III-9. Comparative aging characteristics of a Gen 2 cell vs. a Gen 3 trial cell that contains an electrolyte additive that stabilizes the passivation films on the negative and positive electrodes.

Fresh Electrode Characterization – Representative SEM images (Figure III-10) from fresh Gen 3 positive electrodes show the $Li_{1.05}(Ni_{1/3}Co_{1/3}Mn_{1/3})_{0.95}O_2$, Super P, and PVdF binder. The oxide secondary particles are typically 5 to 10μm in size and are composed of faceted primary particles (Figure III-10b). TEM examination showed that the oxide particles have similar surface and bulk structures, which is different from that of the Gen 1 ($LiNi_{0.8}Co_{0.2}O_2$) and Gen 2 ($LiNi_{0.8}Co_{0.15}Al_{0.05}O_2$) particles that had a ~3 to 10 nm Li_xNiO surface layer even on the fresh oxide particles. XPS spectra on the Gen 3 particles were consistent with the presence of Ni^{+2}, Co^{+3}, and Mn^{+4}. In addition, the oxygen XPS spectra showed strong oxide peaks and weak surface impurity peaks; again this is different from that of the Gen 1 and Gen 2 oxide particles that showed strong Li_2CO_3 peaks and weak oxide peaks. The XPS data suggest that the Gen 3 oxide is less prone to form Li_2CO_3 on the particle surfaces. However, the effect of long-term air exposure on the surface Li_2CO_3 formation is not known and will be examined at a later time.

Representative SEM images (Figure III-7) of fresh Gen 3(-) electrodes show the MCMB-10 graphite, VGCF carbon fibers and PVdF binder. The graphite particles are 10μm in size, but smaller particles in the 1μm size range are also observed; and the carbon fibers are ~2-3μm in length. XPS spectra obtained on the electrodes showed the expected graphite and PVdF peaks in the C1s and F1s spectra, respectively.

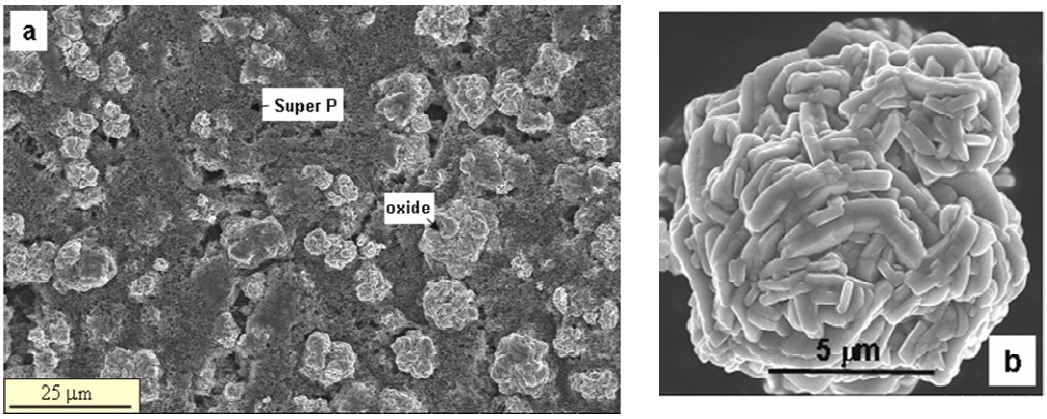

Figure III-10. (a) SEM image of Gen 3 positive electrode, (b) Enlarged view of oxide particle.

Testing of laboratory cells with Gen 3 electrodes – Electrochemical data on cells with Gen 3 electrodes were obtained from both 2032-type coin cells and from larger cells that incorporated a Li-Sn reference electrode. The electrolyte in these cells was 1.2 M $LiPF_6$ in an EC:EMC (3:7 by wt.) solvent. A 25μm thick Celgard 2325 separator was used. Typical data from a Gen 3+/$Li_4Ti_5O_{12}$- coin cell cycled at 55°C shows ~ 15% capacity fade after 100 cycles (Figure III-11a) and impedance rise (Figure III-11b) of ~30%. Because the $Li_4Ti_5O_{12}$ negative electrode contributes little to cell performance degradation, the measured capacity fade and impedance rise are most likely associated with the Gen 3+ electrode. In contrast, a Gen 3+/Gen 3- coin cell cycled under similar conditions showed a much higher capacity fade (~ 40%) after 100 cycles (Figure III-12a) and impedance rise (Figure III-12b). That is, the capacity fade and impedance rise are worse in cells containing graphite negative electrodes.

The negative electrode contribution to cell impedance rise was confirmed in Gen 3+/Gen 3- cells containing a Li-Sn reference electrode; both the oxide-positive and graphite-negative electrode

contributed to impedance rise in these cells. The capacity fade in cells containing the Gen 3+ electrodes may be associated with the dissolution of Mn from the cathode. The positive electrode impedance rise probably results from the blocking of the oxide edge planes by organo-phosphate and flourophosphate surface films. The negative electrode impedance rise probably results from a thickening of the SEI layer, which impedes Li-ion transport. Further tests are underway to determine and delineate the performance degradation mechanisms in this cell chemistry.

It has been found that additives that stabilize the negative and positive electrode surface passivation films produce a significant reduction in the rate of impedance rise with this cell chemistry during accelerated aging. These electrolyte additives will be incorporated into some of the Gen 3 high-power 18650 cells to quantify their impact and understand the mechanism(s), via diagnostic studies on aged cells.

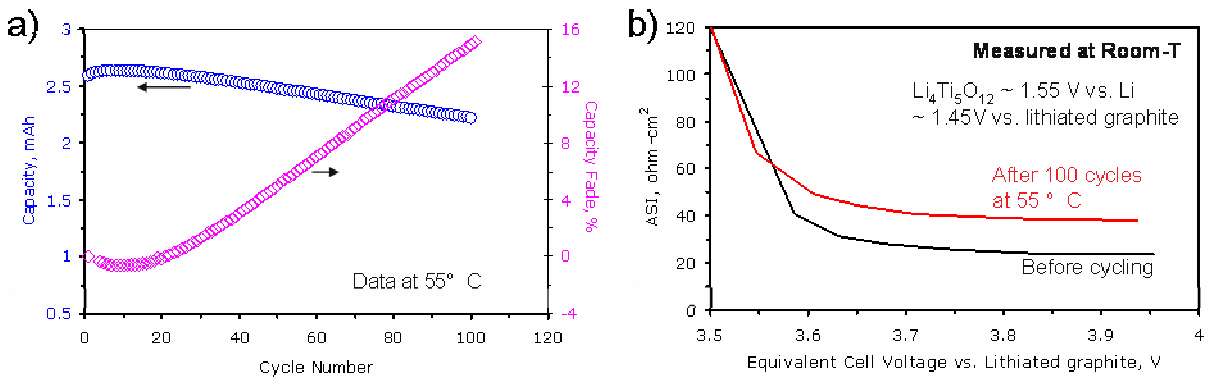

Figure III-11. (a) Capacity and capacity fade data from a Gen 3+/$Li_4Ti_5O_{12}$- coin cell cycled from 1.5 – 2.7 V cycles (Equivalent range: 2.95 - 4.15V in graphite anode cells) at a C/4 rate. (b) ASI data obtained by the current-interrupt technique.

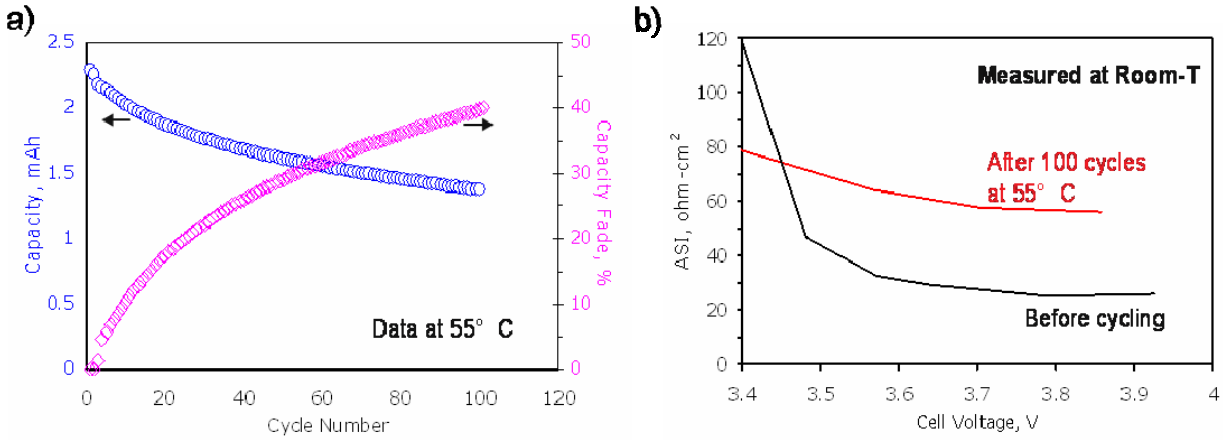

Figure III-12. (a) Capacity and capacity fade data from a Gen 3 +/- coin cell cycled from 3 to 4.1V at a C/4 rate. (b) ASI data obtained by the current-interrupt technique.

III.C Understand and Enhance Low-Temperature Performance

OBJECTIVES

- Understand factors that limit low-temperature performance and identify approaches to enhance that performance.
- Develop models of low-temperature electrolyte and cell behavior.
- Thoroughly characterize the Gen 3 cell chemistry at low temperatures, including the power loss during high-current pulse discharge and possible Li plating during charging.

APPROACH

- Use *in-situ* and *ex-situ* diagnostics, including EIS, FTIR, XRD and modeling to aid in identifying sources of the problem.
- Investigate the SEI and its characteristics at low temperatures.
- Identify methods for enhancing low-temperature performance and evaluate them.

ACCOMPLISHMENTS/FINDINGS

- In general, changes in active material and electrolyte do not significantly impact the poor low-temperature performance.
- Results from binder and carbon free electrodes show that the impedance rise at low temperature is due to interfacial effects on the active material particles.
- High surface area particles improve the low-temperature performance but provide only part of the solution.
- Several electrolyte formulations based on $LiBF_4$ in carbonate and ester mixtures show improved performance over Gen 2 electrolytes at –30ºC:
    - $LiBF_4$ is superior to $LiPF_6$ if no phase changes take place at low temperatures,
    - $LiBF_4$ needs higher dielectric constant solvents for avoiding phase changes,
    - The addition of γBL increases the solubility of $LiBF_4$ at low temperature.
- The addition of methyl butyrate significantly reduces viscosity and increases wet-ability to separator.

FUTURE STUDIES

- Understand and modify interface, investigate additives (vinyl ethylene carbonate (VEC), vinylene carbonate (VC), vinyl propionate (VP), *etc.*).
- Continue to investigate non-EC based electrolytes, and additional salts ($LiBF_4$, LiBOB, new proprietary salts).
- Continue testing hard carbons, alternative electrodes for use at low temperatures.
- Perform *in-situ* XRD on Gen 3 and $LiFePO_4$ cathode materials at low temperatures.
- Continue data analysis and parameter development for cell model for Gen 3 cells.
- Further investigate solid-phase formation at interphases.

III.C.1 Introduction

This subsection provides highlights and progress on understanding the factors that limit the low-temperature performance of high-power Li-ion cells and identifying methods to enhance that performance via cell material and component changes. The limitations include possible Li plating on the negative electrode during charging and a major loss of discharge power ≤-10ºC. The latter

cannot be explained by the conductivity of the electrolyte. Efforts this year involved further studies to thoroughly characterize these limitations in the Gen 3 chemistry, isolating the source(s) of these issues, employing electrolyte modeling, evaluating alternative electrolyte salts and solvents, and developing a low-temperature cell transport model. Table III-7 provides a summary of how the participating DOE laboratories, together with ARL, contribute to this focus area.

Table III-7. Summary of how the DOE laboratories and the Army Research Laboratory contribute to the "Low-Temperature Performance" focus area.

	ANL	BNL	INL	LBNL	SNL	ARL
Characterize Gen 3 Cell Chemistry	X		X			
Reference Electrode Diagnostics	X	X				
Electrolyte Modeling			X			
Electrochemical Cell Modeling	X					
Evaluate Alternative Materials						X

III.C.2 Low-Temperature Performance Characterization

It was well established in last year's effort that the active material did not affect the low-temperature performance to any significant extent in the Gen 2 electrolyte. The electrolyte influence was explored this year with results summarized in Figure III-13 for three sets of electrodes. All of the electrolytes studied exhibited similar low temperature power loss with nearly identical activation energy. It appears that the low-temperature problem may be inherent to electrolytes based on EC or, perhaps, carbonate solvents in general. This will be explored further next year.

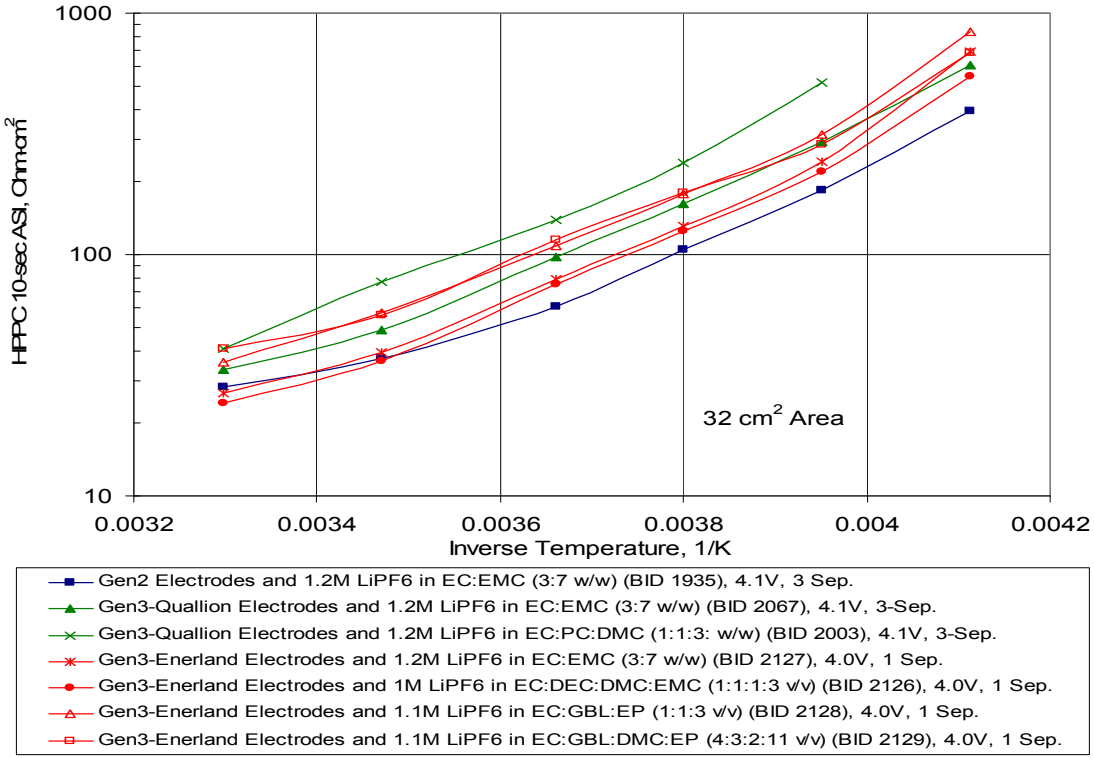

Figure III-13. HPPC ASI of various combinations of electrodes and electrolytes.

Salt molarity and temperature were found to have a significant influence on viscosity. An order of magnitude change in viscosity was measured by increasing the salt molarity from 0.6 to 1.8 moles/liter of $LiPF_6$ or by decreasing the temperature from 30°C to -30°C (Figure III-14). Despite such large changes in viscosity, the HPPC ASI of full cells made with 0.6, 1.2 and 1.8 M electrolytes changed very little. This reinforces the observation that the low-temperature power problem occurs at the electrode-electrolyte interface; viscosity is a bulk property and, hence, not likely to affect the interface.

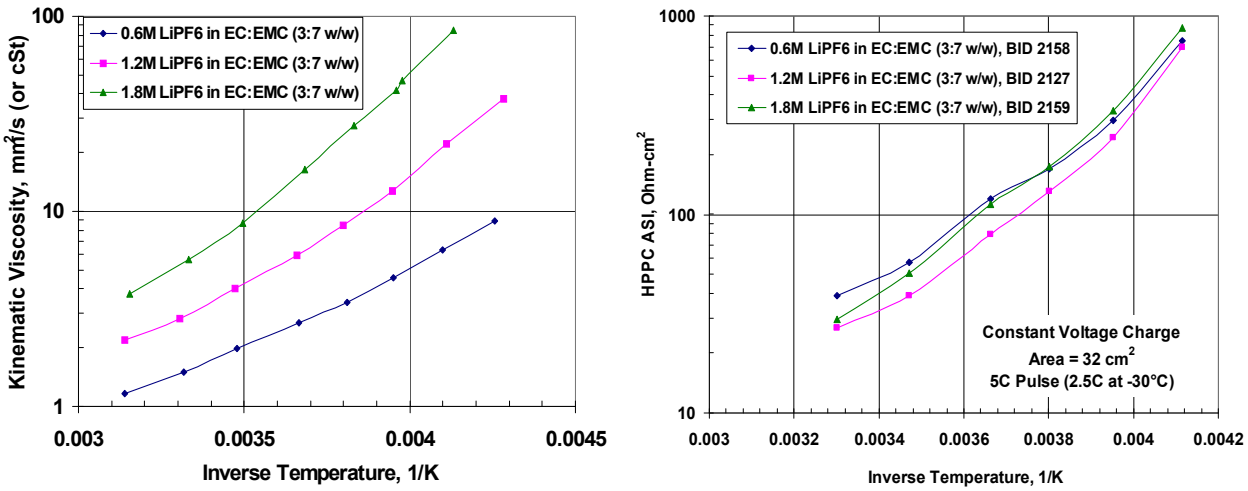

Figure III-14. Effect of salt molarity and temperature on kinematic viscosity and HPPC ASI.

Binder and Carbon Free (BCF) thin film electrodes were developed in this program to aid in diagnostic studies of Li-ion systems. These BCF cells also offer a unique perspective on the low-temperature studies of the electrode-electrolyte interface. Three cathode materials ($Li_{1.1}(Ni_{1/3}Co_{1/3}Mn_{1/3})_{0.9})_2$, $LiMn_2O_4$, and $Li_4Ti_5O_{12}$) were produced successfully as BCF thin film electrodes. BCF cells made with $Li_4Ti_5O_{12}$ electrodes are particularly interesting because of its stability to electrolytes (V_{OCV} = 1.55 V vs. Li), which creates a relatively "clean" interface.

The BCF thin film electrode experiments are typically conducted as half-cell studies using lithium as a counter electrode, which is unacceptable for low-temperature studies due to the instability of the lithium electrode. A lithium-preloaded Ti spinel composite (LTOc) electrode with low interfacial impedance (2 Ω-cm^2 at 30°C) was developed for use as a counter electrode. The interfacial impedance of the LTOc composite electrode was established using a symmetric LTOc composite electrode cell. The BCF thin film electrode's interfacial impedance was found by subtracting the LTOc composite electrode impedance from the total cell's interfacial impedance. Results (Figure III-15) were obtained at temperatures from 30°C to -30°C.

Attention should be directed to the slopes of the lines in Figure III-15, and not the magnitude of the resistances. Differences in R_w from one material to the next reflect differences in each electrode's electrochemically active area, which can only be estimated (Ti Spinel > Mn Spinel > Gen 3 Positive). The Gen 3 positive electrode also suffers from the fact that Li diffusion can only occur in two dimensions, while the spinels enable 3D Li diffusion. The interfacial impedance of all thin film BCF electrodes studied exhibit a strictly Arrhenius type behavior (*i.e.* no change in slope at 0°C). Like the data of Figure III-13, the interfacial impedance of all three BCF oxides studied had

similar activation energies (E_a). This further confirms the observation that the choice of active material has little influence on low-temperature performance.

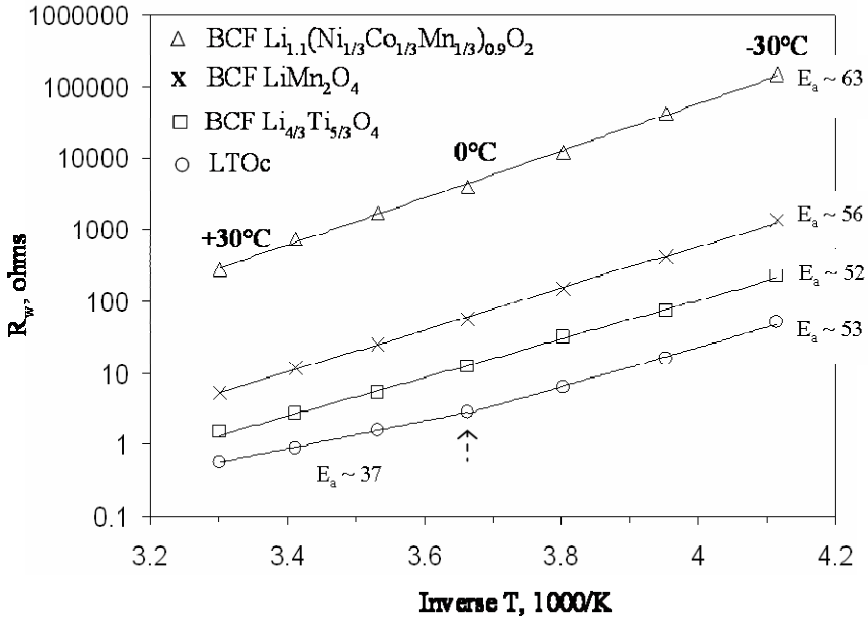

Figure III-15. Arrhenius plot showing R_w (real portion of resistance associated with mid-frequency arc) as a function of test temperature for BCF and LTOc electrodes. E_a in kJ/mole.

Note that the activation energy of the LTOc is nearly identical to the activation energy of the Ti spinel BCF electrode below 0°C. However, the activation energy for the LTOc electrode above 0°C is lower and indicates that an additional mechanism dominates in this region for composite electrodes but not for BCF electrodes. This suggests that the binder and carbon may play a significant role at room temperatures, but only a minor role at low temperature. All data to date confirm that the problem lies at the interface between the active material and the electrolyte.

III.C.3 Low Temperature Electrolyte Modeling

Based on FY 2005 ATD work and supporting literature, additional electrolyte systems were modeled relevant to ATD using the Advanced Electrolyte Model (AEM). These new systems typically involved the addition of one or more ester solvents to improve the overall transport performance at low temperatures. A comparison of the Gen 2 electrolyte (EC-EMC-$LiPF_6$) with two systems based on ethyl propionate (EP) was made, with results given in Figure III-16. The addition of EP can greatly improve electrolyte viscosity, conductivity, and diffusivity.

The AEM was also extended to model asymmetric electrolytes (where the cation and anion have disproportionate charges relative to each other), achieving excellent predictive accuracy for test cases involving an asymmetric Air Products salt. This advancement expands AEM capabilities to model many other electrolytes past the common 1:1 salt systems.

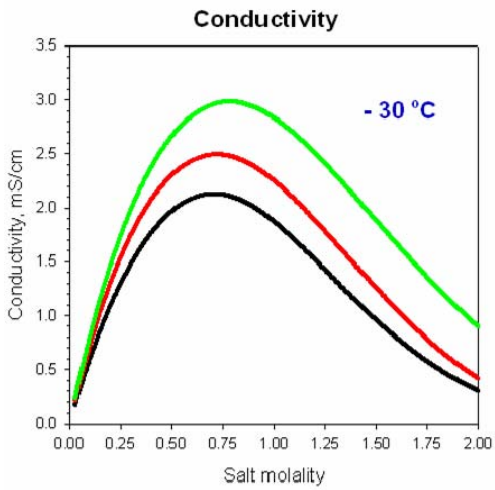

Figure III-16. Conductivity of Gen 2 and EP-amended electrolytes, top = EC-γBL-EP (1:1:3)+$LiPF_6$, middle = EC-EMC-EP-γBL (3:3:3:1)+ $LiPF_6$, bottom = EC-EMC (3:7)+ $LiPF_6$

Lastly, it has been reported that the addition of fluorinated solvents can improve the low-temperature cyclability of Li-ion cells. Solvents such as mono-fluoroethylene carbonate (mFEC) have shown a clear benefit when added in small amounts.[10] Preliminary AEM results indicate that mFEC does provide an advantage regarding Li desolvation energy and the time required for Li desolvation, but this benefit may be minimal for electrolyte solutions with low amounts of mFEC. In mFEC + salt electrolytes, modeling has shown that the activation energy required for the Li desolvation process is lower than for carbonate-based systems, which varies with temperature and salt concentration. This activation energy quantity is related to activation energies of charge transfer resistance measured in cells containing a given electrolyte. The solvent-to-Li binding energy and solvation numbers for mFEC determined by the AEM are generally 10-15% lower than for conventional solvents. These modeling results underscore the advantage mFEC provides in lowering the effective interaction between solvent and Li.

Evaluation of solid solvate formation – Gen 2 18650 baseline cells were used to investigate EIS-derived complex impedance profiles of cells that have undergone pulses (become polarized) just prior to EIS measurements, specifically at low temperatures. The results show a lower bulk electrolyte conductivity (by a small amount,) *indicating a possible phase transitions at the electrode-electrolyte interfaces.* The most plausible phases formed under discharge-driven concentration polarization include EC to its own solid phase (cathode side), and a solid solvate (anode side). Solid solvates are stable or metastable solvated salt complexes (macroscale) that can form under favorable thermodynamic conditions, especially at energy-lowering interfaces. Formation of such phases under low-temperature cycling would significantly decrease lithium transport through interfacial regions, and would explain the dramatic drop in performance at low temperatures for cells containing EC.

Based on this work, the AEM was expanded to evaluate the equilibrium constant for solid solvate species. An Arrhenius analysis of this quantity over several salt concentrations indicated

[10] N.-M. Choi et al., *J. Power Sources* (in press); T. Abe et al., *JECS.*, Vol. 152 (11), A2151-A2154 (2005)

inflection points where the equilibrium constant started to increase more at lower temperatures. A plot of these inflection points (Figure III-17) provides a thermodynamic contour that defines the probable region for the onset of solid solvates. The data in Figure III-17 is for the Gen 3 system EC-PC-DMC (1:1:3)-$LiPF_6$, and shows the general trend that solid solvate species will start to form at lowering salt concentrations as the temperature decreases. Also, the predicted contour temperature value at 1.2 molar salt is -13.9°C, which compares well with the ANL laboratory value of approximately -17°C.

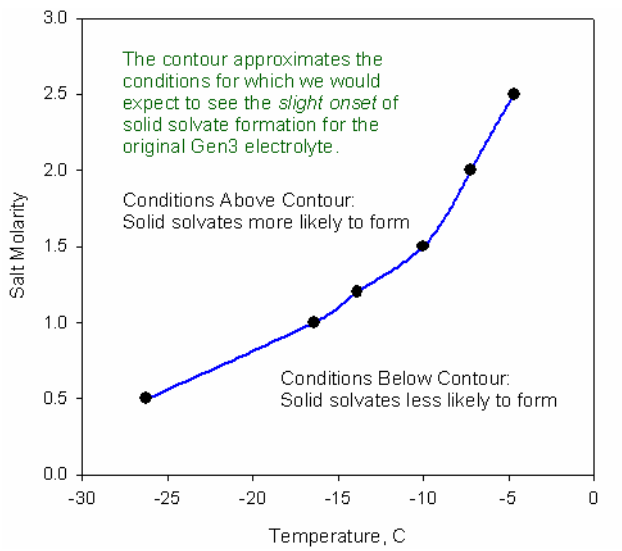

Figure III-17. AEM-derived thermodynamic contour for the onset of solid solvate formation within the Gen 3 electrolyte.

Lithium desolvation as a rate-driven process – Due to the nature of the ligand binding mechanism between polar solvents and Li, there is necessarily a *process* involved with desolvating a Li ion from its equilibrium solvated state to a bare ion prior to intercalation. A mechanistic model was developed based on a chemical kinetics framework that enables estimates of the net time required to desolvate a lithium ion ($\Delta t_{desolvate}$), given the electrolyte composition and temperature. In general, $\Delta t_{desolvate}$ is greater at lower temperatures and at lower salt concentrations, indicating that the desolvation process could become a problematic element in Li-ion cells at low temperatures where concentration polarization has produced a salt-depleted region (as will occur, for example, at cathode particle surfaces under discharge). Values for the net Li desolvation time are dependent on the choice of solvents, and most ATD-related electrolyte systems exhibit $\Delta t_{desolvate}$ ~5 to 20 nanoseconds. An excessively high desolvation time is detrimental and can act to increase the charge transfer resistance in Li-ion cells.

III.C.4 Low Temperature Cell Performance Modeling

The emphasis this year was focused on the Gen 3 cell technology and to determine the factors that contribute to the poor low-temperature performance of Li-ion cells. This year, particular importance was placed on the issue of Li plating on graphitic negative active materials during low-temperature charging. To accomplish this task, an effort was initiated to examine and modify the models previously developed in this program for the Gen 2 technology. One version of the model is used to simulate the cell response from AC impedance studies, and the other version is used for examining HPPC tests. Both of these experimental techniques are used extensively in the

program to quantify the cells' and its components' electrochemical performance. The underlying basis for both models is the same, as well as their parameter set.

The methodology for the model follows the work of Prof. Newman at LBNL. Concentrated solution theory is used to describe the transport of salt in the electrolyte. Volume- averaged transport equations account for the composite electrode geometry. Electrode kinetics, thermodynamics, and diffusion of Li in the oxide active particles are also included. The detailed theoretical description of the oxide active material SEI, is based on post-test analytical diagnostic studies. The SEI region is assumed to be a film on the oxide and an oxide layer at the surface of the oxide. The film on the oxide is taken to be an ill-defined mixture of organic and inorganic material through which Li ions from the electrolyte must diffuse and/or migrate to react electrochemically at the surface of the oxide. The Li is then assumed to diffuse through the oxide surface layer into the bulk oxide material. Capacitive effects are incorporated at the electrochemical interfaces and a localized electronic resistance between the current carrying carbon and the oxide interface can also be included.

A comparison of the Gen 2 and Gen 3 electrode active materials suggests that the electrochemical models developed for the Gen 2 cells would be directly applicable to the Gen 3 technology with only a change in parameter sets. Both positive active materials are layered transition metal oxides and the negatives are graphitic carbons. However, a close examination of the electrodes' AC impedance suggests that the Gen 3 positive electrodes' characteristic interfacial time constant is much greater than that for the Gen 2 positive electrode. The AC impedance model was easily able to handle this difference and estimation of the positive electrode interfacial parameters, as well as other model parameters, was initiated. The variations of electrode coatings of the Gen 3 technology offers an important opportunity to use the model to examine changes in coating thickness and loading, as well as more subtle changes in microstructure that may occur from different manufactures. However, the multiple electrode variations requires a unique parameter set for each electrode, and considering temperature and state-of-charge ranges, it soon becomes a huge effort to conduct these studies properly.

The slow interfacial time constant was much more problematic for the HPPC model. While the HPPC model is based on the same underlying assumptions as the AC impedance model, for numerical speed and simplicity the interfacial time constant was assumed to be relatively fast (*i.e.* the interfacial effects were assumed to be at steady-state). This was an excellent assumption for the Gen 2 positive electrode at room temperature, but not for the Gen 3 positive, and not for any Li-ion electrode at low temperature. A significant effort was undertaken to modify the HPPC model to properly account for the slower interfacial effects. This has resulted in an HPPC model with expanded capabilities, but with somewhat limited numerical stability. Further work is being conducted to improve the model's stability.

The greatest challenge this year has been to develop an electrochemical model applicable to the negative electrode. While both Gen 2 electrodes were simulated with the electrochemical cell models, the modeling effort concentrated on the positive electrode because of its importance in the cell's impedance rise. Similarities between the Gen 2 and Gen 3 negative electrodes suggest that all the previous questions concerning the modeling of the negative electrode have carried over to the new technology. Analysis of the negative electrode observations indicate two possible issues

that are not properly accounted for in the previous model. First, it is not clear that the interfacial phenomena are being accurately described. Second, intercalation of Li into the graphite may be occurring through a two-phase process, as opposed to single phase diffusion assumed in the model. Understanding both these issues requires the separation of interfacial and bulk active material phenomena. To accomplish this task a combined theoretical and experimental effort was initiated to examine the intercalation of Li into the active material using an established electrochemical titration technique (GITT).

The existing analytical GITT theory was expanded using an electrochemical model to account for electrolyte and counter electrode effects, as well as particle diffusion and the porous electrode geometry. A series of experiments with a Gen 2 positive electrode exhibited the importance of using a reference electrode in the cell and relevance of this technique to elucidating the bulk active material diffusion process. After success with the positive electrode, the emphasis has switched to the Gen 3 negative electrode. An experimental investigation of the negative electrode is underway and the model is being modified to allow for the possibility of phase change during the charge/discharge process. Once the active particle diffusion effects have been quantified, the AC impedance model can be modified to elucidate the interfacial phenomena.

III.D Understand and Enhance Abuse Tolerance

OBJECTIVES

- Understand cell component roles in the abuse characteristics of high-power Li-ion cells.
- Identify and develop more stable cell components that enhance the inherent abuse tolerance of Li-Ion cells.
- Validate inherent abuse tolerance enhancements at the cell level and quantify them.

APPROACH

- Use accelerated rate calorimetry (ARC) and differential scanning calorimetry (DSC) to identify the role of each cell component on the thermal characteristics of the Gen 3 and other cell chemistries.
- Identify methods to enhance overcharge and thermal abuse tolerance and evaluate them in 18650 cells.
- Fabricate 110 mAh sealed prismatic cells and 18650 cells with the most promising cell components and additives to validate and quantify respective enhancements.

ACCOMPLISHMENTS/FINDINGS

- Heat observed below 180ºC due to continuous breakdown and formation of the anode SEI may initiate thermal runaway of the cell. This heat could be reduced through use of:
    - Low surface area round edge carbon, and
    - Additives that form a more stable SEI.
- $Li_4Ti_5O_{12}$ anode shows no heat generation below 200ºC.
- The entropy change of $Li_4Ti_5O_{12}$ during cycling is 10 times lower than that of MCMB graphite, indicating a much better thermal stability.
- The oxidation of the electrolyte due to O_2 release from the cathode is the main cause of thermal runaway in many cathodes.
- Spinel and olivine cathodes show by far the best thermal abuse response.
- Gen 2 and $LiFePO_4$ cathodes show significant heat during cycling, specifically at the end of charge and discharge.
- Electrolyte additives can reduce reactivity and gas phase flammability.
- Separator breakdown can result after shutdown and is dependent on temperature above shutdown, voltage applied to cell, and time duration of applied voltage.
- Non-shutdown separators may give enhanced abuse tolerance for cell strings and modules.
- Anode reactivity is of equal magnitude compared to the new stabilized NMC ($Li_{1.1}(Ni1_{/3}Co_{1/3}Mn_{1/}3)_{0.9}O_2$] cathodes.
- The NMC cathode shows improved overcharge tolerance compared to NCA ($LiNi_{1/3}Co_{1/3}Mn_{1/3}O_2$) cathodes.
- Improved the fidelity of Li-ion thermal abuse model based on measured cell reactions.

FUTURE STUDIES

- Investigate the reason behind the large heat observed at the end of charge and discharge of the olivine cell. Carry out similar study for Mn-spinel and Gen 3 cathode.
- Demonstrate the effect of the use of low surface area carbon and electrolyte additives on the 18650 Gen 3 cell's thermal abuse.

Thermal Abuse

- Investigate the thermal abuse characteristics of 18650 Mn-Spinel/$Li_4Ti_5O_{12}$ cells and compare to the other systems.
- Determine the benefit of shutdown separators on thermal abuse tolerance.
- Determine effect of solvent composition on thermal stability.
- Demonstrate improved abuse response with more stable anode materials.
- Develop thermal reaction parameters for cell components for a wide range of chemistries.
- Further develop Thermal Abuse Model to more accurately predict cell thermal response.

Overcharge Response

- Measure effect of improved shutdown separators on overcharge response.
- Investigate reactivity of overcharged electrodes at regions of reaction and thermal runaway.
- Determine effect of alternative electrolytes on overcharge response and gas generation.
- Determine effect of newly developed redox shuttle on the overcharge response of Li-ion cells
- Perform diagnostic studies of overcharge samples.

III.D.1 Introduction

This subsection provides highlights and progress on understanding the factors that limit the inherent abuse tolerance of high-power Li-ion cell chemistries and using this knowledge to identify alternative materials and cell components that enhance their abuse tolerance. The cell chemistries used in conventional Li-ion cells are thermodynamically unstable. During the initial charge/discharge cycle, passivation films are formed on the active surfaces of the electrodes which stabilize the system. Detailed studies have been performed on the individual components of the Gen 3 cell and the cell chemistry system was thoroughly studied in terms of its thermal and overcharge abuse characteristics. Also, an effort was continued to model the abuse behavior of 18650 cells, employing different materials and cell chemistries, with the goal of predicting the behavior of full-size HEV cells. Table III-8 provides a summary of how the DOE laboratories contribute to this focus area.

Table III-8. Summary of how the DOE laboratories contribute to the "Abuse Tolerance" focus area.

	ANL	BNL	INL	LBNL	SNL
DSC and ARC on Advanced Materials	X				
ARC and Thermal Block Tests on 18650 Cells					X
Overcharge Tests with Advanced Materials					X
Diagnostics on Abused Cell Materials and Components	X	X			X
Model 18650 Cell Behavior					X

III.D.2 Thermal Abuse

III.D.2.1 Component-Level Studies

Li-ion batteries used for high-power applications are expected to encounter significant temperature excursions during power pulse discharge. Consequently, the critical challenge in designing a high energy/power Li-ion battery is its safety under normal cell conditions as well as under abusive conditions. Under abusive conditions (including internal shorts), Li-ion cells may

undergo thermal runaway producing high temperatures, smoke, and sometimes explosion and fire. For example, under high rate discharge or pulse power discharge, the large exothermic chemical processes may cause heat to accumulate inside the battery if the heat transfer to the surrounding is not efficient. This in turn may create "hot spots' within the battery which may result in thermal runaway. There are a number of exothermic chemical reactions that contribute to thermal runaway. The most important reactions are believed to involve the reaction of cathode and anode with the electrolyte and thermal decomposition of salts. Therefore, the safe use of high power Li-ion batteries requires better understanding of the abuse tolerance of the cell components at higher operating temperatures, including the stability limits of the electrolyte.

In this section is reported the investigation of the impact of the cathode, and anode on the thermal behavior of Li- ion batteries. ARC, isothermal microcalorimeter (IMC), and DSC were used to investigate the performance of Li-ion cell components at elevated temperature, including thermal stability and thermal runaway as a function of temperature and SOC. These studies were focused on studying the thermal effects in normal and abusive conditions and understanding the thermal behavior at a level to allow conclusions for diagnostics and design.

Thermal behavior of the carbon anode – Figure III-18 shows the DSC of fully lithiated MCMB-10-28 in the presence of 1.2M$LiPF_6$/EC:EMC (3:7). The figure shows an early initiation of heat with an onset temperature of ~70ºC caused by the breakdown of the SEI at the anode surface. Once the SEI film is broken down, a continuous heat was observed up to 200ºC.

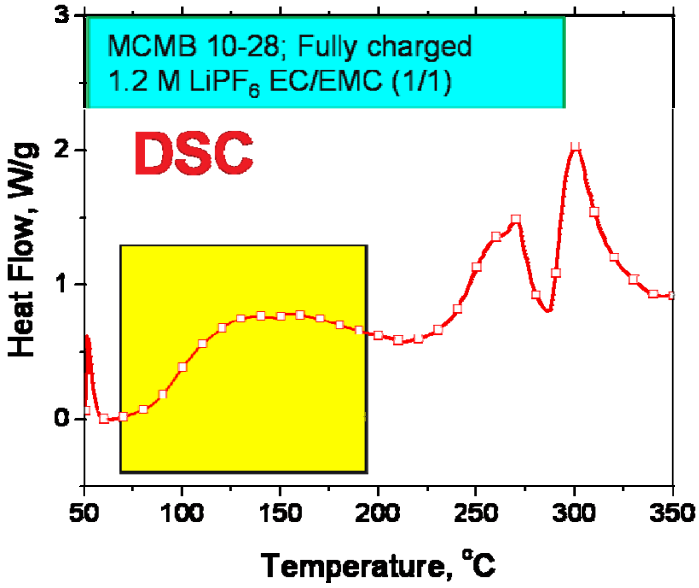

Figure III-18. DSC of fully lithiated MCMB-10-28

The energy involved with this heat was calculated from the total heat of a sample that has been subjected to a full DSC scan and another sample that has been preheated in a separate furnace to 200ºC, and then further tested using DSC. The amount of heat generated from this broad DSC thermal signature between 70 and 200ºC is ~507 J/g (Figure III-19), which may be enough to cause a safety hazard, especially for large batteries that use large quantities of carbon anode. The main reason behind this continuous heat is once the SEI film is broken down, Li inside the carbon is

deintercalated, reacts at the surface with the electrolyte and forms a secondary passivation film. This new film is decomposed with the increase in the temperature of the DSC resulting in further heat generation. This continuous formation and breakdown of the secondary SEI continuous until the amount of Li inside the carbon becomes small and no deintercalation of Li takes place. Since this early heat is associated with the continuous formation and breakdown of the SEI, the intensity of the heat associated with this broad DSC thermal signature will depend on the surface area of the carbon used in the cell.

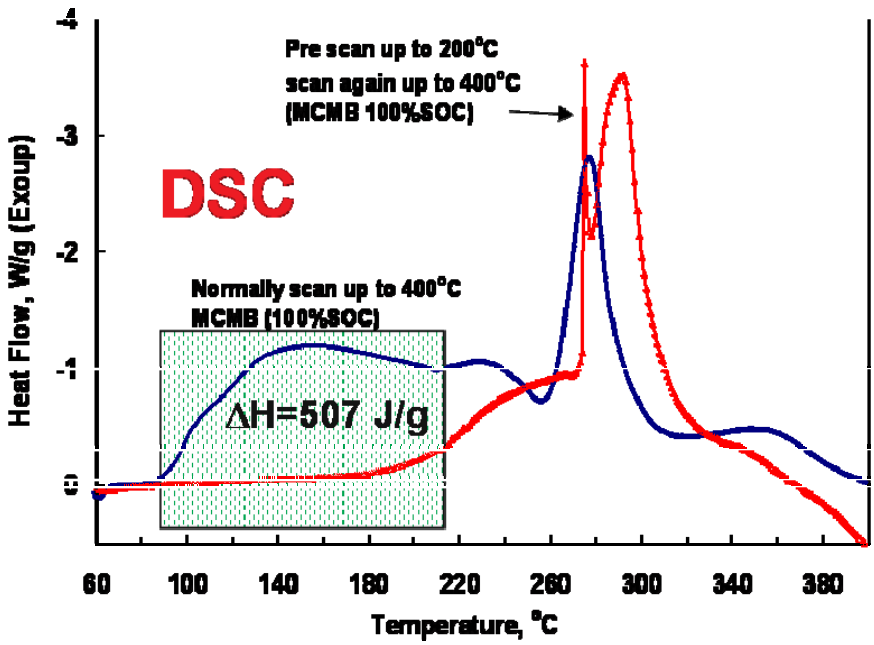

Figure III-19. DSC of two lithiated MCMB carbons. One fully scanned using DSC and one preheated to 200ºC and then scanned by DSC.

Figure III-20 shows the exothermic heat from the continuous formation and breakdown of the SEI using two different carbons (MCMB from Osaka Gas & MAG 10 from Hitachi Chemical) with different surface areas. The MCMB carbon with 2.2m^2/g surface area shows almost half of the heat generated from the MAG-10 which has 5.2m^2/g surface area. Therefore, one possible way of reducing the early heat from the carbon is to select a carbon with low surface area. It should be noted that the heat generated beginning at 70ºC could accelerated other reactions in the cell, such as the cathode decomposition, which can lead to thermal run away of the cell. Another way of delaying this type of reactions is to use a functional additive that can form a more stable SEI at the carbon surface which would resist the early breakdown and heat generation.

Figure III-21 shows the accumulated heat with increasing temperature of lithiated MCMB carbon using 1.2M$LiPF_6$/EC:PC:DMC(1:1:3), the same electrolyte+1wt% vinylene carbonate (VC) additive and then the same electrolyte + 1wt% LiBOB. VC and LiBOB are known to form a stable passivation film that protects the carbon interface from reaction with the electrolyte even at high temperatures. In the case of LiBOB additive, the breakdown of the SEI film takes place at 120ºC resulting in much lower overall accumulated heat of the cell. The VEC additive shows a breakdown onset temperature at 100ºC which also results in lower accumulated heat compared with a cell with no additive.

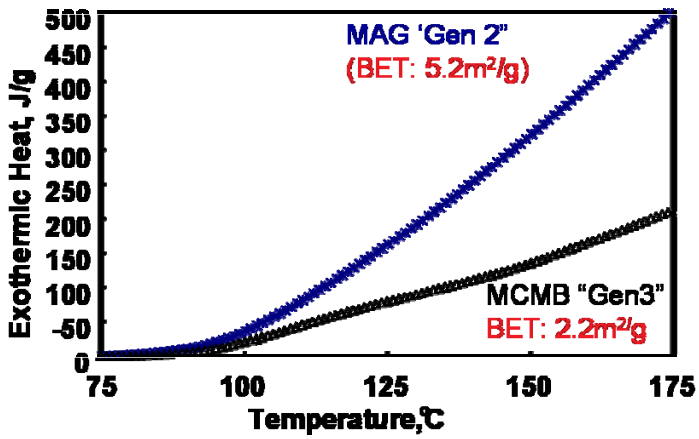

Figure III-20. Accumulated heat from 75°C to 175°C caused by the continuous formation and breakdown of two different carbons with two different surface areas.

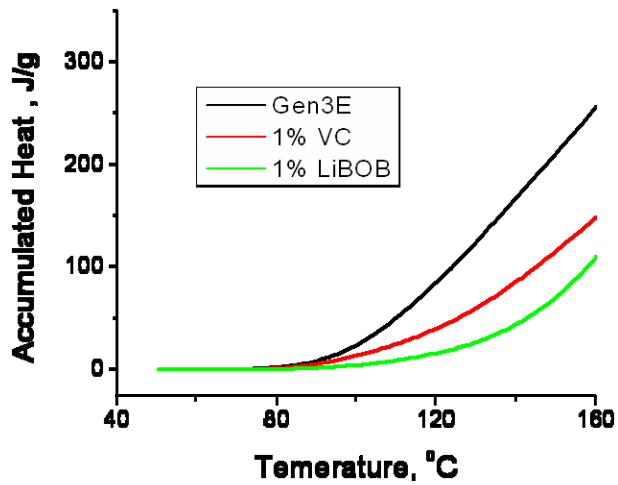

Figure III-21. Accumulated heat of lithiated MCMB -10-28 carbon with 1wt%VEC, 1wt%LiBoB and without additive. Electrolyte used is 1.2M$LiPF_6$/EC:PC:DMC(1:1:3) (Gen3E).

Thermal behavior of different cathode materials – ATD has been investigating several cathode materials that offer outstanding power capability and have the potential of being used in HEV batteries, including $LiNi_{0.8}Co_{0.15}Al_{0.05}O_2$, $Li_{1+x}(Mn_{1/3}Co_{1/3}Ni_{1/3})_{1-x}O_2$, $Li_{1+x}Mn_{2-x}O_4$ and $LiFePO_4$. One of the concerns is that most of these oxides, when delithiated, can readily reduce and generate oxygen that can react with other cell component leading to the thermal runaway of the cell.

Figure III-22 shows the ARC test of fully charged 18650 cells having similar carbon but different cathode materials. The capacity of the cell is 0.9Ah, therefore, the effect of carbon on the heat generation is relatively small. The cell with $LiNi_{0.8}Co_{0.15}Al_{0.05}O_2$ shows significant heat generation with the onset temperature ~200°C. The $Li_{1+x}(Mn_{1/3}Co_{1/3}Ni_{1/3})_{1-x}O_2$ material exhibits better stability because of the stabilizing effect of the Mn and Co on the structure, this material shows 1/10 the heat generation of $LiNi_{0.8}Co_{0.15}Al_{0.05}O_2$.

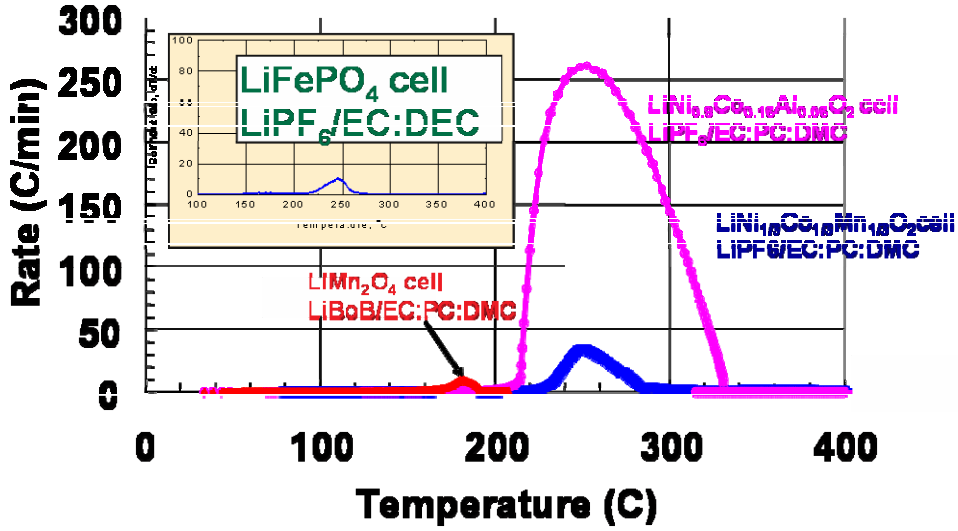

Figure III-22. ARC test of 18650 cell having similar carbon and different cathode materials

To understand the reason behind this significant improvement in the safety of Gen 3 compared to Gen 2, layered $Li_{0.45}(Ni_{0.8}Co_{0.15}Al_{0.05})O_2$ and $Li_{0.55}(Ni_{1/3}Co_{1/3}Mn_{1/3})O_2$ powder materials were prepared from $Li(Ni_{0.8}Co_{0.15}Al_{0.05})O_2$ and $Li(Ni_{1/3}Co_{1/3}Mn_{1/3})O$, respectively, by a chemical delithiation method using NO_2BF_4 oxidizer in an ACN medium. The thermal degradation of these deintercalated powders was studied using thermal gravimetric analysis (TGA) (Figure III-23).

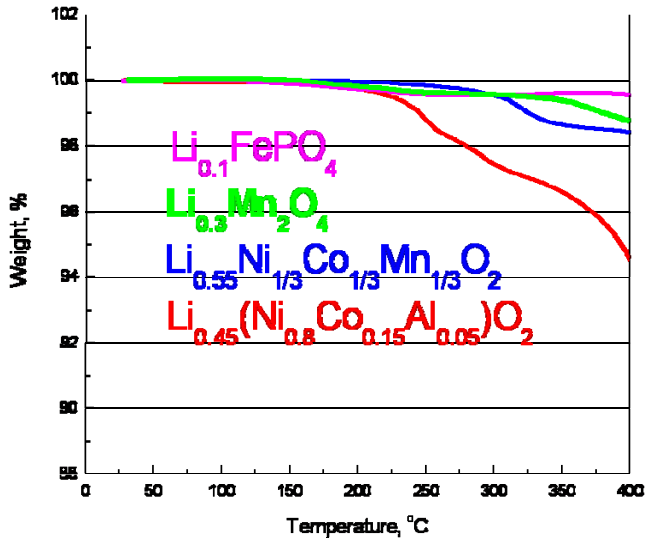

Figure III-23. TGA, conducted under purified air atmosphere, of the $Li_{0.45}(Ni_{0.8}Co_{0.15}Al_{0.05})O_2$ and $Li_{0.55}(Ni_{1/3}Co_{1/3}Mn_{1/3})O_2$ delithiated cathode

In the case of $Li_{0.45}(Ni_{0.8}Co_{0.15}Al_{0.05})O_2$, significant O_2 loss was observed starting at ~200ºC which is the same temperature as the onset temperature of reaction observed by the ARC test. The oxygen release from the cathode reacts exothermically with the electrolyte resulting in the large observed heat for this system.

However, $Li_{0.55}(Ni_{1/3}Co_{1/3}Mn_{1/3})O_2$ does show a small amount of oxygen release near 250ºC which explains the reactivity with the electrolyte and the delayed reaction observed in the ARC test. This result confirms that oxide cathodes that generate the least oxygen should exhibit enhanced abuse tolerance since the major reaction of the cell is the oxidation of the electrolyte. $Li_{1+x}Mn_{2-x}O_4$, which generates a very small amount of oxygen, and $LiFePO_4$ olivine, which doesn't generate any oxygen, provide by far the least heat in the cell as shown in Figure III-22.

Figure III-24 shows the heat profile for Li/Gen 2 (+), Li/Gen 3(+), Li/$Li_{1+x}Mn_{2-x}O_4$ and Li/ $LiFePO_4$ during the charge and discharge process. The heat flow rate of these cells was obtained using the IMC and consists of the reversible heat (q_{rev}) and irreversible heat (q_{irr}) according to the energy balance equation:

$$q = |i\eta| + (-iT\left(\frac{\partial E}{\partial T}\right)_P) \qquad [1]$$

Where: q stands for the heat rate of the cell, which is positive when the cell generates heat; i, the current, is positive during the cathodic reaction process; T the cell temperature (K), is constant during the IMC experiment; P the pressure in the half cell, which is considered constant; E is the cell potential during cycling; and η is the over-potential, whish is the voltage difference between the end of pulse charge and the end of one hour current interruption in this study. Since q_{irr} can be determined from the over-potential and the total heat flow can be obtained from IMC, the entropy change (dE/dT) can be calculated using this equation. Figure III-24 shows that as expected, Li/Gen 2(+) shows continuous heat during both charge and discharge with significantly more heat occurring at the end of the discharge.

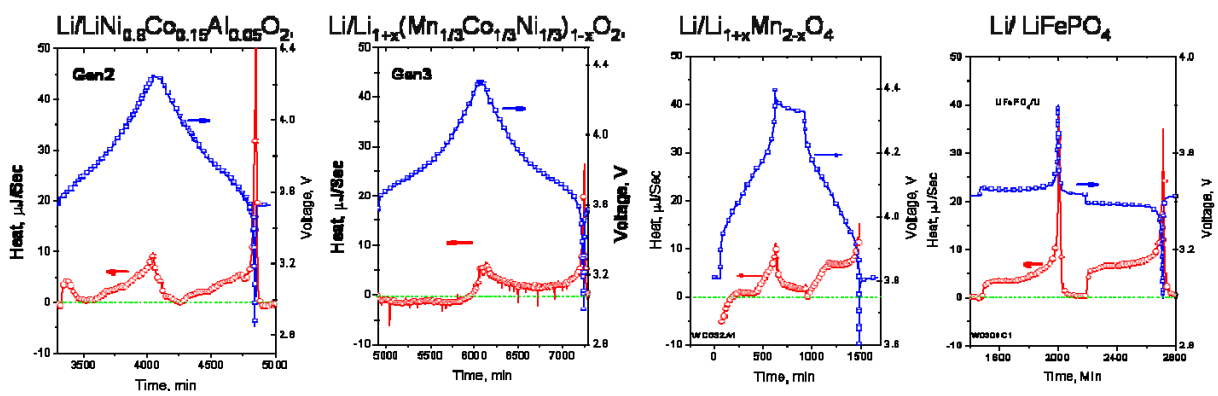

Figure III-24. Heat profile from the isothermal microcalorimeter for Gen 2, Gen 3, a spinel and an iron phosphate cathode during the charge and discharge process

Li/Gen 3(+) shows no heat generation during charge or discharge and only small heat at the end of discharge. The spinel cell shows an endothermic heat at the beginning of the charge and no heat during the charging process until the end of charge where a very small heat is observed. The same phenomenon happens during the charge process. The olivine however, shows a surprising result with a behavior similar to that of Li/Gen 2(+). In this case, the cell shows continues heat generation during both the charge and discharge process with significant heat taking place both at the end of charge and discharge.

This result indicates that the $LiFePO_4$/carbon cell is expected to generate significant heat when charged or discharge at high rate. Heat sensing infrared camera tests on commercial olivine cells

designed for power application shows that the cell temperature could reach approximately 70ºC when discharged at 13C rate.

III.D.2.2 Cell-Level Studies

This program has demonstrated significantly improved abuse tolerance in 18650 size cells (constructed at SNL) using stabilized cathodes in combination with different electrolyte/solvent components. New materials evaluated have included stabilized cathodes, anodes, electrolytes and electrolyte additives. The thermal properties of these materials have been characterized and used to determine the effect on full cell abuse response including heat generation, gas generation and flammability. The major cell chemistries and components evaluated were:

- Gen 2: Cathode – $LiNi_{0.8}Co_{0.15}Al_{0.05}O_2$ (NCA); Anode – 6%GDR,
- Gen 3: Cathode – $Li_{1.0}Ni_{1/3}Co_{1/3}Mn_{1/3}O_2$ (NMC); Anode – 6%GDR,
- Gen 3: Cathode – $Li_{1.1}(Ni_{1/3}Co_{1/3}Mn_{1/3})_{0.9}O_2$; Anode – MCMB,
    - Electrolyte: EC:EMC/1.2M $LiPF_6$; EC:PC:DMC/1.2M $LiPF_6$,
    - Additives: SEI enhancer –VEC, Flame retardant – "Phoslyte B and C",
    - Separators: Celgard2325, Separion®,

ARC Study – 18650 cells with 950 mAh nominal capacities were built using these chemistries for abuse measurements. ARC measurements allowed comparison of the heat generation enthalpies and reaction kinetics as well as the gas evolution profiles. Measurements were performed on full cells and also on complete cell electrodes removed from fully charged cells and resealed in 18650 cans. These measurements have allowed determination of the relative contributions of the anode and cathode to the full cell heat and gas generation.

The new stabilized Gen 3 $Li_{1.1}(Ni_{1/3}Co_{1/3}Mn_{1/3})_{0.9}O_2$ showed further improvement in thermal stability over the previous $Li_{1.0}Ni_{1/3}Co_{1/3}Mn_{1/3}O_2$ cathode material which showed significant improvement over the Gen 2 material. Figure III-25 shows higher thermal runaway onset temperature, lower peak heating rate and reduced enthalpy of reaction for this new chemistry.

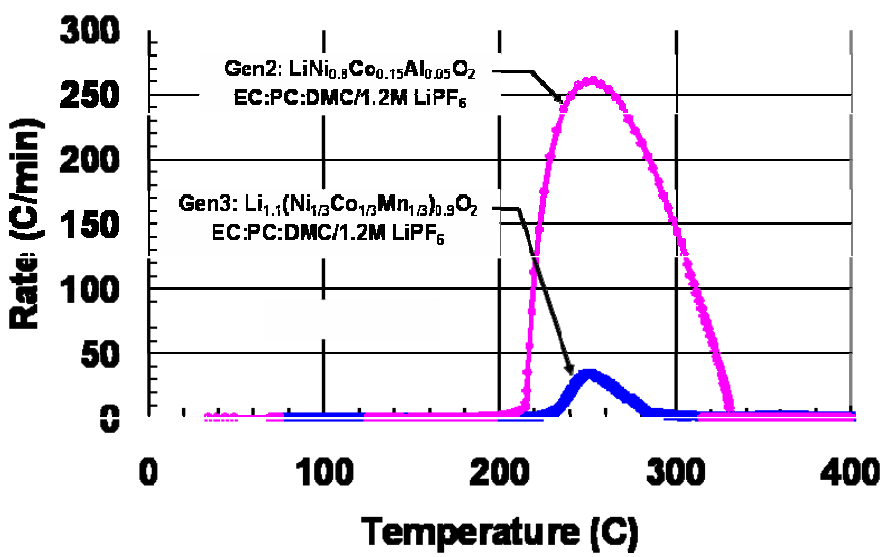

Figure III-25. ARC heating rates for stabilized Gen 3 cathode materials compared to Gen 2 baseline cell.

Initial measurements (Figure III-26) have shown reduced thermal runaway energies for electrolytes with EC:PC:DMC (1:1:3) solvents compared to EC:EMC (3:7). Similar reductions in peak heating rates were also seen for the Gen 2 NCA material but not to the same extent as seen for the Gen 3 NMC cathodes. Optimized cell abuse tolerance must consider interactions between all cell components.

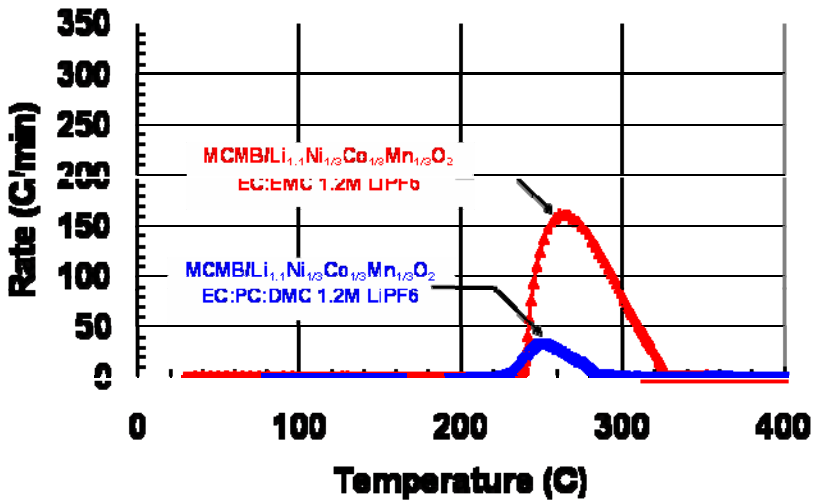

Figure III-26. ARC heating rates for Gen 3 cells with EC:EMC or EC:PC:DMC based electrolytes.

The relative contributions of the Gen 3 MCMB anode and NMC cathode electrodes to full cell thermal runaway were determined by disassembling a charged Gen 3 18650 cell and re-sealing the individual electrodes/electrolyte in 18650 cans. ARC runs shown in Figure III-27 clearly reveal that the reduced NMC cathode reactions are now comparable to the anode reactions and the full cell response is equal to the sum of the two electrode components. Further cell improvements must also be accompanied by reduced anode reactions.

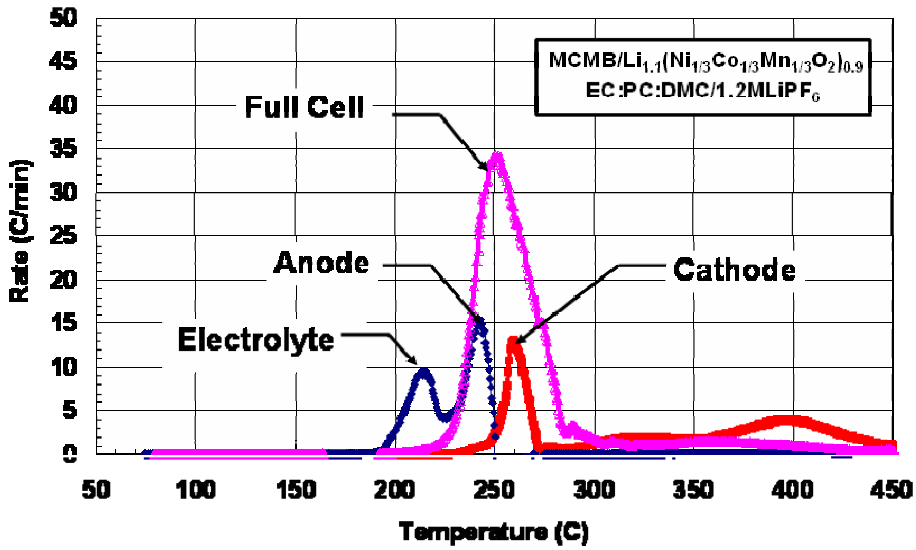

Figure III-27. ARC profiles of full Gen 3 cell compared with individual electrodes and electrolyte.

Gas generated by the cell components during thermal runaway was equal to that from anode and cathode accounting for the total volume of gas from the full cell. Gas evolution begins around 150°C corresponding to the thermal breakdown temperature of the electrolyte (Figure III-28).

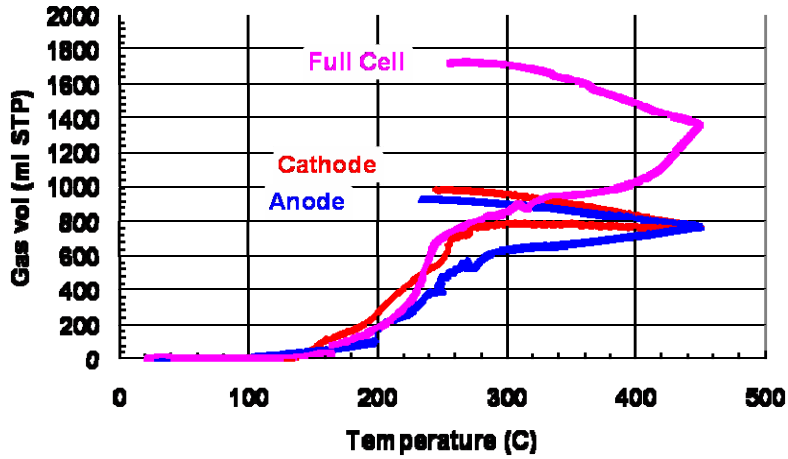

Figure III-28. Gas generation of Gen 3 cell and electrodes during thermal runaway and cool down.

The high-rate cathode reaction is believed to come from solvent combustion by oxygen released by the cathode. TGA measurements of cathode materials have shown that the mass loss is a function of the degree of lithiation and is given by:

$$Li_yMO_2 \rightarrow (1+y)\,Li_{\frac{y}{1+y}}\,M_{\frac{1}{1+y}}\,O + \frac{1-y}{2}O_2$$

The rate of the thermal runaway will be affected by the kinetics of this decomposition reaction. TGA scans show that the Gen 2 NCA cathode has very high kinetics indicated by the overlapping TGA curves with increasing scan rate (Figure III-29, left). These cells have shown rapid disassembly during runaway. The TGA curves for the Gen 3 NMC cathode material are shown in Figure III-29 (right) and indicate that the decomposition kinetics are slower. Thermal runaway for these cells were seen to be less energetic without cell disassembly.

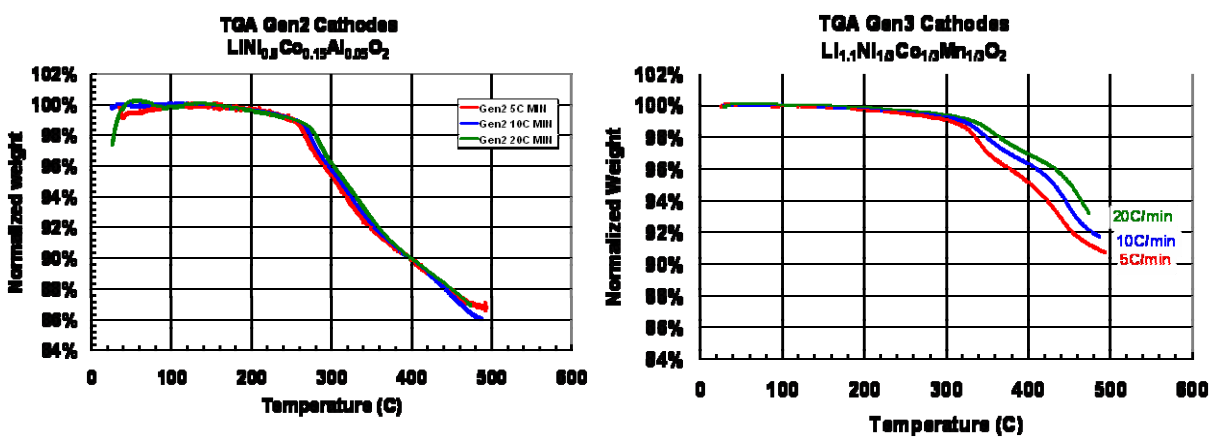

Figure III-29. TGA profile of Gen 2 (left) and Gen 3 (right) cathodes with increasing scan rate showing high-rate (left) and lower rate (right) kinetics.

Thermal Ramp Response/Flammability Study – The thermal abuse response of these cells and the flammability of the vented gases were measured using a thermal block apparatus developed at SNL that allows determination of the onset of cell heat generation and also records the flammability of the vented gases/electrolyte in the presence of an external ignition source. Cells were ramped in open air at a rate of 6˚C/min until thermal runaway.

The thermal ramp of a cell with the stabilized $Li_{1.1}(Ni_{1/3}Co_{1/3}Mn_{1/3})_{0.9}O_2$ cathode showed a lower self-generated heating rate between the 140°C onset temperature and the 190°C runaway temperature compared to the early non-stabilized NMC cells (Figure III-30). Cell venting was seen to be more benign and low-rate, reflecting the reduced reaction kinetics of these cathodes.

The thermal abuse tolerance of these stabilized Gen 3 cells was improved even further using electrolyte additives. VEC was used to improve the protective SEI layer on the anode which delayed the onset of the anode reactions. Fire retardant additives not only reduced the flammability of the vent gases but also helped passivate the electrode surfaces. The effects of these additives (VEC/Phoslyte B) are shown in Figure III-31. The thermal runaway temperature for this cathode material with these two additives increased by about 25°C. The flammability of the vapors was also reduced although the liquid electrolyte at the cell vent still burned at a low rate.

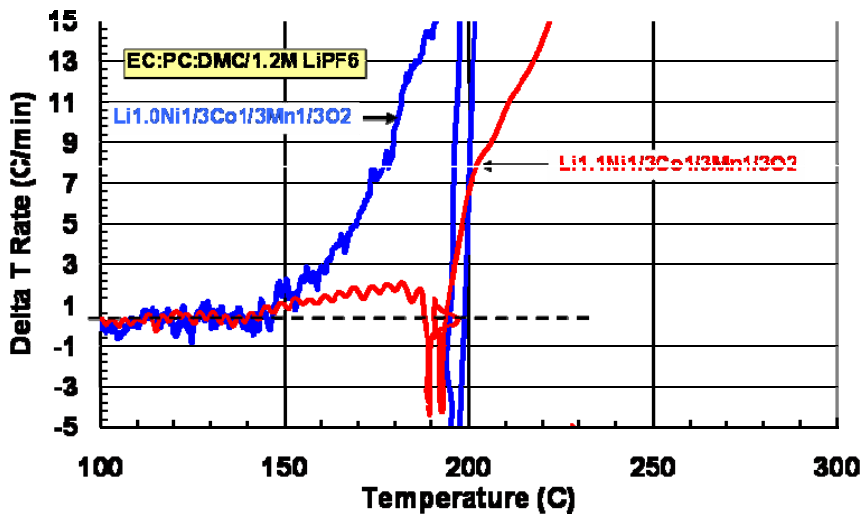

Figure III-30. Thermal ramp profile comparing cells with Gen 3 cathodes and stabilized Gen 3 cathodes.

Thermal Abuse Modeling - A thermal abuse model has been developed in collaboration with Battery Design Co. as part of the Battery Design Studio® cell design program. This model is based on cell construction parameters and material properties to simulate the thermal response profiles for ARC, DSC and Thermal Ramp. Cell properties can be entered into the model or the program can determine these values as best fits to the data. Arrhenius-based thermal reaction terms are used with generalized reaction order expressions to model anode, cathode and electrolyte decomposition reactions.

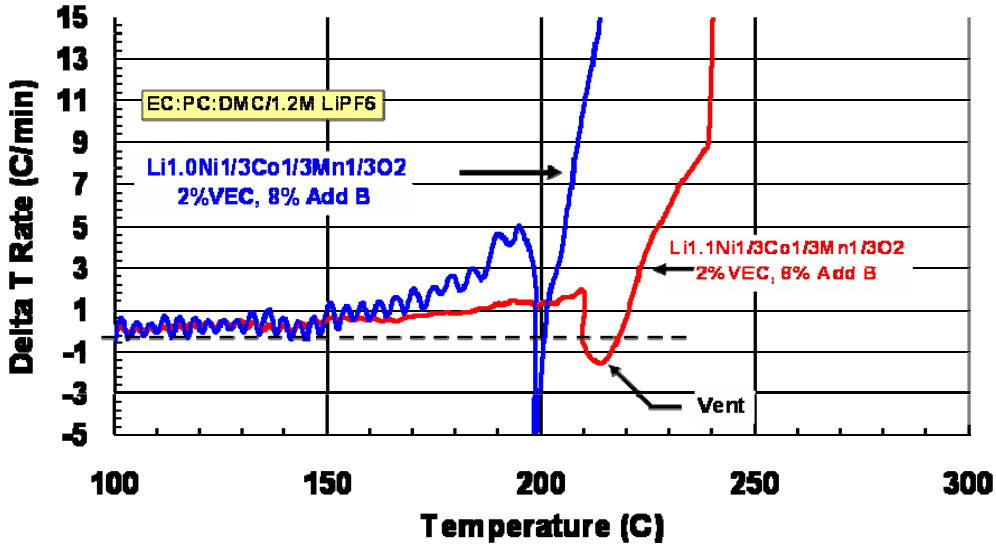

Figure III-31. Thermal ramp profile comparing cells with normal and stabilized Gen 3 cathodes with SEI and flame retardant additives.

An example of a generalized cathode rate expression is (α is degree of conversion):

$$R = k\exp\left[\frac{-E_a}{RT}\right]\alpha_{pos}^{m}\left(1-\alpha_{pos}\right)^{n}\left[-\ln\left(1-\alpha_{pos}\right)\right]^{p}c_{solvent}^{r}$$

This model has successfully simulated measurements using a consistent set of material reaction parameters. A two-step cathode reaction with the electrolyte was found to determine the cell response: an initial Arrhenius-type surface reaction with the electrolyte followed by the cathode decomposition/solvent combustion reaction. Figure III-32 (left) shows the fit of the model to experimental Gen 2 cell ARC data using the initial cathode surface/electrolyte reaction. At the end of this reaction temperature regime the cathode decomposition reaction dominates and drives the cell into the peak runaway regime. The model fit to this reaction used a function based on the measured TGA curves and closely fit the peak runaway profile, Figure III-32 (right). The model can closely simulate actual experimental data and will be very useful for predicting larger cell performance using these values.

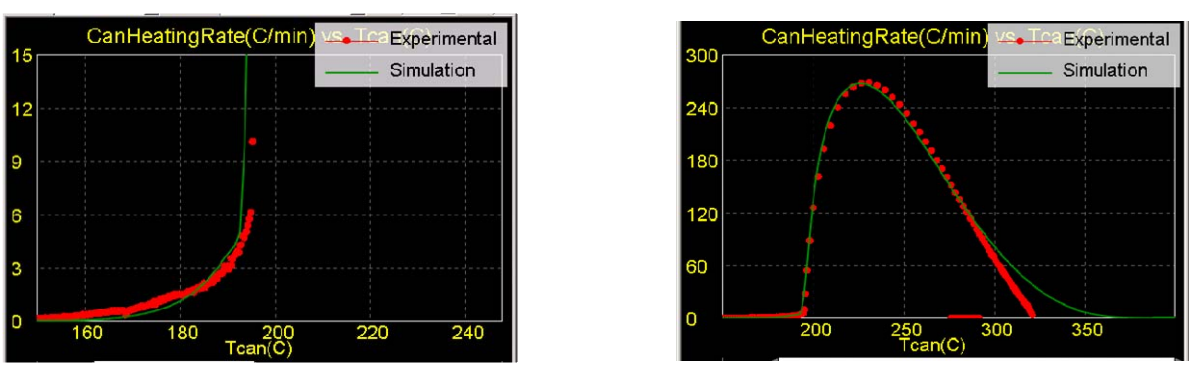

Figure III-32. Model simulation results compared with experimental ARC data for Gen 2 cathode material showing onset reactions (left), and peak thermal runaway reactions (right) .

III.D.3 Overcharge Abuse

The goal of this work is to determine the effects of overcharge and thermal decomposition leading to cell thermal runaway. Overcharge studies have been performed using a custom apparatus designed to allow quantitative measurements of the heat generation of the cells during overcharge and simultaneous real-time gas monitoring. It has been previously demonstrated that high-rate overcharge can lead to thermal runaway. It was also found that, for extended overcharges at low rates, thermal runaway does not automatically occur for Gen 2 and Gen 3 based cells as long as the cell temperature remains below the separator melt temperature (135ºC). Overcharge response was seen to be largely a thermal reaction often resulting from failure of the separator leading to internal shorts. The high-temperature material-based thermal response during overcharge was demonstrated using cells with a non-shutdown separator that eventually reached the runaway temperature of the cathode material. This resulted only after extensive overcharging with low heat removal from the cell.

The effect of increasing cell capacity on overcharge response was measured using Gen 2 NCA cells with capacities of 1 Ah and 1.4 Ah but identical cell configurations. Charging was performed at a 1C rate for each cell. Figure III-33 shows that the two different capacity cells had the same temperature response up to about 130% SOC but the higher capacity 1.4 Ah cell then began to heat more rapidly, going into runaway sooner at a lower SOC. The cells went into runaway after the internal temperature reached the separator shutdown temperature followed by separator failure. This heating began after depletion of the cathode Li level and resulted from internal ohmic heating. The higher capacity cell had higher current levels and thus higher heating rates. Overcharge in high-capacity cells may be more problematic.

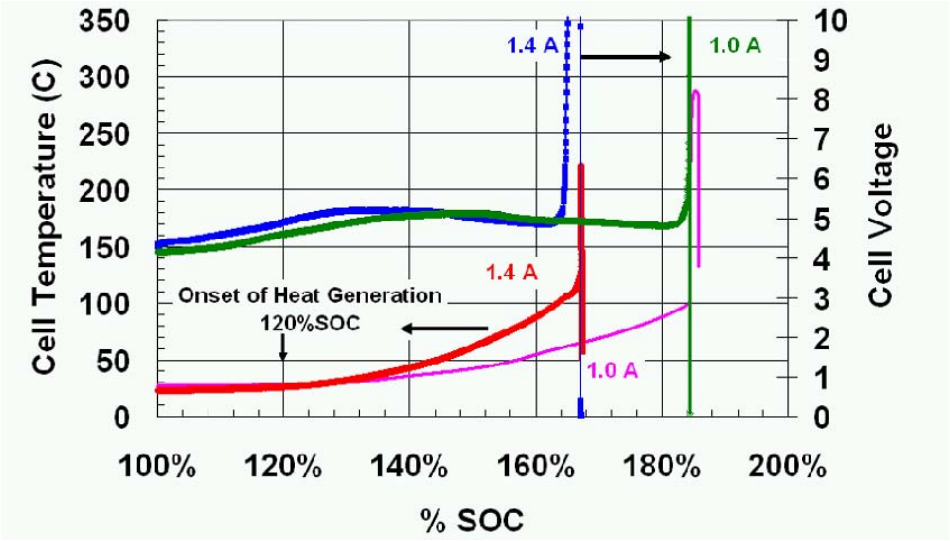

Figure III-33. Cell voltage and temperature profile of two Gen 2 cells with different capacities (1Ah and 1.4 Ah) during 1C overcharge showing heating to separator shutdown followed by thermal runaway.

Overcharge of cells with the new stabilized NMC cathodes showed improved overcharge abuse tolerance compared to the Gen 2 cells. Figure III-34 shows that the NMC cathode cells showed a greater overcharge range before heat generation and higher SOC before reaching separator shutdown and runaway.

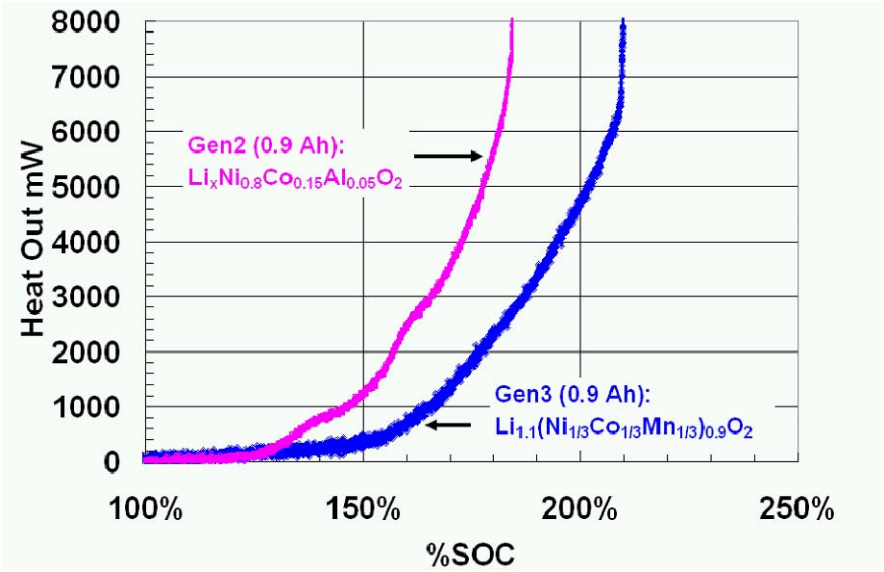

Figure III-34. Comparison of overcharge response of Gen 2 cells with stabilized Gen 3 NMC cells at 1C rate.

Overcharge cell response can be determined by the response of the shutdown separator. If the cell heats up to the shutdown temperature, the cell impedance increases and the full power supply potential appears across the separator. Figure III-35 shows the cell response during shutdown with 29V across the cell. The shutdown separator did not completely stop all current flow and thus the cell continued to heat. After one minute a short developed through the separator and the cell went into thermal runaway. Figure III-36 shows the corresponding heat output from the cell compared with the electrical power input. Decreasing the potential across the cell increases the time before failure. As shown in Figure III-37, the cell maintained its integrity for two minutes with 22V applied potential. Lower potentials can result in much longer times before failure but failures can still occur even after the cell appears stable.

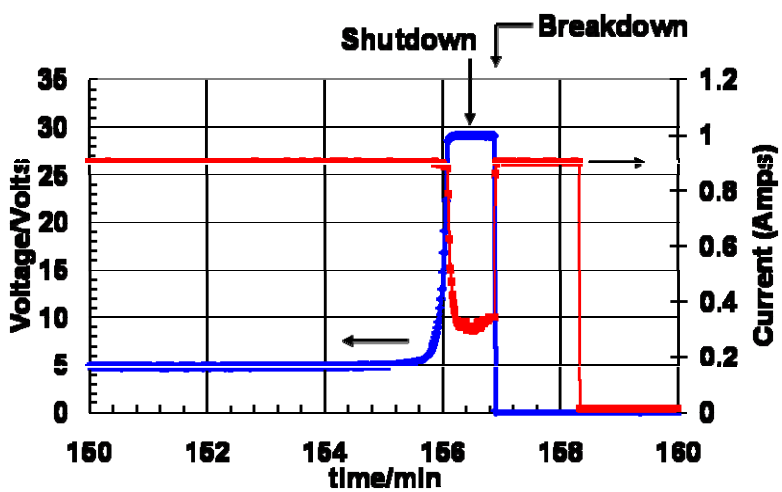

Figure III-35. Cell voltage and current profile showing continued current flow through cell even after separator shutdown with continued applied potential (29V).

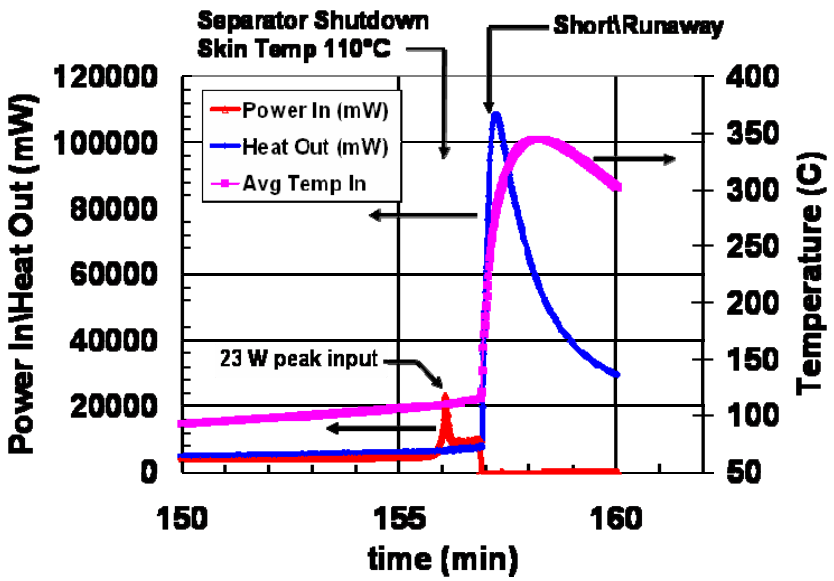

Figure III-36. Cell heat output and power input during separator shutdown after overcharge showing delayed time to failure and runaway.

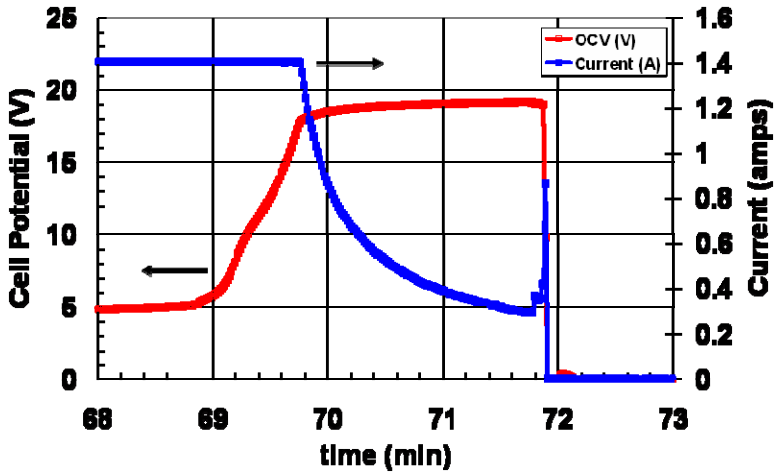

Figure III-37. Cell voltage/current profile showing increased time to failure with lower applied potential (22V).

Cells without a shutdown separator can be overcharged up to the thermal stability limits of the electrodes. Gen 2 cells were built using a non-shutdown separator (Separion®). Figure III-38 shows that the cell did not go into thermal runaway until 300% SOC at which the cell temperature reached the cathode runaway temperature of 180°C.

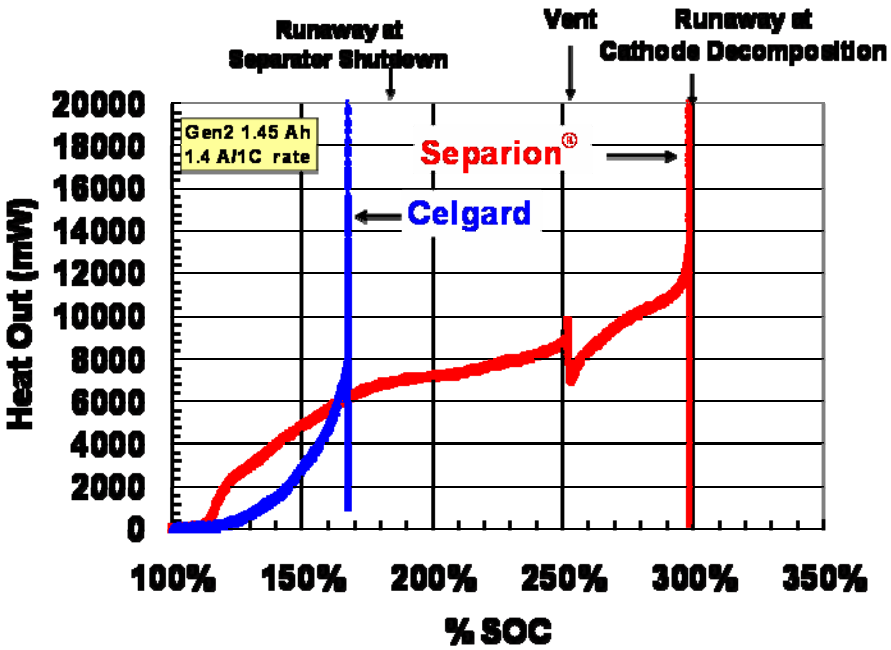

Figure III-38. Comparison of heat output during overcharge of cells with a shutdown separator (Celgard) and a cell with a non-shutdown separator (Separion®).

III.E Cell-Level Cost Reduction

OBJECTIVES

- Identify and secure advanced low-cost cell materials from material suppliers and evaluate samples for high-power HEV applications and report most promising materials to the USABC-sponsored industrial battery developers.
- Develop lower-cost high-power cell chemistries — using the most promising materials — and conduct preliminary evaluations to establish their viability.
- Evaluate the ability of a novel lithium titanate (LiTO) electrode (manufactured from nanophase primary and micron sized secondary particles) to provide a high rate, low cost, cell when coupled with Mn spinel.

APPROACH

- Secure samples of the most advanced materials from material suppliers.
- Refine rapid screening test protocols to assess the suitability of novel materials. Employ protocols to evaluate material capabilities, provide feedback to the material suppliers.
- Produce cells from the most promising materials and conduct preliminary evaluations on their performance, life, and safety characteristics, using sealed prismatic cells.
- Prepare laboratory sized LiTO/Mn cells and characterize their room temperature and high temperature performance and compare against other SOA cells.

ACCOMPLISHMENTS/FINDINGS

- Established and maintained contacts with material suppliers in Japan, Korea, and Europe.
- Obtained samples of advanced natural and synthetic graphite materials, lithium titanates, advanced layered and 3D spinel cathode materials, electrolyte salts, separators, and binder materials for evaluation.
- Conducted screening tests on advanced materials and provided feedback to suppliers.
- Established that the nano composite LiTO cells performed as well or better than similar cells and continued with development efforts.
- Established that electrolyte additives can stabilize the electrode/electrolyte interfaces to extend the calendar life of the graphite/L333 cell chemistry, without reducing its power.

FUTURE STUDIES

- Evaluate Li iron phosphate as a low cost, abuse tolerant cathode material.
- Continue securing advanced materials and evaluating them for HEV applications.
- Conduct preliminary accelerated aging studies on the nano-phase LiTO/Mn spinel cell system to establish its aging characteristics.

III.E.1 Introduction

Since the beginning of this program, researchers have been searching for lower cost cell materials and components that possess enhanced stability. These cell materials include: electrode active materials, conductive additives for the positive electrode, electrode binders, electrolyte salts, electrolyte solvents, and electrolyte additives. Where it makes sense to do so, a limited amount of internal R&D is performed to develop more stable materials (primarily in terms of electrolyte components and positive electrode materials). Recently, ANL has developed a novel

nano-composite LiTO negative electrode material that, when combined with a high rate positive material like Mn spinel, offers the promise of an extremely high rate, low cost, and abuse tolerate system.

Table III-9 provides a summary of how the DOE laboratories contribute to this focus area.

Table III-9. Summary of how the DOE laboratories contribute to the "Cost Reduction" focus area.

	ANL	BNL	INL	LBNL	SNL
Secure and Evaluate Advanced Materials	X				
Develop Electrode and Electrolyte Materials	X				
Preliminary Accelerated Aging Studies	X				
Cell Component Diagnostics	X				
Evaluate LiTO for High Power Cell Applications	X				

III.E.2 Material Screening and Development

Recently, this program has been investigating $Li_{1+x}(Ni_{1/3}Co_{1/3}Mn_{1/3})_{1-x}O_2$ (Gen 3) as a potential cathode material for high power applications. The investigation has shown that this material has several advantages compared to $LiNi_{0.8}Co_{0.2}O_2$ and $LiNi_{0.8}Co_{0.15}Al_{0.05}O_2$ (Gen 2) cathodes that were investigated previously. The Gen 3 material was found to have similar or higher capacity, much higher power, and better safety characteristics compared to other nickelate systems. One of the reasons why this material offers better cycling and safety performance is that the concentration of active nickel in the material is small and the average oxidation of Ni during charge is less than 3.5 which is more stable than Ni^{4+}, which reacts with the electrolyte in $LiNi_{0.8}Co_{0.2}O_2$ and Gen 2 cathodes. The oxidation of all available divalent nickel to the tetravalent state in the case of $Li_{1+x}(Ni_{1/3}Co_{1/3}Mn_{1/3})_{1-x}O_2$ takes place at 4.6 V. In addition, Mn^{4+} ions play a stabilizing role which could prevent a structural stress and collapse during cycling. By considering these factors, good calendar life and improved safety is expected with the Gen 3 electrode system.

$LiFePO_4$ has also attracted significant attention due to its low cost and outstanding safety characteristics. As mentioned above, removing all the Li in the lithium transition metal oxides can result in significant performance degradation as well as safety concerns. Hence, a specific upper cutoff voltage needs to be maintained. In the case of $LiFePO_4$, all the lithium can be removed without leading to performance degradation and safety concerns since $FePO_4$ is a stable phase and oxygen release is no longer an issue. Therefore, one expects higher thermal stability and better overcharge tolerance for $LiFePO_4$-based Li-ion batteries.

$Li_{1+x}[Ni_{1/3}Mn_{1/3}Co_{1/3}]_{1-x}O_2$/graphite system – Figure III-39 shows the ASI of MCMB/ $Li_{1.1}[Ni_{1/3}Mn_{1/3}Co_{1/3}]_{0.9}O_2$ Li-ion cells vs. DOD during the HPPC test. The electrolyte used was 1.2 M $LiPF_6$ in EC/EMC (3:7, by weight). With an interval of 10% DOD, a pair of 10 C charge/discharge pulse currents was applied for 10 seconds. The voltage change of the cell was used to calculate the ASI at each specific DOD. The ASI of the cell is ~25 $\Omega\cdot cm^2$, which is less than the requirements set for the ATD program of 35 $\Omega\cdot cm^2$. Therefore, it appears that MCMB/$Li_{1+x}[Ni_{1/3}Mn_{1/3}Co_{1/3}]_{1-x}O_2$ is an viable candidate for HEV applications.

Figure III-40 shows the normalized discharge capacity of MCMB/$Li_{1.1}[Ni_{1/3}Mn_{1/3}Co_{1/3}]_{0.9}O_2$ cells cycled with a constant current of C/2. The cell has excellent capacity retention with no observable capacity fade at room temperature. However, when the cell was cycled at 55ºC, more than 20%

capacity fade was observed after 100 cycles. This capacity fade raised some concern on the calendar life, since HEV batteries are required to have 15 year calendar life. Hence, there is a need to understand and address the poor capacity retention at elevated temperatures.

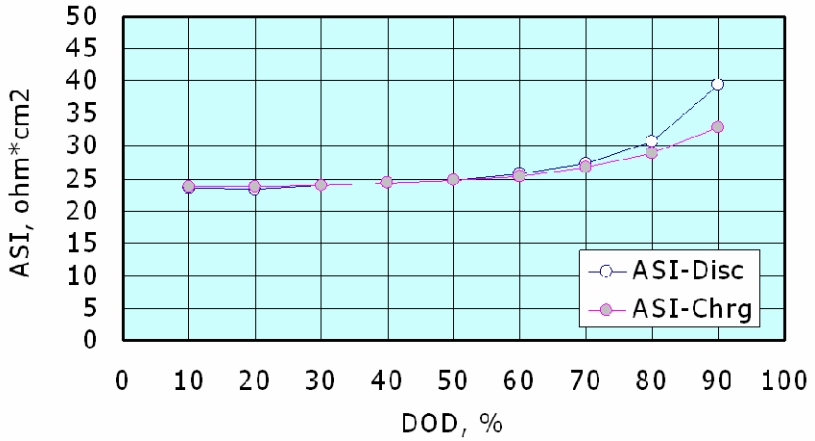

Figure III-39. ASI of a MCMB/$Li_{1.1}[Ni_{1/3}Mn_{1/3}Co_{1/3}]_{0.9}O_2$ cell during the HPPC test at 25ºC. The electrolyte used was 1.2 M $LiPF_6$ in EC/EMC (3:7, by wt), the HPPC test was carried out with 10 C pulses.

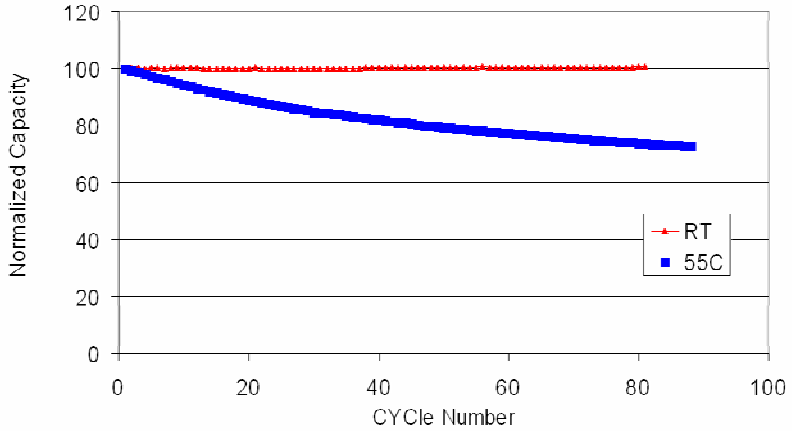

Figure III-40. Normalized discharge capacity of a MCMB/$Li_{1.1}[Ni_{1/3}Mn_{1/3}Co_{1/3}]_{0.9}O_2$ cell cycled with a constant current of C/2. The electrolyte is as in Figure III-39.

In order to understand the capacity fade at elevated temperatures, a Li reference electrode was inserted between the positive and the negative electrode. Then, the cell was cycled at 55ºC and the lithium electrode was used as a reference to monitor the potential change of the positive and the negative electrodes. Figure III-41 shows the ASI of the whole cell, the positive electrode, and the negative electrode obtained using this technique. The cell impedance increases quickly with the cycle number, resulting in the rapid capacity fade as shown in Figure III-40. Figure III-41 also illustrates that the impedance growth is mostly due to the negative electrode, while the ASI of the positive electrode remained constant. This result is quite different from that observed with the Gen 2 chemistry. In the case of Gen 2 chemistry, Ni(IV) in the charged positive electrode material can readily oxidize the electrolyte components, especially carbonates, and coat the by product on the surface of the positive electrode resulting in interfacial impedance growth on the positive electrode

while the impedance growth on the negative electrode was much lower. One possible explanation for the impedance increase at the carbon electrode in the Gen 3 system is that the Mn ion from the cathode may dissolve and poison the SEI of the carbon as observed in the spinel system.

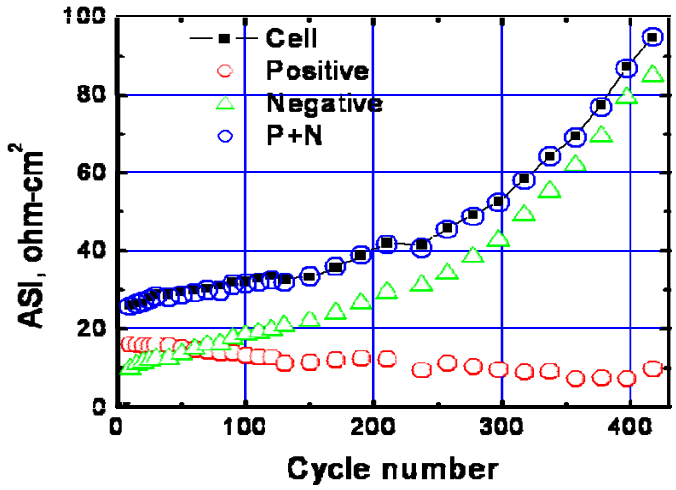

Figure III-41. ASI of the whole cell, the positive and the negative electrode during the cycling at 55ºC.

Figure III-42 shows the leaching metals detected the electrolyte after soaking the Gen 3 positive electrode material in the electrolyte at 55ºC for one month. Significant amounts of metal (Ni, Co, and Mn) were detected regardless of the source of the materials. Unlike Mn-spinel, where pure Mn metal deposition at the carbon surface appears to play a strong catalytic role in poisoning the anode SEI, the dissolution of Mn, Ni, and Co in this material may form less active Mn-Ni-Co alloys that don't poison the SEI of the anode as effectively. As a result, one may be able to overcome the capacity fade of the Gen 3 system by selecting a more stable SEI at the carbon using functional electrolyte additives.

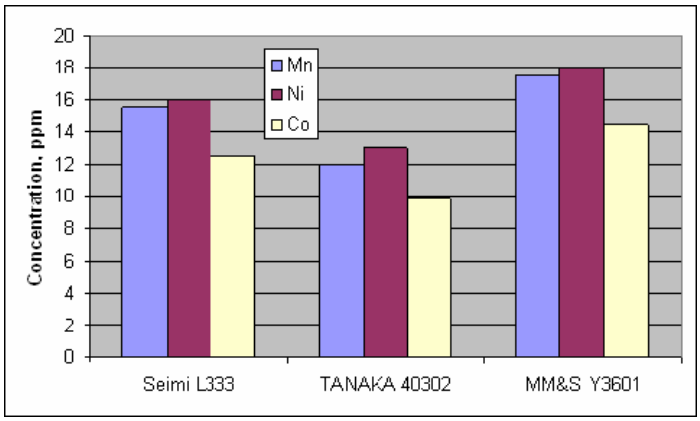

Figure III-42. Amount of metal elements in electrolyte after soaking Gen 3(+) at 55ºC for 1 month.

ANL has been testing several electrolyte additives, including LiBOB and VEC. These additives typically provide excellent protection but result in high interfacial impedance of the cell. ANL developed a unique electrolyte additive, lithium difluoro(oxalate)borate (LiDFOB), which

provides strong protection of the negative electrode similar to LiBOB. However, the addition of LiDFOB to the electrolyte does not result in an increase of cell impedance. Figure III-43 shows the AC impedance of MCMB/Gen 3(+)cells using different electrolytes. The electrolytes used were 1.2 M $LiPF_6$ and 1.0 M LiDFOB in EC/PC/EMC (1:1:3, by weight) respectively. The overall impedance of the cell using LiDFOB is about 15% higher than that of the cell using $LiPF_6$-based electrolyte. This suggests that the power capability of the cells could be slightly reduced by completely replacing $LiPF_6$ with LiDFOB. Therefore, it may be possible to maintain the power capability of Li-ion cells by adding a small (2-5%) amount of LiDFOB, to permit the LiDFOB to act as the passivation additive to effectively protect the negative electrode from being attacked by other cell components such as dissolved Mn, Ni, and Co ions.

Figure III-43. AC impedance of MCMB/L333 cells using 1.2 M $LiPF_6$ and 1.0 M LiDFOB in EC/PC/DMC (1:1:3, by weight).

Figure III-44 shows the ASI as a function of aging time for MCMB/Gen 3(+) cells with and without LiDFOB additive. Both cells were aged at 55ºC and at 60% SOC. It can be seen that the ASI of the cell without LiDFOB increases by more than 200% in 72 days while the cell with 2% LiDFOB experienced a 30% ASI increase during the same period.

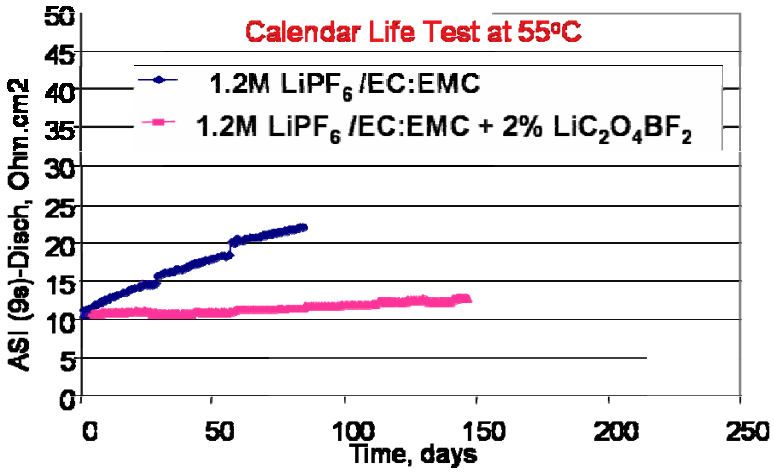

Figure III-44. Area specific impedance of MCMB/L333 cells during aging test.

Another activity in this area is to screen advanced positive electrode materials for high power applications and recommend promising materials to the industrial partners of the USABC. Figure III-45 shows a comparison of the power performance of different Gen 3(+) materials from different commercial sources. It can be seen that the material from Nippon Chemicals has the lowest ASI at low rate (<25 C), and the ASI increases quickly with the current applied. Alternatively, the material from Daejung showed very stable performance with increasing rate.

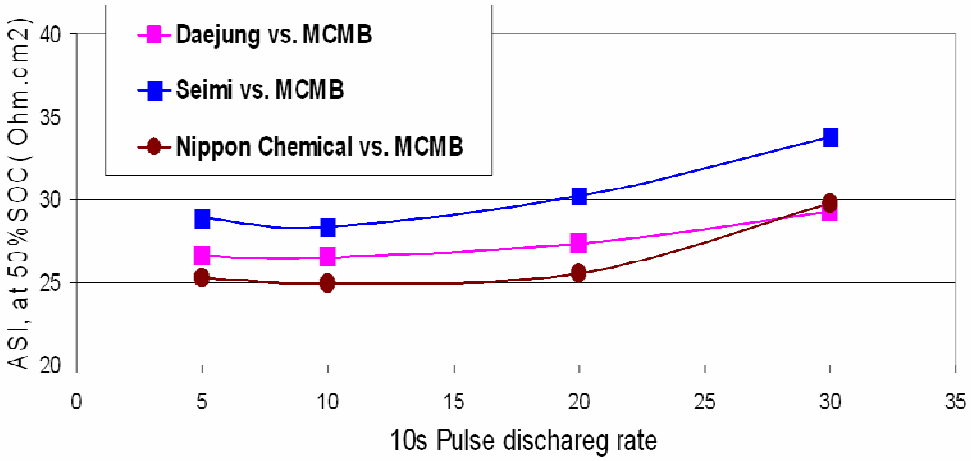

Figure III-45. ASI of Li-ion cells using Gem 3(+) from different commercial sources

$LiFePO_4$/Graphite system – As mentioned above, $LiFePO_4$ is an attractive positive electrode material for HEV applications due to its low cost and excellent safety characteristics. Several $LiFePO_4$ positive electrode materials from different commercial sources were evaluated. Figure III-46 shows a comparison of the ASI of different positive electrode materials. Only $LiFePO_4$ from A123Systems had enough power capability to meet the HEV applications. Figure III-47 shows the discharge capacity of the A123 cell cycled at 55ºC. Only 10 % capacity fade was observed for 200 cycles. However, most of the other olivines show significant capacity fade at 55ºC. The result of the capacity fade was correlated with the Fe dissolution observed in most of theses olivine materials.

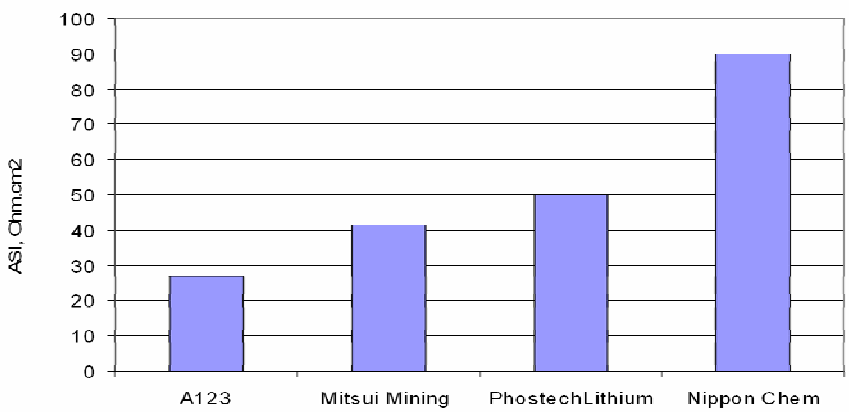

Figure III-46. ASI of Li-ion cells using $LiFePO_4$ from different commercial sources.

Conclusions – Several positive electrode materials were evaluated as promising candidates for high-power Li-ion cells. The main focus of this work is the $Li_{1+x}[Ni_{1/3}Mn_{1/3}Co_{1/3}]_{1-x}O_2$ layered positive electrode materials and $LiFePO_4$. It has been demonstrated that $Li_{1+x}[Ni_{1/3}Mn_{1/3}Co_{1/3}]_{1-x}O_2$ had several advantages, including cost, life, and safety characteristics, over the Gen 2 positive electrode material. However, the cells using $Li_{1+x}[Ni_{1/3}Mn_{1/3}Co_{1/3}]_{1-x}O_2$ suffered some capacity fade at elevated temperature. Hence, LiDFOB was proposed as a functionalized electrolyte additive to improve both the capacity and the power retention of Li-ion batteries based on this system.

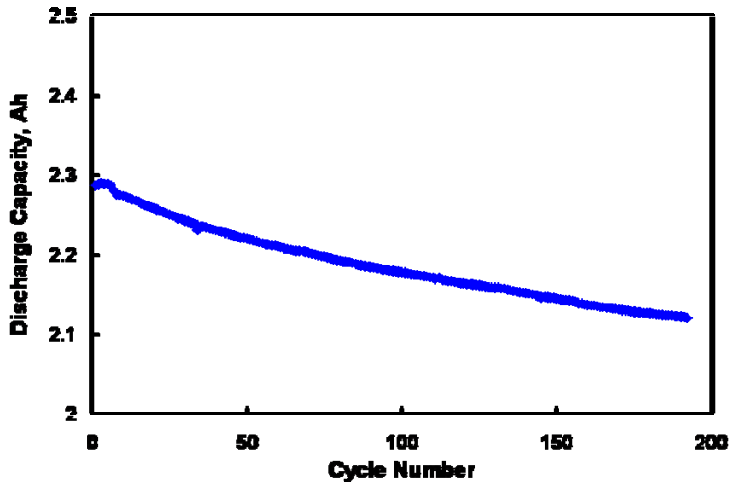

Figure III-47. Discharge capacity of MCMB/$LiFePO_4$ cell at 55ºC.

Several $LiFePO_4$ olivine materials were evaluated for their power and cycle life performance. While most of the olivines tested show low power and poor cycle life at 55ºC, cells from A123Systems shows excellent power capability and good capacity retention at 60ºC.

III.E.3 Evaluation of $Li_4Ti_5O_{12}$ Nano Materials

Li-manganese oxide spinels have attracted significant attention for high-power applications due to their low cost, outstanding power capability, and low reactivity towards electrolytes when charged. However, the migration of manganese from spinel to the negative electrodes, which results in rapid capacity fade, remains a major barrier to enable this technology in HEVs.

Several approaches to reduce the dissolution of Mn in the electrolyte have been carried out. One is to dope the spinel with low-valence-state metals to increase the valence state of manganese and to eliminate the disproportionation reaction that leads to the Mn^{2+} dissolution. Alternatively, the spinel particles were coated with an acid scavenger to locally reduce the acidity of the electrolyte on the surface of spinel particles and hence to suppress the manganese dissolution. Meanwhile, it was also proposed to use high *p*H non-aqueous electrolytes, such as LiBOB-based ones, to improve the capacity retention at elevated temperatures. It has also been reported that the capacity retention of the spinel Mn-based Li-ion cells could be improved by mixing the spinels with Li-Ni-Co-Mn oxides. Finally, there have been efforts to deposit a protection layer on the surface of graphite to suppress the deposition of manganese.

The approaches mentioned above are meant to slow the manganese migration from the spinel to the graphite negative electrode and prevent the poisoning of the anode SEI. However, these approaches do not offer complete solutions. A more promising solution is to replace the graphite negative electrode with $Li_4Ti_5O_{12}$, which has a redox potential of 1.55 V vs. Li^+/Li and doesn't require a SEI. The advantages of $Li_4Ti_5O_{12}$ with a higher redox potential over lithiated graphite is to eliminate the self discharge reaction of lithiated graphite that results in both capacity fade and power fade of Li-ion cells. Moreover, the low reactivity of $Li_{4+x}Ti_5O_{12}$ towards non-aqueous electrolytes is a significant advantage. A disadvantage of $Li_4Ti_5O_{12}$ is that the cell voltage is reduced by about 1.5 V compared to carbon based batteries, which translates to reduced energy density. In the case of HEV, the main bottleneck for Li-ion batteries is life and power (and cost), but not energy density. Therefore, the use of $Li_4Ti_5O_{12}$ for HEV applications should not be problematic because of the reduced energy density. In this work, nano-structured $Li_4Ti_5O_5$ was investigated as a promising negative electrode material to work with Li-manganese oxide spinels. The nano structure was adopted to overcome the disadvantage of low electric conductivity of $Li_4Ti_5O_{12}$. It was demonstrated that cells using nano-$Li_4Ti_5O_{12}$ as the negative electrode and $Li_{1.06}Mn_{1.94}O_4$ as the positive electrode had excellent capacity retention at 55ºC, outstanding rate and power capability, and long life.

Result and Discussion – The material investigated was a prototype nano-structured $Li_4Ti_5O_{12}$ developed at ANL whose SEM images are shown in Figure III-48. XRD patterns were also taken. The specific surface area (BET) was ~1.9 m^2/g. The SEM images show that the nano-$Li_4Ti_5O_{12}$ is round-shaped with 1-2 µm secondary particles and less than 15 nm primary particles. Also, the primary particles are loosely packed with voids among them; the voids appear to provide tunnels for the electrolyte to diffuse into, reducing the diffusion length of the lithium/electron during intercalation/deintercalation reactions. The positive electrode material investigated was $Li_{1.06}Mn_{1.94}O_4$ with an average particle size of 8 µm.

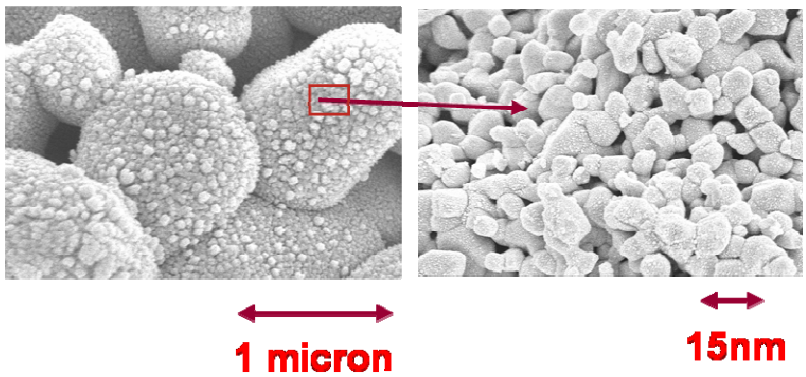

Figure III-48. Scanning electron microscopic images of the prototype nano-$Li_4Ti_5O_{12}$ developed at ANL.

Figure III-49 shows the charge and discharge capacity of a $Li_4Ti_5O_{12}/Li_{1.06}Mn_{1.94}O_4$ cell vs. cycle number. The electrolyte used was 1.2 M $LiPF_6$ in EC/EMC (3:7, by weight), and the cell was cycled between 1.5 V and 2.6 V at 55ºC with a constant current of 6Cduring the charge and discharge. The cell has experienced only 7% capacity fade up to 500 cycles at 55ºC. Thus, it appears that the rapid capacity fade of spinel-based Li-ion cells can be resolved by replacing the graphite anode with $Li_4Ti_5O_{12}$. Figure III-50 shows the ASI of a nano-$Li_4Ti_5O_{12}/Li_{1.06}Mn_{1.94}O_4$

cell as a function of the DOD during an HPPC test. For each data point, a 30 C pulse discharge current for 18 seconds and a 22.5 C pulse charge current for 10 seconds were applied, and the voltage change was used to calculate the ASI. Figure III-50 shows that the ASI of the cell greatly exceeded the standard requirements set for HEV applications (35 $\Omega \cdot cm^2$) during the whole course of charge/discharge window. In a real HEV application, the battery is generally kept at about 50% DOD and is charged /discharged with a very narrow DOD window. One can also see that the ASI of the cell within the window of 30%-70% DOD was ~17 $\Omega \cdot cm^2$ for 18-second pulse discharge.

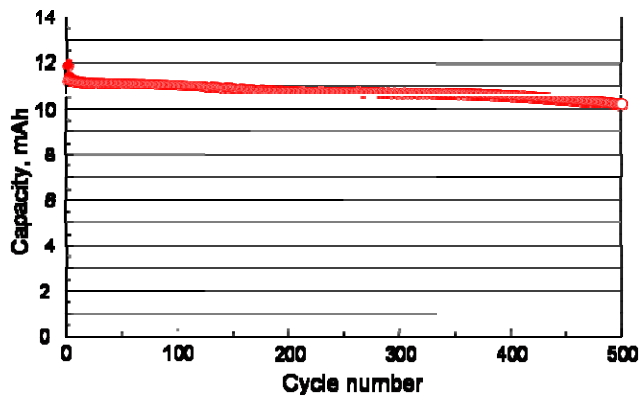

Figure III-49. Charge and discharge capacity of a $Li_4Ti_5O_{12}/Li_{1.06}Mn_{1.94}O_4$ Li-ion cell.

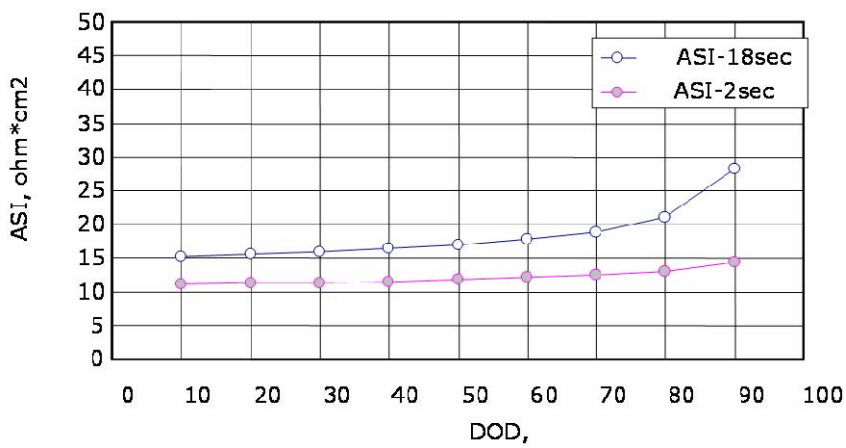

Figure III-50. ASI of nano-$Li_4Ti_5O_{12}/Li_{1.06}Mn_{1.94}O_4$ cell during the HPPC test at 30C. The ASI for 18-sec pulse discharge is presented by the open circles, and the ASI for 2-sec regen charge is presented by the solid circles.

Figure III-51 shows a comparison on ASI for a nano-$Li_4Ti_5O_{12}$ electrode and a graphite electrode using a lithiated tin reference electrode in the Li-ion cell configuration. The ASI was measured at 60% SOC using a 5 C pulse current for 10 seconds. The ASI of the nano-$Li_4Ti_5O_{12}$ electrode is much lower than that on the graphite electrode between -30ºC and 30ºC. The major difference can be explained by: (1) the much shorter diffusion length (~15 nm) in nano-structured $Li_4Ti_5O_{12}$; (2) the lack of a conventional SEI on the surface of the nano-$Li_4Ti_5O_{12}$ to impede the heterogeneous phase charge transfer; and (3) unlike carbon based systems, there is no Li plating taking place in this system when the temperature is below 0ºC.

Another major challenge for Li-ion batteries is the 15-year battery life. Under the charged condition, Li is removed from the positive electrode material and inserted into the negative electrode material. The resulting high oxidation state transition metal oxides in the positive electrode can oxidize the non-aqueous electrolyte while the lithiated negative electrode, particularly stage 1 Li_xC_6, can reduce the non-aqueous electrolyte. Both reactions will increase the cell impedance and lead to the loss of power. In this work, lithium manganese oxide spinel was chosen because the MnO_2 has very low reactivity towards non-aqueous electrolyte.

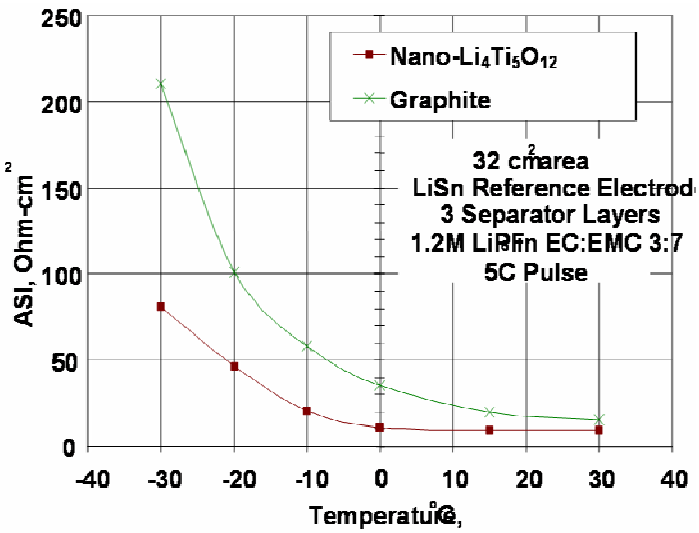

Figure III-51. Comparison of the ASI for nano-$Li_4Ti_5O_{12}$ and graphite at various temperatures. The reference electrode technique was used to measure the contribution from the negative electrodes.

Figure III-52 shows the results of calendar life tests of two cells. One of the cells used a graphite negative electrode, and the other used nano-$Li_4Ti_5O_{12}$. Both cells were charged to 60% SOC and then stored in an oven at 55ºC. Once a day, one pair of 9 second/10 C pulse currents were applied to charge and discharge the cell, and the change of the voltage profile was used to calculate the ASI. The $Li_4Ti_5O_{12}$-based cell showed very stable performance with no significant ASI increase during the course of 50-day aging at 55ºC. As a comparison, the ASI of the control cell increased from 15 $\Omega \cdot cm^2$ to 35 $\Omega \cdot cm^2$ after the 60-day test. Therefore, a much longer life can be expected for nano-$Li_4Ti_5O_{12}$/$Li_{1.06}Mn_{1.94}O_4$ Li-ion cells than that for graphite/$Li_{1.06}Mn_{1.94}O_4$ ones.

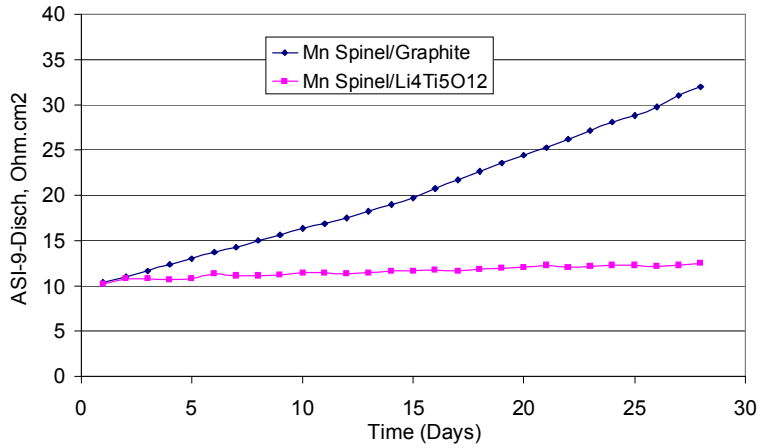

Figure III-52. ASI of Mn spinel vs. LiTO and graphite during calendar life test at 55ºC.

Conclusion – Nano-structured $Li_4Ti_5O_{12}$ was investigated as a promising negative electrode material to work with lithium manganese oxide spinels for HEV applications. It has been demonstrated that nano-$Li_4Ti_5O_{12}/Li_{1.06}Mn_{1.94}O_4$ Li-ion system is a promising battery technology for HEV applications with high power capability, low reactivity towards non-aqueous electrolytes, excellent capacity retention, and long life.

Selected Publications

1. B. Barnett, E. Roth, K. Thomas-Alyea, & D. Doughty, "Abuse Tolerance vs. Field Failure: Two Different Issues for Lithium-Ion Safety," Accepted for publication in JPS[11] for IMLB 2006 (Biarritz).
2. C. Johnson, K. Lauzze, N. Kanakaris, A. Kahaian, M. Thackeray, K. Amine, G. Tapia, S. Hackney & R. Rigney, Electrochemical Performance of Ni/Cu metallized & carbon coated graphite for lithium batteries, *New carbon Based Materials for Electrochemical Energy Storage Systems (2006) 357-376*
3. D. Abraham, E. Reynolds, E. Sammann, A. Jansen, & D. Dees, Aging characteristics of high-power Li-ion cells with $LiNi_{0.8}Co_{0.15}Al_{0.05}O_2$ and $Li_{4/3}Ti_{5/3}O_4$ electrodes, *Electrochimica Acta 51 502 (2005).*
4. D. Abraham, E. Reynolds, P. Schultz, A. Jansen, D. Dees, Temperature Dependence of Capacity and Impedance Data from High-Power Lithium-ion Cells, *JECS*[12] *153, A1610 (2006).*
5. D. Abraham, E. Roth, R. Kostecki, K. McCarthy, S. MacLaren, D. Doughty, Diagnostic Examination of Thermally Abused High-Power Lithium-Ion Cells, *JPS 161, 648 (2006).*
6. D. Doughty, E. Roth, C. Crafts, G. Nagasubramanian, G. Henriksen & K. Amine, Effects of additives on thermal stability of Li ion cells, *JPS*, 146, 116 (2005).
7. E. Roth, D. Doughty, & D. Pile, "Effects of Separator Breakdown on Abuse Response of 18650 Li-Ion Cells,"Accepted for publication in JPS for IMLB 2006 (Biarritz).
8. H. Bang, H. Joachin, H. Yang, K. Amine & J. Prakash, Contribution of the structural changes of $Li(Ni_{0.8}Co_{0.15}Al_{0.05})O_2$ cathodes on the exothermic reactions in Li-ion cells, *JECS*, 153: A731 (2006).
9. H. Yang, G. Zhuang, & P. Ross, "Thermal stability of $LiPF_6$ salt and Li ion battery electrolytes containing $LiPF_6$," JPS, 161, 573 (2006).
10. H. Yang, H. Bang, K. Amine & J. Prakash, Investigations of the exothermic reactions of natural graphite anode for Li-ion batteries during thermal runaway, *JECS*, 152, A73 (2005).
11. I. Belharouak, C. Johnson & K. Amine, Synthesis and electrochemical analysis of vapor-deposited carbon-coated $LiFePO_4$, *Electrochemistry Communications*, 7, 983 (2005).

[11] JPS = Journal of Power Sources
[12] JECS = Journal of the Electrochemical Society

12. I. Belharouak, D. Vissers & K. Amine, Thermal Stability of the $Li(Ni_{0.8}Co_{0.15}Al_{0.05})O_2$ Cathode in the Presence of Cell Components, *JECS*, 153, A2030 (2006).
13. I. Belharouak, W.Q. Lu, D. Vissers & K. Amine, Safety characteristics of $Li(Ni_{0.8}Co_{0.15}Al_{0.05})O_2$ and $Li(Ni_{1/3}Co_{1/3}Mn_{1/3})_{1-x}O_2$, *Electrochemistry Communications*, 8, 329 (2006).
14. I. Bloom, B. Potter, C. Johnson, K. Gering, & J. Christophersen, "Effect of cathode composition on impedance rise in high-power lithium-ion cells: Long term aging results," *JPS*, 155, 415 (2006).
15. I. Bloom, J. Christophersen, D. P. Abraham, K. Gering, "Differential Voltage Analyses of High-Power Lithium-Ion Cells. 3. Another Anode Phenomenon," *JPS*, 157, 537 (2006).
16. J. Christophersen, C. Ho, C. Motloch, D. Howell, & H. Hess, "Effects of Reference Performance Testing during Aging Using Commercial Cells," *JECS.,*153, A1406 (2006).
17. J. Liu, D.R. Vissers, K. Amine, Surface Treated natural Graphite as Anode material For High Power Li-ion battery Applications, *New carbon Based Materials for Electrochemical Energy Storage Systems 283 (2006).*
18. K. Amine, J. Liu & I. Belharouak, High-temperature storage and cycling of C-$LiFePO_4$/graphite Li-ion cells, *Electrochemistry Communications*, 7, 669 (2005).
19. K. Amine, J. Liu, I. Belharouak, S.H. Kang, I. Bloom, D. Vissers & G. Henriksen, Advanced cathode materials for high-power applications, *JPS*, 146, 111 (2005).
20. K. Chung, H. Lee, W-S. Yoon, J. McBreen, X.Q. Yang, Studies of $LiMn_2O_4$ Capacity Fading Mechanism at Elevated Temperature Using In Situ Synchrotron XRD, *JECS*, 153, A774 (2006).
21. K. Chung, W. S. Yoon, H. Lee, X.Q. Yang, J. McBreen, B. Deng, X.Q. Wang, M. Yoshio, R. Wang, J. Gui, & M. Okada, Comparative Studies between Oxygen Deficient $LiMn_2O_4$ and Al-doped $LiMn_2O_4$, *JPS* 146, 226 (2005).
22. K. Chung, W-S. Yoon, H. Lee, J. McBreen, X.Q. Yang, S. Oh, W. Ryu, J. Lee, W. Cho, & B. Cho, In Situ XRD Studies of the Structural Changes of ZrO_2 Coated $LiCoO_2$ during Cycling and Their Effects on Capacity Retention in Lithium Batteries, *JPS*, Available online 13 February 2006.
23. K. Edstrom, M. Herstedt, D. Abraham, A New Look at the Solid Electrolyte Interphase on Graphite Anodes In Lithium-Ion Batteries, *JPS* 153, 380 (2006).
24. K. Gering, Low-Temperature Performance Limitations of Li-ion Batteries, *ECS Trans*. 1, 119 (2006).
25. K. Gering, Prediction of electrolyte viscosity for aqueous and non-aqueous systems: Results from a molecular model based on ion solvation and a chemical physics framework, *Electrochim. Acta*, 51, 3125 (2006).
26. M. Otsuki, T. Ogino & K. Amine, Investigation of Flame-Retardant Additives for Safety Usage of Lithium-Ion Batteries, *ECS Transactions*, 1, 13 (2006).
27. R. Spotnitz, J. Weaver, G. Yeduvaka, D. Doughty & E. Roth, Simulation of abuse tolerance of lithium-ion battery packs, *JPS* 163, 1080, (2007).
28. W. Lu, I. Belharouak, D. Vissers & K. Amine, In Situ Thermal Study of $Li_{1+x}(Ni_{1/3}Co_{1/3}Mn_{1/3})_{1-x}O_2$ Using Isothermal Micro-calorimetric Techniques, *JECS*, 153, A2147 (2006).
29. W. Lu, Z. Chen, H. Joachin, J. Parakash, J. Liu & K. Amine, Thermal and electrochemical characterization of MCMB 10-28/LiNi{sub 1/3}Co{sub l/3}Mn{sub l/3}O{sub 2} with excess Li using LiBOB as an electrolyte additive *JPS*, in press (2006).
30. W-S. Yoon, J. Hanson, J. McBreen, & X.Q. Yang, A Study on the Newly Observed Intermediate Structures during the Thermal Decomposition of Nickel-Based Layered Cathode Materials Using Time Resolved XRD, *electrochemistry communications*, 8, 859 (2006).
31. W-S. Yoon, K. Chung, J. McBreen, & X.Q. Yang "A Comparative Study on Structural Changes of $LiCo_{1/3}Ni_{1/3}Mn_{1/3}O_2$ and $LiNi_{0.8}Co_{0.15}Al_{0.05}O_2$ during First Charge Using in situ XRD" *electrochemistry communications*, 8, 1257 (2006).
32. W-S. Yoon, K. Chung, J. McBreen, D. Fischer, & X.Q. Yang "Changes in Electronic Structure of the Electrochemically Li-ion Deintercalated $LiNiO_2$ System Investigated by Soft X-ray Absorption Spectroscopy" *JPS,* Available online 20 February 2006.

33. W-S. Yoon, K. Chung, J. McBreen, K. Zaghib, & X.Q. Yang "Electronic Structure of the Electrochemically Delithiated $Li_{1-x}FePO_4$ Electrodes Investigated by P K-edge X-ray Absorption Spectroscopy" *ESSL*[13], 9, A415 (2006).
34. W-S. Yoon, K. Chung, K-W. Nam, & K-B. Kim "Characterization of $LiMn_2O_4$ - Coated $LiCoO_2$ Film Electrode Prepared by Electrostatic Spray Deposition" *JPS*, Available online 15 February 2006.
35. W-S. Yoon, K. Chung, M. Balasubramanian, J. Hanson, J. McBreen, & X.Q. Yang, "Time Resolved XRD Study on the Thermal Decomposition of Nickel-Based Layered Cathode Materials for Li-ion Batteries" *JPS,* Available online 20 February 2006.
36. W-S. Yoon, M. Balasubramanian, K. Chung, X.Q. Yang, J. McBreen, C. P. Grey, & D. A. Fischer "Investigation of the Charge Compensation Mechanism on the electrochemically Li-ion deintercalated $Li_{1-x}Co_{1/3}Ni_{1/3}Mn_{1/3}O_2$ Electrode System by Combination of Soft and Hard X-ray Absorption Spectroscopy" *Journal of the American Chemical Society*, 127, 17479 (2005)
37. W-S. Yoon, M. Balasubramanian, X.Q. Yang, J. McBreen, & J. Hanson "Time Resolved XRD Study on the Thermal Decomposition of $Li_{1-x}Ni_{0.8}Co_{0.15}Al_{0.05}O_2$ Cathode Materials for Li-ion Batteries" *ESSL,* 8, A83 (2005).
38. Z. Chen & K. Amine, Capacity fade of $Li_{1+x}Mn_{2-x}O_4$-based Li-ion cells, *JECS*, 153: A316 (2006).
39. Z. Chen & K. Amine, Electrochemical and kinetic studies of $Li_{1.156}Mn_{1.844}O_4$, *JECS* 153, A1279 (2006).
40. Z. Chen & K. Amine, Tris(pentafluorophenyl) borane as an additive to improve the power capabilities of lithium-ion batteries, *JECS*, 153, A1221 (2006).
41. Z. Chen, Q. Z. Wang & K. Amine, Improving the performance of soft carbon for lithium-ion batteries, *Electrochimica Acta*, 51, 3890 (2006).
42. Z. Chen, W. Q. Lu, J. Liu & K. Amine, $LiPF_6$/LiBOB blend salt electrolyte for high-power lithium-ion batteries, *Electrochimica Acta*, 51, 3322 (2006).
43. Z. Chen, Y. K. Sun & K. Amine, Electrochemical properties of lithium-rich $Li_{1+x}(Ni_{1/3}Co_{1/3}Mn_{1/3})_{1-x}O_2$ at high potential, *JECS*, 153, A1818 (2006).

Extended Abstracts and Invited Talks

1. J. McBreen, H. Lee, W-S. Yoon, & X.Q. Yang, "Nickel-Metal Hydride and Lithium-Ion Batteries for HEV Applications", **Invited,** Technical Conference of China International Battery Fair 2006 (CIBF2006), Beijing, China, June 28-30, 2006
2. X.Q. Yang, H. Lee, W-S. Yoon, K. Chung, & J. McBreen, "The Structural Changes of New Cathode Materials for Lithium Batteries and their Implication on Safety Related Characteristics Studied by X-ray Absorption and Diffraction", **Invited,** Technical Conference of China International Battery Fair 2006 (CIBF2006), Beijing, China, June 28-30, 2006

[13] ESSL = Electrochemical and Solid-State Letters

IV. FOCUSED LONG-TERM RESEARCH

The Focused Long-Term Research Program, also called the Batteries for Advanced Transportation Technologies (BATT) program, is supported by the DOE's FreedomCAR and Vehicle Technologies program (DOE-FCVT) to research and analyze new materials for high-performance, next generation, rechargeable batteries for use in HEVs and EVs.

Background and Program Context

The development of an advanced battery for automotive applications is difficult, although companies are making progress each year. Current HEV batteries are all NiMH, but Li-ion continues to show promise due to the promise of improved performance, reduced weight and volume, and potentially lower price and longer life. Thus, there remains a need to identify and understand performance and lifetime limitations to help guide the search for new materials to enable the use of Li-based batteries. The Focused Long-Term Research Program addresses fundamental issues of chemistries and materials associated with lithium battery candidates for vehicular applications. The program emphasizes the identification and mitigation of failure modes, coupled with materials synthesis and evaluation, advanced diagnostics, and improved electrochemical models. Battery chemistries are monitored continuously with periodic substitution of more-promising components based on advice from within this program, from outside experts, and from assessments of world-wide battery R&D.

The work is carried out by the Lawrence Berkeley National Laboratory (LBNL) and a number other organizations. The program's investigations center around three baseline systems:

1. The $LiFePO_4$ system promises to be low cost and abuse tolerant. The program is working to develop lower cost synthesis methods and significantly improved materials using liquid or gel electrolytes. This is regarded as a moderate-energy, low-voltage system that is inherently stable and low cost.

2. The spinel system with a liquid-electrolyte provides good high-rate capability, which aids work in the applied research program to develop a low-cost high-power battery. The program is working to understand the capacity fade at high temperature to prolong this material's life.

3. The $LiNi_{1/3}Mn_{1/3}Co_{1/3}O_2$ (called 123 or 1/3) cathode material with a carbon-coated graphite anode is a high-energy cell. The cathode is less expensive than the Gen 2 cathode and promises a combination of high energy and power. The program is working on understanding the fade mechanisms and improving the rate capabilities of other layered materials.

The program, and this document, is organized into the following research areas:

IV.A New Cathode Systems, Performance and Limitations

IV.A.1 $LiFePO_4$ Systems
IV.A.2 Mn Spinel and Spinel Composite Systems
IV.A.3 Nickelate Systems

IV.B New Anode Materials
IV.C Novel Electrolytes and their Characterization,
IV.D Li-Ion Modeling, Diagnostics, and Cell Analysis

These task areas provide the program with additional focus on the issues and possible solutions associated with some of the most promising chemistries in the Li-ion battery field while also permitting the researchers to collaboratively address the barriers common to all of these chemistries. Brief descriptions of each research area follow.

- The ***$LiFePO_4$ System*** task includes studies of capacity and power fade in the iron phosphate system, including the performance of iron phosphate with gel polymer electrolytes. This cathode material promises more abuse tolerant performance at a relatively low cost. Researchers investigate lower cost synthesis methods and the impact of processing steps on performance, and perform theoretical investigations on the impact of carbon coatings on performance.

- The ***Mn Spinel Systems*** task aims to understand the failure and degradation modes in the Mn spinel system using various material doping, cell cycling, and advanced diagnostics. Researchers are also evaluating electrode materials from multiple suppliers.

- The ***Nickelate Systems*** task aims to understand the failure and degradation modes in the 123 and other nickelate systems using cell builds, cell cycling, empirical and *ab-initio* calculations, and advanced diagnostics.

- The ***New Anode Materials*** task aims to find improved composite negative electrodes containing one (or more) metal components within a graphite matrix, for example, C/Sn and C/Sb systems, and nano-composite alloys.

- The ***Novel Electrolyte Materials*** task involves investigating the limitations of polymers, ionic liquids, and single-ion conducting gels in Li-polymer and Li-ion cells that offer promise for low cost and abuse tolerant batteries. Post-test analyses and spectroscopic and microscopic techniques are used to investigate morphology, structure, and compositional changes of electrode materials.

- The ***Modeling and Diagnostics*** tasks involve the use of advanced diagnostics techniques, such as FTIR, to investigate interfacial properties of batteries by studying the SEI formation and its change with cycling. It also involves studying the changes in electrode structure at high temperatures using XAFS, XRD, NMR and other techniques. Several modeling approaches are used to understand cell behavior and fundamental material properties, including *ab-initio* calculations, macroscopic cell calculations, finite element, and molecular dynamics simulations.

This chapter summarizes the research activities of this program in FY 2006. The website for the BATT Program is found at http://berc.lbl.gov/BATT/BATT.html.

IV.A New Cathode Materials

The overall objective of the following tasks is to evaluate advanced cathode materials for Li-ion batteries. Current materials suffer a number of shortcomings, including expensive raw materials and relatively poor response to abuse conditions. As a result, this program is investigating three baseline chemistries, $LiFePO_4$, $LiMn_2O_4$, and $LiNi_{1/3}Mn_{1/3}Co_{1/3}O_2$, and several more exploratory systems including composite cathodes, that offer improvements over $LiCoO_2$.

IV.A.1 $LiFePO_4$ and other Phosphate Systems: Performance and Limitations

OBJECTIVES

The primary objective of the iron-phosphate research is to understand and overcome the inherently poor conductivity of this material to permit cell developers to take advantage of its relatively low cost and good abuse tolerance characteristics. In addition, researchers are investigating new manufacturing methods that would further lower the cost of this material.

APPROACH

A fairly large number of approaches are being used to improve the conductivity, lower the processing cost, and understand the behavior of this material, including:

- Investigating novel low cost synthesis techniques, including low-temperature hydrothermal synthesis, and then evaluating the resulting performance of the cathode materials.

- Investigating the use of conductive polymers to enhance both the rate capability and storage capacity of the iron phosphate materials. Determining the physical and electrochemical properties (e.g., structure, surface characteristics) and correlating them with both performance and manufacturing approaches.

- XRD, *in-situ* microscopy, vibrational spectroscopies, and electroanalytical techniques are used to determine signatures and correlations with performance.

- Using solid state nuclear magnetic resonance (NMR) and diffraction/TEM to characterize local and long range structure respectively, as a function of sample preparation method, state of charge, and number of charge cycles.

- Using first principles calculations (density functional theory) to identify redox-active metals, relative stability of different structures, and the effect of structure on cell voltages.

- Adding carbon fibers to improve high-rate performance and diminish the capacity fade due to loss of conductivity/connectivity. This involves improving the point-to-point electronic connections between the fibers, active material particles, and current collector.

- Using microwave assisted chemical deposition to improve the carbon coating on $FePO_4$ particles and thereby improve its high rate performance.

ACCOMPLISHMENTS

Hydrothermal Synthesis of $LiFePO_4$: Control of Particle Size & Morphology, and Phase Transition Study (Richardson[14]) – This project involves the study of various conditions in hydrothermal synthesis and their affects on the morphology and size distribution of crystalline $LiFePO_4$. It has been found that $LiFePO_4$ crystals grow in aqueous solutions containing lithium, iron (II), phosphate, and sulfate ions through a heterogeneous dissolution and reprecipitation process. Reaction parameters including reaction temperature and time, pH of the initial mixture, and overall reactant concentrations are critical. Discrete, well-formed $LiFePO_4$ crystals with dimensions ranging from 50 nm to tens of μm are synthesized through fine-tuning of these parameters. Smaller crystals are obtained at higher reactant concentrations and a slightly basic pH. These adopt a thin hexagonal plate shape with large *ac* surfaces (Figure IV-1, left). The larger crystals obtained in dilute solutions and at lower pH are typically prismatic, with diamond-shaped 010 (ac) faces, and much thicker in the *b* direction, (Figure IV-1, right).

Well-formed, carbon free crystals of $LiFePO_4$ were synthesized using the above described hydrothermal method at 220ºC and a pH close to neutral. Lithium extraction from crystals of different sizes was investigated using chemical oxidation by bromine diluted in ACN. Although crystals with a *b*-axis thickness <2μm were completely converted to $FePO_4$ by a slight excess of oxidant, thicker crystals were only partially oxidized under the same conditions. For example, the crystals in Figure IV-1, right, which are 10μm along *b*, were only 20% oxidized even after prolonged exposure to bromine. Optical and electron microscope images indicate that Li was extracted to a depth of ~ 1μm from a region parallel to the 010 faces. It is proposed that as Li is removed at the $LiFePO_4/FePO_4$ phase boundary, which proceeds in the *a* direction across the face of the crystal, there is a limit to the depth from which Li can be removed before the boundary has moved on and left only $FePO_4$ behind. Once the surface has been converted to $FePO_4$, it is no longer possible to establish a phase boundary and delithiation ceases, because Li cannot pass through the $FePO_4$ layer.

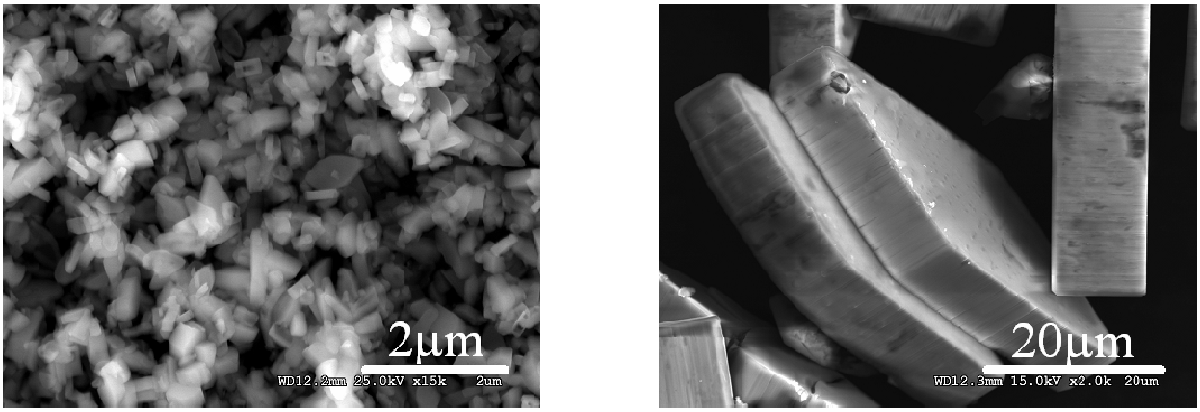

Figure IV-1. SEM images of hydrothermally synthesized $LiFePO_4$ crystals

Also, electron microscopy studies revealed that oxidation of $LiFePO_4$ led to formation of cracks along the *bc* plane of the crystals, clearly seen on both SEM and TEM images. The extent of cracking increased with the level of oxidation. Selected area electron diffraction of $Li_{0.5}FePO_4$

[14] Most projects in the BATT program involve multiple collaborations, often at several institutions. However, the primary POC is identified for each specific task. PI contact information is provided in Appendix A.

crystals showed co-existing crystalline domains of $LiFePO_4$ and $FePO_4$. Alternating light and dark domains of $LiFePO_4$ and $FePO_4$ appeared in TEM images (Figure IV-2, left), and HRTEM revealed crystalline domains separated by a disordered transition zone (Figure IV-2, right).

As lithium is extracted from $LiFePO_4$, the transformation to $FePO_4$ is initiated at the surface parallel to the *ac* plane, where the diffusion paths for both Li^+ and e^- are the shortest. The *a* and *b* axes shrink by 5% and 3.6%, respectively, while the *c* axis expands 2%. The resulting lattice mismatch leads to structural defects such as dislocations. The formation of $FePO_4$ generates the strongest dislocation stress fields in the *ac* plane as Li ions leave the parent phase along *b* during chemical delithiation. The strain is accommodated through the development of an extended disorder zone in the *bc* plane, which translates in the *a* direction leaving $FePO_4$ behind. Since Li is constrained to move only along *b* at room temperature, only the *ac* plane is active for Li extraction or insertion. The next step is to investigate ways to prepare small, thin $LiFePO_4$ plates to further increase the percentage of *ac* surface area, which may improve the electrochemical performance of the material.

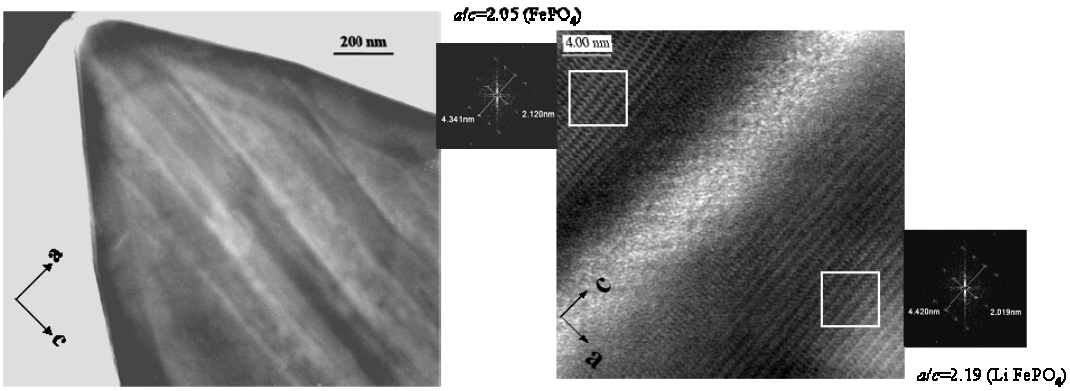

Figure IV-2. TEM image (left) and HRTEM image (right) of a $Li_{0.5}FePO_4$ crystal

Low-Temperature (Low-Cost) Formation of Lithium Iron Phosphate (Whittingham) – This project is studying a low-cost method for forming high-quality $LiFePO_4$. As previously reported, the crystal-structure volume is critical in determining good material, with a minimum temperature of 175°C being desirable. Above this temperature, the lattice volume is the same as materials formed at 700°C, as shown in Figure IV-3. The electrochemical behavior of $LiFePO_4$ formed in the presence of ascorbic acid and carbon nanotubes at 200°C was also investigated. Over 90% of the lithium capacity was removed on charging and 86% inserted on the first discharge. These were tested in a bag cell configuration and showed the same capacity as $LiFePO_4$ formed at 700°C in the same configuration at room temperature. It therefore appears that the hydrothermal low energy synthesis procedure is viable.

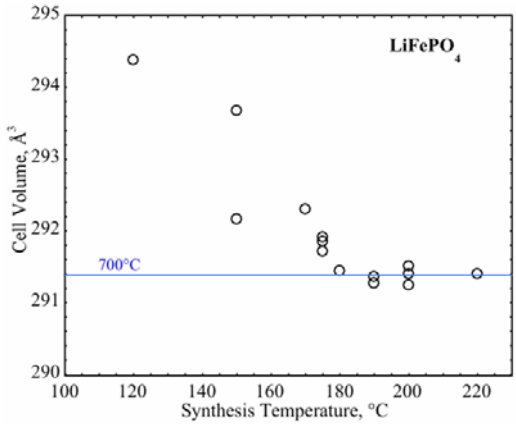

Figure IV-3. Cell volume of $LiFePO_4$, showing the need for a synthesis temperature > 175°C

Theoretical Investigation of Iron Phosphate Phase Diagram (Ceder and Grey) - Using a novel *ab-initio* approach, the phase diagram of the $FePO_4$ – $LiFePO_4$ system has been computed (Figure IV-4). Even though the phase diagram has a highly unusual shape, it is in excellent agreement with the experimental work performed by the groups of Masquelier in France and Fultz at Caltech. The system is phase separating between $FePO_4$ and $LiFePO_4$ at room temperature, but moderately elevated temperature leads to the formation of a solid solution. This work shows that this solid solution is driven by electronic disorder rather than by the typical ionic configurational entropy. This is the first system in which electronic disorder has been shown to drive solid solution formation and is further confirmation that in this material the Li-vacancy motion is strongly coupled to the electronic structure.

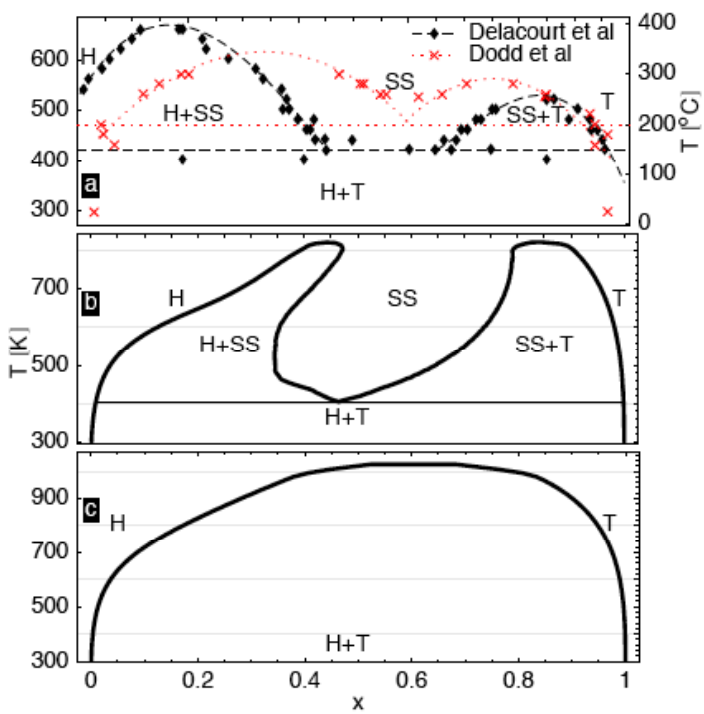

Figure IV-4. $LixFePO_4$ phase diagram: a) experimental phase boundary data taken from Delacourt et al and from Dodd et al; b) calculated with both Li and electron degrees of freedom and c) with explicit Li vacancy disorder only.

Conductive and Electroactive Polymers (Goodenough) – In previous work, an improvement in the rate capability and capacity of cathodes was observed using carbon-coated $LiFePO_4$ (from Phostech Lithium, Inc.) by replacing the carbon and Teflon additives with electroactive polypyrrole (PPy) bonded to the oxide particles by the carbon coat. An excellent charge/ discharge performance at a rate as high as 10C, and even a 3-minute (20C) charge, was achieved with a C-$LiFePO_4$/PPy cathode containing 16 wt% PPy. Both high rate charge and discharge is shown in Figure IV-5.

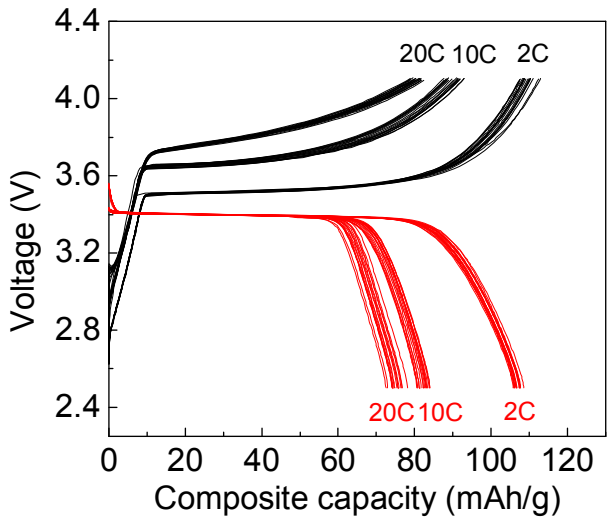

Figure IV-5. Improved discharge and charge rate capability for $(C\text{-}LiFePO_4)_{0.84}(PPy)_{0.16}$

Microwave Assisted Plasma (MPA) Carbon Deposition (Kostecki) – The first objective of this work was to improve the high-rate performance of $LiFePO_4$ by microwave-assisted plasma chemical vapor deposition of graphitic carbon films. The concept is to expose organic precursors to traditional microwave radiation, and to use the resulting graphitic cloud to coat raw cathode particles held in an adjacent container, not exposed to the microwaves. It was determined that improved electrochemical properties of $LiFePO_4$ are associated with a larger ratio of sp2-coordinated carbon, which exhibits better electronic conductivity than disordered or sp3-coordinated carbon. Preliminary experiments revealed that interaction of the organic precursors with low-pressure Ar-plasma and strong electromagnetic radiation led to vaporization and immediate pyrolysis. Thin-films of highly crystalline graphitic carbons of a consistent graphene domain size and excellent electronic conductivity were produced and characterized.

Raw $LiFePO_4$ commercial powder was coated with a thin film of conductive carbon. The carbon film consists of densely packed ~50 nm particles. TEM images of individual carbon grains reveal ~40Å graphene domains. Raman spectra (Figure IV-6) show that the carbon film exhibits graphitic structure that is very similar to the carbons pyrolized at temperatures above 1200ºC. However, XRD and Raman spectra of the microwave carbon-coated $LiFePO_4$ show no indication of structural damage due to overheating.

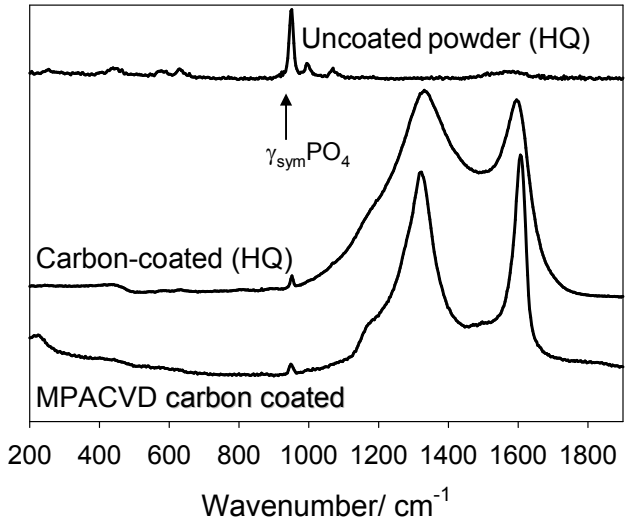

Figure IV-6. Raman spectra of carbon-coated $LiFePO_4$ powders

A preliminary electrochemical evaluation of the carbon-coated powders was carried out. Electrochemical cycling tests of $LiFePO_4$ cathodes with the MPA carbon-coated powder vs. Li anode show a significant improvement of material utilization and power performance compared to electrodes made from the uncoated powder. On the other hand, the MPA carbon-coated electrodes fall short of matching the performance of the-state-of-the-art $LiFePO_4$ cathodes, Figure IV-7. However, there are significant differences in the powders' particle size (1-5 μm vs.200 μm) and morphology which may be responsible for the discrepancies in performance. A new batch of uncoated 200 nm particle-size $LiFePO_4$ powder was procured from Hydro-Québec. The comparative experiments of MPA-coated $LiFePO_4$ electrodes are still being conducted and a full evaluation of this technology will be completed.

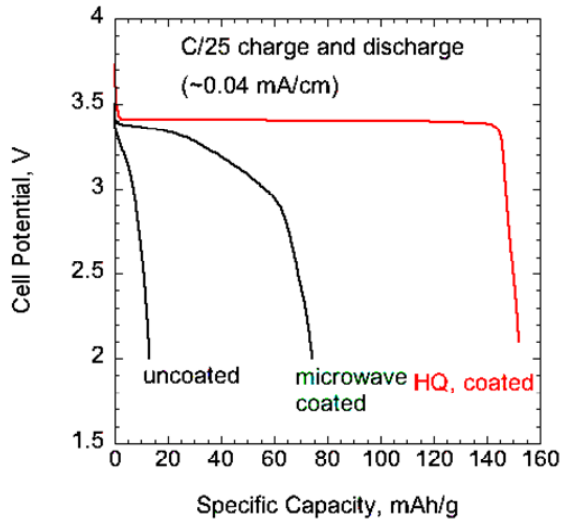

Figure IV-7. C/25 discharge capacity of uncoated, HQ carbon-coated, and MPA carbon-coated $LiFePO_4$.

Carbon Films and Their Impact on Capacity Fade (Doeff) – A recent TEM study (with H. Gabrisch, U. of New Orleans) of a $LiFePO_4$ sample containing 1.45 wt. %C, which was produced in the LBNL laboratory, shows that there is a carbon coating approximately 5nm thick on the active material. Two electrodes containing this material were cycled in lithium cells, and a postmortem TEM analysis was carried out to determine the fates of the coatings. One cell was cycled at low current densities (JF-1C, C/25) with good capacity retention, while the other was discharged at higher rates (JF-1B-A, C/2) and exhibited losses (Figure IV-8). The TEM work shows that the carbon coatings remained nearly intact in both cases, although cracks along the 020 lattice plane (using setting Pnma) were also observed. Furthermore, electron diffraction patterns show evidence of stacking faults. The virgin material is now being re-examined to determine whether the stacking faults were present initially or were induced by cycling. However, these changes in the cathode active materials cannot be responsible for the observed capacity fading in cell JF-1B-A, as they were seen for both samples. The reason for the degradation in performance cell JF-1B-A remains, as yet, undetermined.

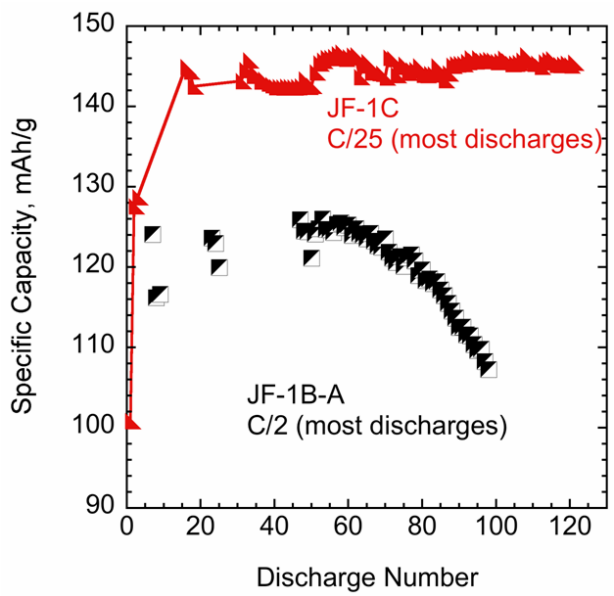

Figure IV-8. Cycling data for two Li/$LiFePO_4$ cells, discharged at two different rates (C/25 for cell JF-1C and C/2 for cell JF-1B-A).

New Conductive Carbons (Wheeler) – The primary tasks in this evaluation of conductive carbons are to fabricate and test cells to determine morphologies and material combinations that enable high-rate performance of $LiFePO_4$ cathodes, and to better understand the associated physical processes. Towards this end, cycle-life testing of cells with different carbon compositions has been undertaken. Additionally alternatives to using carbon-coated aluminum current collectors, which have been found to improve $FePO_4$ performance, are being tested.

Figure IV-9 shows HEV cycle-life data for four different $LiFePO_4$ cells. Two of the cells contained carbon fibers and carbon black (4% each) while the other two contained graphite and carbon black (4% each). The cells with fibers show lower ASI as compared to cells with graphite. The cells containing graphite initially show a drop in ASI, which is not observed in fiber-containing cells. It appears that "settling" or other short-term physical changes may occur

with lower-aspect-ratio carbons that are not observed with the carbon fibers. Based on this data, it appears that the growth in ASI during long-term cycling is similar for the different compositions, and so it is important for the initial ASI to be as low as possible. In addition, the ASIs are almost a factor of five too high for HEV use, thus better performing cells will be constructed to further test the usefulness of carbon fibers.

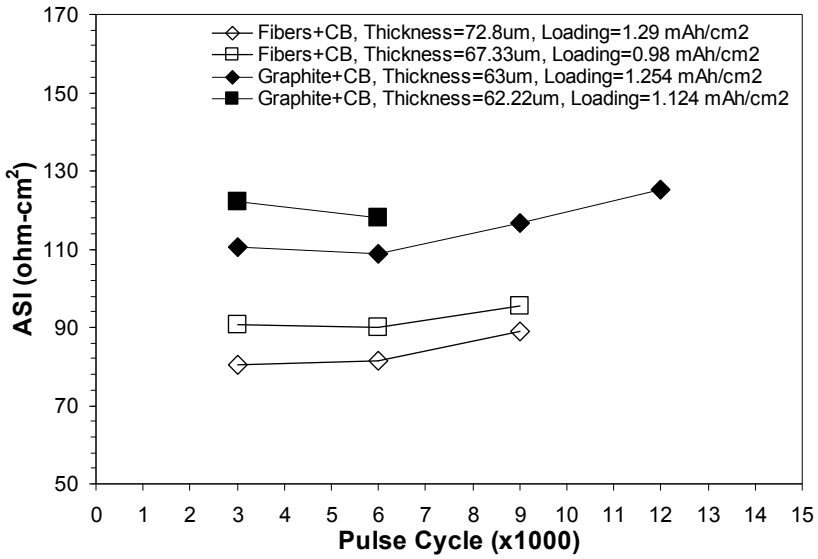

Figure IV-9. HEV cycle-life testing of ASI for cells with different conductive fillers. Each cycle consists of 10s discharge, 40s rest, 10s charge, and 40s rest. Pulses were performed at the 5C rate and at 30% DOD.

In addition, cathodes that utilize current collectors (CCs) with rough (abraded) aluminum surfaces as opposed to carbon-coated aluminum surfaces are being tested. If an abraded aluminum surface performs well as a current collector, then its use would be attractive from a manufacturing standpoint. For cells with small active-material loadings, the rough-aluminum cells have similar ASIs as cells with carbon-coated CCs, whereas for higher-loading cells the carbon-coated cells perform better.

Investigation into Higher Energy Phosphates (Goodenough) – Since Fe^{2+} and Mn^{2+} are stable in a reducing atmosphere, $LiFe_{1-x}Mn_xPO_4$ can be coated with carbon for the composite cathodes with PPy. $LiFe_{1-x}Mn_xPO_4$ was prepared via a wet-chemical route with *in-situ* carbon coating. Although all the as-prepared samples were phase-pure, $LiFePO_4$ showed a specific capacity of 130 mAh/g at C/10 whereas $LiFe_4Mn_{0.75}PO_4$ and $LiMnPO_4$ showed poorer capacities. With substitution of Fe^{2+} with Mn^{2+}, the capacity dramatically decreased. The inability to extract Li from $LiMnPO_4$ despite a V_{oc} (4.1 V vs. Li+/Li) suggests that the larger Mn^{2+} ion is not well-ordered and tends to block the Li-ion channels.

In-situ and Ex-situ Investigation of Phosphates (Yang) – This work is investigating changes in the electronic structural of electrochemically delithiated $Li_{1-x}Fe_{1-y}M_yPO_4$ (M=Mn, Co, Ni) materials using *in-situ* metal K-edge XAS and *ex-situ* P K-edge XAS. The major charge compensation of $LiFe_{0.5}Co_{0.5}PO_4$ during Li extraction is achieved by the oxidation of Fe^{2+} and Co^{2+} to Fe^{3+} and Co^{3+} resulting in more covalent Fe-O and Co-O bonds. In the olivine $LiMPO_4$ structure, polarization of the electrons of the oxygen ions towards the phosphorus ion reduces the

covalent bonding to the iron ion by the inductive effect. Likewise the increased covalency of M (= Fe, Co) -O bonds makes P-O bonds less covalent by the same inductive effect.

It is notable that chemical changes beyond the first coordination sphere around the phosphorus atoms have a systematic influence on the observed XANES spectrum. No pre-edge peak was observed in P K-edge XANES spectrum for the pristine $LiFe_{0.5}Co_{0.5}PO_4$. Upon Li deintercalation, however, pre-edge peaks start to appear in the lower energy region of the main edge, Figure IV-10. The gradual increase of pre-edge peak intensities with the Li-ion extraction at low states of charge ($x<0.4$) shows that these peaks are mainly due to the hybridization of P 3p states with the Fe 3d states. In contrast, at high states of charge ($x>0.4$) the peak intensity of the pre-edge shows relatively smaller change indicating that Co is not rigorously involved in the hybridization of P 3p states with the M 3d states. It is important to note that such hybridization between P 3p and M 3d states occurs in spite of the presence of oxygen atoms that separate phosphorus ions from metal ions. Consequently, the electronic structure of orthophosphates cannot be regarded as composed of traditional ion pairs for $(Li^{+})(M^{2+})$-(PO_4^{3-}) and (M^{3+})-(PO_4^{3-}) which are charged according to their formal valence.

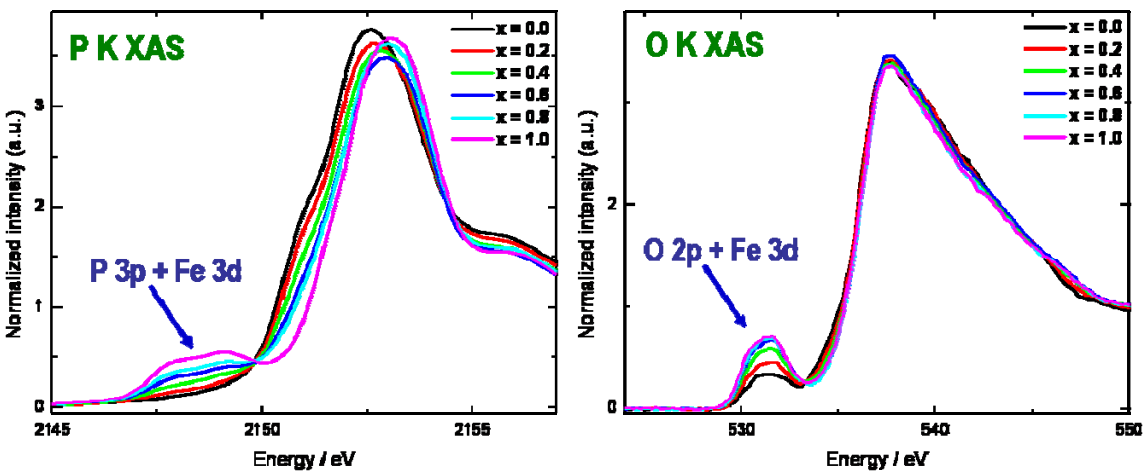

Figure IV-10. XAS of iron phosphate during charge

FUTURE PLANS

Low-Temperature Formation of Lithium Iron Phosphate

- Investigate how to form material with smaller particle sizes, which should enhance the rate capability (the present material is ~one to two μm in size).
- Investigate dopants to increase single phase regions and Li mobility.
- Control particle shape.
- Test cells near 60°C to see if 100% capacity can be obtained.

Theoretical Investigation of Phase Diagram

- Construct an integrated model for the intrinsic rate capability of $LiFePO_4$ electrodes using structural information gained from this study with the previously obtained migration barriers for electrons and Li ions.
- Investigate the timescales of Li-ion mobility through variable temperature 6,7Li and 31P NMR studies.

Conductive and Electroactive Polymers

- Investigate ways to carbon coat other cathode oxides that are susceptible to reduction during the coating process.
- Prepare C-coated $LiFePO_4$ particles from amorphous $FePO_4 \cdot xH_2O$ powders synthesized by a controlled crystallization method and then bond the particles to PPy via electro deposition.

New Conductive Carbons

- Continue investigations into improved power and HEV cycle life of fiber-containing $LiFePO_4$ cathodes and into possible failure mechanisms.
- Model $LiFePO_4$ cathodes and perform experiments to determine main contributor to resistances.
- Develop and investigate novel structured current collectors.

Evaluation of new $FePO_4$ materials

- Study effects of impurities in $LiFePO_4$ on cell performance.
- Introduce a new generation of $LiFePO_4$ (molten state) from Phostech; use with water soluble binder (WSB) in laminate cells and compare electrochemical performance to standard $LiFePO_4$.
- Investigate Co-synthesis of $LiFePO_4$ and carbon nanotubes
    - Addition of conducting nanotubes to electrodes can reduce the amount of carbon that needs to be added to composite electrodes,
    - Cost, health, safety, and fabrication advantages to co-synthesis over mixing in pre-made nanotubes.

***In-situ* diagnostics**

- Perform *in-situ* XRD studies of $LiFePO_4$ at different temperatures (-30ºC to 50ºC) at various cycling rates.

IV.A.2 Spinel and Composite Systems: Performance and Limitations

OBJECTIVES

Mn is inexpensive, environmentally benign, and has inherently high rate capability. However, it suffers large capacity loss at high temperatures, particularly when cycled against carbon-based anodes. Thus, the objective of this task is to develop low-cost spinel manganese oxides that offer excellent capacity retention, low irreversible capacity loss, and good storage characteristics at elevated temperatures, all consistent with the goals of the FreedomCAR program. Another objective is to develop low-cost, high-energy and high-power Mn-oxide-based cathodes with two-component structures.

APPROACH

One approach is to develop a firm scientific understanding of the factors that influence the performance of spinel cathodes and utilize that knowledge to design and develop improved materials. In this regard, a variety of single and multiple cationic substitutions for manganese, anionic substitutions for oxygen, and an optimization of the microstructure and morphology are being pursued. The resulting compositions are characterized by diffraction, spectroscopic, and electrochemical techniques to establish a structure-composition-property-performance relationship.

A second approach is to search for, characterize, and develop low-cost manganese oxide cathodes using high-voltage, high-capacity electrodes with two-component 'composite' structures, e.g., 'layered-layered' $xLi_2M'O_3 \bullet (1-x)LiMO_2$ and 'layered-spinel' $xLi_2M'O_3 \bullet (1-x)LiM_2O_4$ electrodes in which M′ is predominantly Mn and M is selected predominantly from Mn, Ni and Co. These electrodes are then evaluated in full cells against graphite and intermetallic anodes in conjunction with this program's anode projects.

The microstructure of oxide-electrolyte interface with and without nanoparticle coating and its stability as a function of potential and cycle number is examined *ex-situ* and *in-situ* by TEM and electrochemical AFM. Transport processes and properties in the bulk cathode and at the oxide-electrolyte interface, and their changes as a function of potential and cycle number, are analyzed by galvanostatic testing at different current densities.

Finally, a combination of *in-situ*, *ex-situ* and time resolved synchrotron based x-ray techniques are used to characterize these spinels, as described in IV.A.1.

ACCOMPLISHMENTS

Doped Spinels (Manthiram) – Previous investigations showed that certain cationic substitutions for Mn, as well as fluorine substitutions for oxygen, in the spinel manganese oxides lowered the lattice parameter difference Δa between the two cubic phases formed during the charge-discharge process and reduced the amount of manganese dissolution, which in turn led to superior capacity retention at elevated temperatures (60ºC) in the Mn/Li metal system. With an aim to elucidate the relationship between Δa and the Mn dissolution, the amount of Mn dissolution in the two-phase region has been monitored by soaking the chemically delithiated $Li_{1-x}Mn_{2-y-z}Li_yM_zO_{4-\eta}F_\eta$ powders with $(1-x) \approx 0.3 - 0.5$ in the electrolyte at 55ºC for 7 days. It is found that the amount of Mn dissolution in the two phase region decreases with decreasing Δa (as found before with a fully

discharged sample,) demonstrating that a larger Δa leads to a higher amount of manganese dissolution, which in turn results in a higher capacity fade.

Also, the Mn dissolution at different DoDs of the oxyfluoride spinel $LiMn_{1.8}L_{0.1}Ni_{0.1}O_{3.8}F_{0.2}$ has been monitored and compared with that of $LiMn_2O_4$ after storing at 55ºC for 7 days at various DoDs. The amount of dissolved Mn from $Li_{1-x}Mn_2O_4$ ($0.14 \leq 1\text{-}x \leq 1$) decreases slightly from 3.2 to 2.9 wt% with decreasing Li content due to an increase in the oxidation state of Mn. In contrast, the amount of dissolved Mn from $Li_{1-x}Mn_{1.8}Li_{0.1}Ni_{0.1}O_{3.8}F_{0.2}$ decreases from 0.8 to 0.6 wt% with decreasing Li content, confirming that the cationic and anionic substitutions help to reduce Mn dissolution and improve the electrochemical performance. Also, the fluorine incorporated spinel cathodes such as $LiMn_{1.8}Li_{0.1}Ti_{0.1}O_{3.9}F_{0.1}$ exhibit improved storage properties compared to their oxide analog, Figure IV-11.

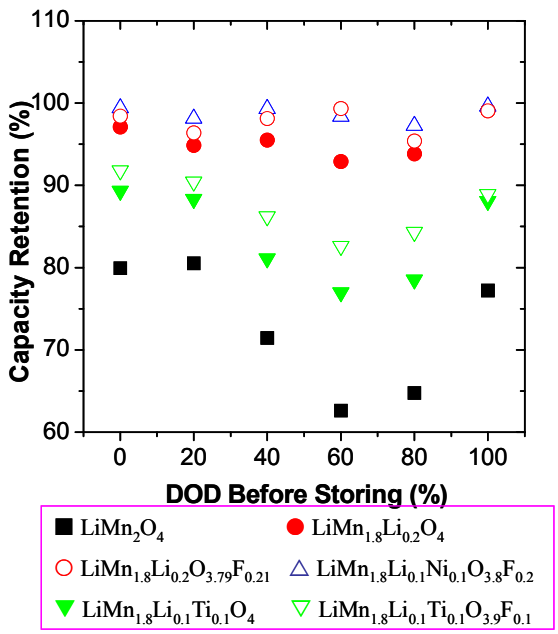

Figure IV-11. Capacity retention of various spinels (vs. Li metal) after storage at 55ºC for 7 days

The ASI of $LiMn_2O_4$, $LiMn_{1.8}L_{0.1}Ni_{0.1}O_4$, and $LiMn_{1.8}L_{0.1}Ni_{0.1}O_{3.8}F_{0.2}$, before and after cycling at 60ºC, has also been measured employing the L-HPPC test at room temperature. Although all three samples have a similar ASI value of 25-35 Ωcm^2 at 50% DOD before cycling, it increases to 120, 87, and 78 Ωcm^2, respectively after cycling at 60ºC, possibly due to changes in electrode kinetics, Li-ion diffusion, and ohmic drop. A smaller rise in ASI for the cation-substituted spinel oxide and oxyfluoride attest to their better electrochemical performance compared to $LiMn_2O_4$.

In addition to the evaluations with Li metal anodes described above, electrochemical tests have been carried out with Li-ion cells fabricated with the spinel cathodes and commercial carbon or $Li_4Ti_5O_{12}$ anodes. While the $LiMn_2O_4$/C cell shows a severe capacity fade of 33% after 30 cycles, the $LiMn_{1.85}Li_{0.075}Ni_{0.04}Al_{0.035}O_4$/C and $LiMn_{1.8}L_{0.1}Ni_{0.1}O_{3.8}F_{0.2}$/C cells exhibit better cyclability with a (still significant) capacity fade of, respectively, 22 and 16% after 30 cycles. The cell fabricated with the $Li_4Ti_5O_{12}$ anode shows better cyclability than that fabricated with the carbon

anode due to the well-known interaction of the dissolved Mn with the carbon anode, as shown in Figure IV-12, where (■) $LiMn_2O_4$/C, (▲) $LiMn_{1.85}Li_{0.075}Ni_{0.04}Al_{0.035}O_4$/C, (▼) $LiMn_{1.8}Li_{0.1}Ni_{0.1}O_{3.8}F_{0.2}$/C, (△) $LiMn_{1.85}Li_{0.075}Ni_{0.04}Al_{0.035}O_4/Li_4Ti_5O_{12}$.

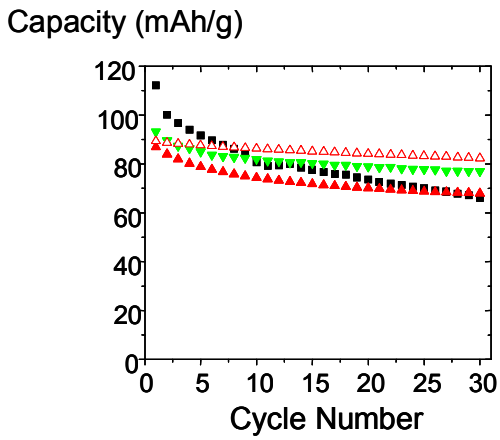

Figure IV-12. Cyclability of Li-ion cells at 60ºC and C/5 rate,

In-situ Diagnostics of Spinels (Yang) – To investigate the origins of the greater stability of the doped spinels, *in-situ* diagnostics were performed on a nearly pristine spinel and a doped spinel. The results, shown in Figure IV-13, show that the "nearly pristine" $Li_{1.04}Mn_{1.96}O_4$ spinel shows a clear phase transition from C1 to C3 via C2, whereas the multi-doped spinel shows continuous phase changes without discrete phase separation. It was also found that the unit cell volume of the multi-doped spinel shows a smaller change than that of the $Li_{1.04}Mn_{1.96}O_4$ spinel, which may give the multi-doped spinel a better structural reversibility for a longer cycling life.

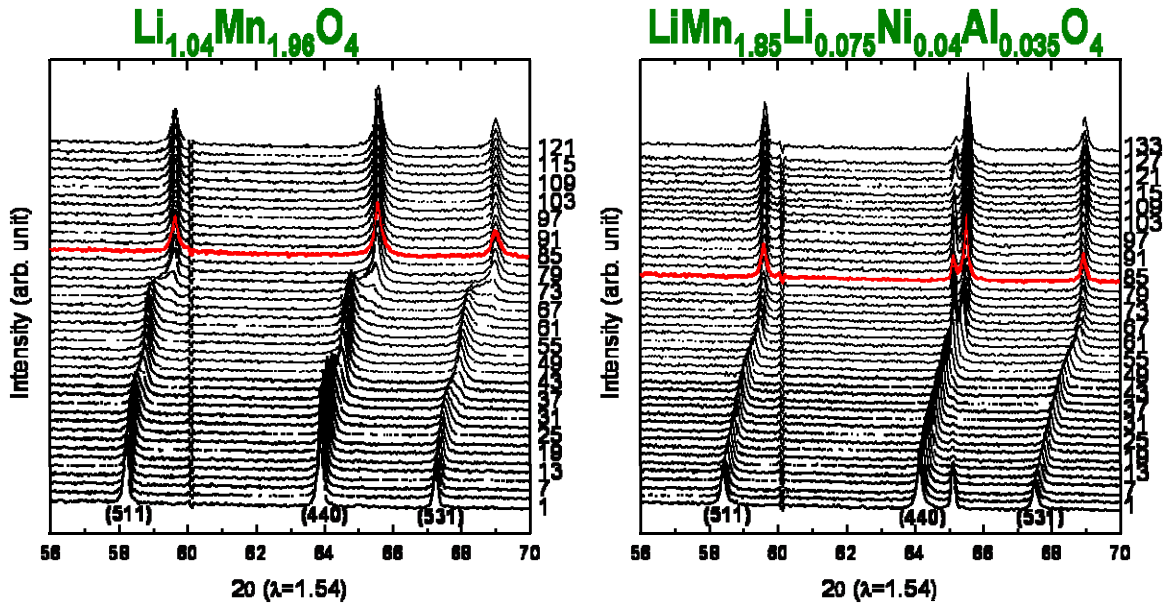

Figure IV-13. *In-situ* XRD of $Li_{1.04}Mn_{1.96}O_4$ and $LiMn_{1.85}Li_{0.075}Ni_{0.04}Al_{0.035}O_4$

Layered and Spinel Composite Cathodes (Thackeray) – In this task, the goal is to develop Mn-rich, high-energy oxide cathodes for Li-ion cells. It has been established that Li- and Mn-rich

Li-Mn-Ni-Co-O electrodes with layered structures deliver high capacities (200-250 mAh/g) when cycled between 4.6 and 2.0 V in lithium cells. The composition of these electrodes can be represented in two-component notation as $Li_2MnO_3 \bullet LiMO_2$ in which M=Mn, Ni and Co. Charging the electrodes to potentials >4.5 V removes Li_2O from their structures, which results in an irreversible capacity loss on the first cycle.

Work continues on an approach to counter this first-cycle capacity loss by leaching Li_2O from the Li_2MnO_3 component of a mildly fluorinated Li- and Mn-rich $0.5Li_2MnO_3 \bullet 0.5LiNi_{0.44}Co_{0.25}Mn_{0.31}O_2$ electrode with acid prior to cell assembly. In principle, such a preconditioning step can be used to balance the anode and cathode of a cell with respect to the amount of Li to be transported between the electrodes during charge and discharge. The first several cycles of this cell between 4.6 and 2.0 V is shown in Figure IV-14.

Acid treatment eliminates the first-cycle capacity loss without compromising the high capacity of the as-prepared electrode (~250 mAh/g); it is also clear that a 2-hour leach is as effective as a 24-hour leach. dQ/dV plots of untreated and acid-treated electrodes develop similar, but not identical, character, suggesting a coalescence and redox interaction of the Mn ions in the MnO_2-rich and $5LiNi_{0.44}Co_{0.25}Mn_{0.31}O_2$ regions of the structure, consistent with the gradual slope of the discharge curve between 4.6 and ~2.7 V. The data (not shown here) demonstrates that the cycling efficiency of the electrodes decreases with increasing leach time, the as-prepared electrodes being >99% coulombic efficient, while electrodes after a 24-h leach were <97% efficient. Thus it appears that the electrode surface is damaged by the acid treatment. Techniques to counter the damage of these acid-treated electrodes are currently being examined.

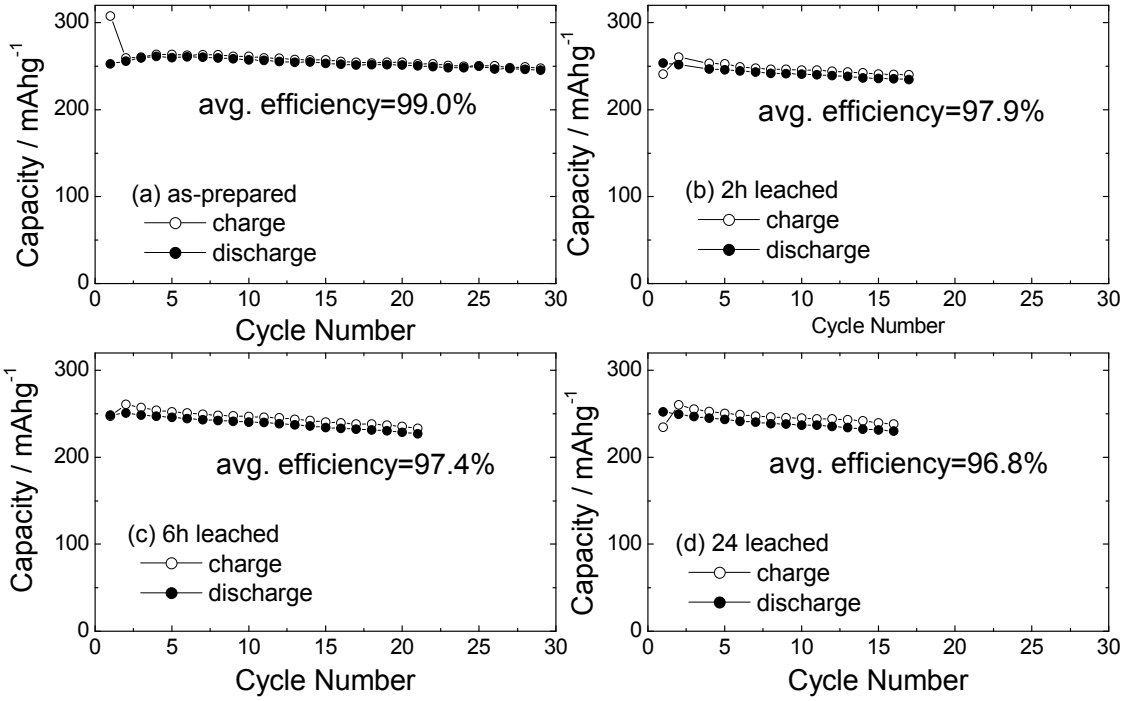

Figure IV-14. Capacity vs. cycle number of cells (a) as-prepared; (b-d) acid-treated cathodes

Structural Changes (Thackeray) – This team is also characterizing the structures of chemically- and electrochemically activated electrode materials. Specifically, they have combined neutron diffraction (ND) and gas analyses of the system $0.5Li_2MnO_3$-$0.5LiNi_{0.5}Mn_{0.5}O_2$. Neutron data sets were collected at three points during the initial charge. The total amount of Li extracted at 4.8 V was 1.13 Li per $Li[Li_{0.2}Ni_{0.2}Mn_{0.6}]O_2$ formula unit, 0.4 of which could be compensated for by Ni(II) oxidation (<4.5 V) and 0.73 by oxygen loss (>4.5 V).

In-situ differential electrochemical mass spectroscopy (DEMS) demonstrated unequivocally that the 4.6V plateau observed experimentally was associated with the loss of oxygen gas. The amount of CO_2 released was estimated to be less than 10% the amount of oxygen. Structural refinements of the electrode during the initial charge to 4.8 V revealed that the small amount of Ni in the Li layer was not significantly mobile; and also confirmed that the removal of Li above 4.5 V was accompanied by the loss of oxygen from the structure. The structural refinements suggest that as oxygen is evolved from the electrode surface at high potentials, Li vacancies in the transition metal layer become occupied through a cooperative displacement of the transition metal ions from the surface of the electrode structure into the bulk, thereby retaining the close-packed layered character of the structure.

A new series of structurally-integrated 'layered-spinel' electrodes, $xLiNi_{0.5}Mn_{0.5}O_2 \bullet (1-x) Li(Ni_{0.5}Mn_{1.5})O_4$ ($0 \leq x \leq 1$), have also been synthesized; produced by reacting Li_2CO_3 with appropriate amounts of co-precipitated $Ni_{1-y}Mn_y(OH)_z$ precursors at 900°C in air. XRD patterns provided clear evidence of the coexistence of the layered and spinel components as shown, for example, in the diffraction pattern of $0.6LiNi_{0.5}Mn_{0.5}O_2 \bullet 0.4Li(Ni_{0.5}Mn_{1.5})O_4$ (Figure IV-15). Electrochemical, NMR and TEM data are currently being collected on this series of electrodes

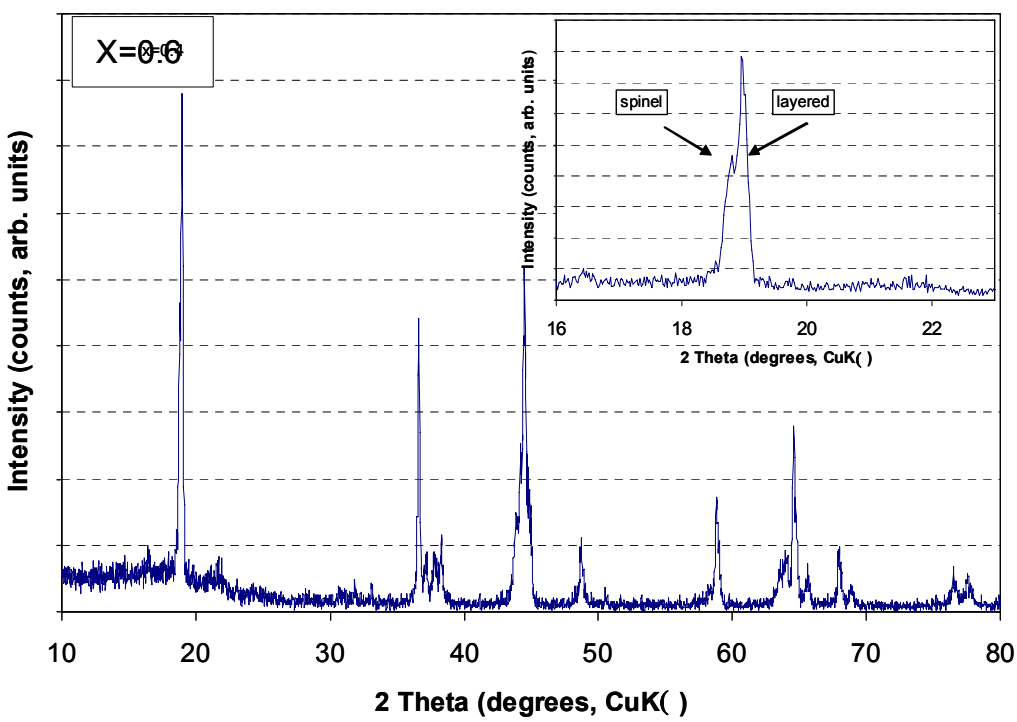

Figure IV-15. XRD pattern showing evidence of layered and spinel phases.

Nanoparticle Coatings and Improved Electrode Stability (Horn) - $AlPO_4$ nanoparticle coatings on $LiCoO_2$ have been reported to show the best rate and cycling stability to high voltages with respect to other coating chemistry. Thus, this group has applied $Al_xP_yO_z$ nanoparticle coatings onto $LiMn_2O_4$ samples and are examining their structure and cycling stability.

TEM studies showed that the nanoparticles had sizes in the range of 20-50 nm and appear to be crystalline. However, the surfaces were not well covered. The exact crystal structures of the nanoparticles are being investigated. Scanning transmission electron microscopy and energy dispersive spectroscopy of 2wt% and 5wt% coated samples showed that both P and Al elements were uniformly distributed on the particles, Figure IV-16.

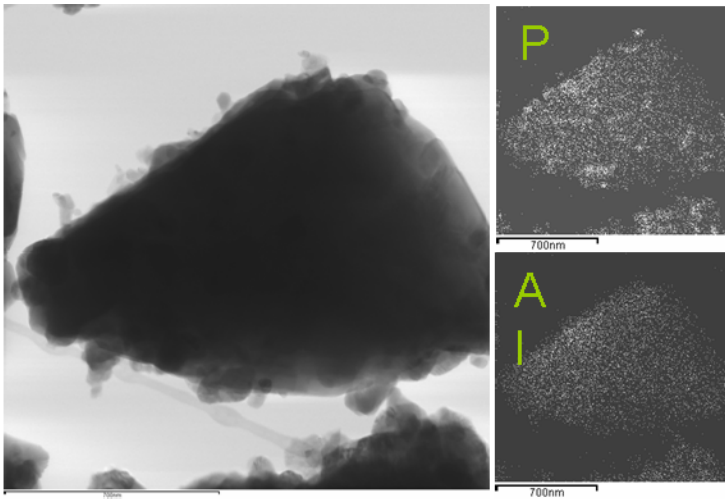

Figure IV-16. TEM image of the 2wt% $Al_xP_yO_z$ coated $Li_{1.05}Mn_{1.95}O_4$ sample (Left); STEM EDX mapping of P and Al on the crystal (Right).

Although the coated samples showed better cycling stability than uncoated samples (Figure IV-17), preliminary results showed that the coated samples had much lower capacities than the uncoated electrodes at intermediate current densities such as C/5. Efforts will be focused on understanding the coating microstructure and chemistry, reducing the particle size and improving particle coverage.

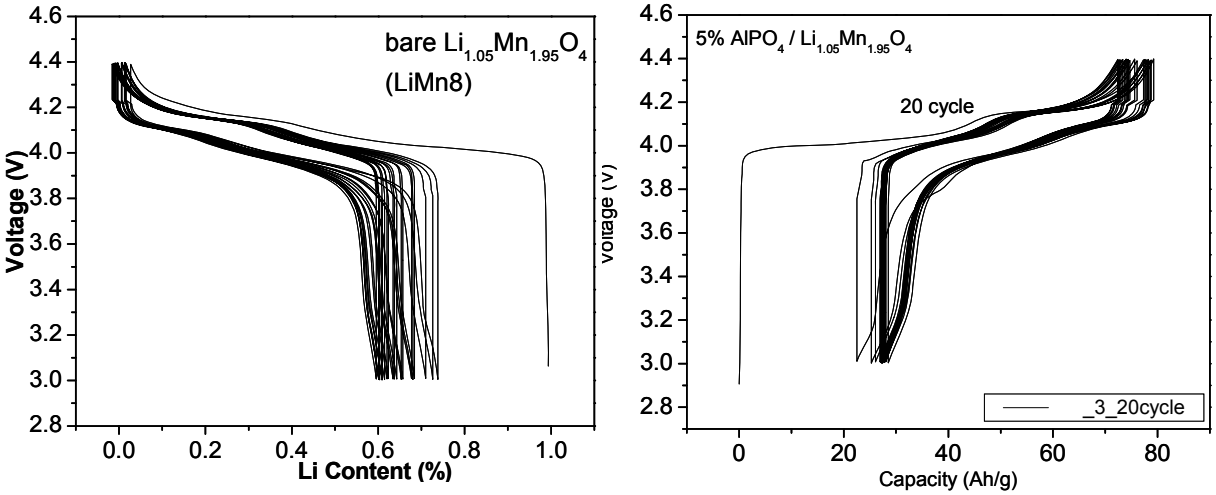

Figure IV-17. Voltage profiles of Li/$Li_{1.05}Mn_{1.95}O_4$-uncoated cycled at a rate of C/5 (Left); Voltage profiles of Li/$Li_{1.05}Mn_{1.95}O_4$-5wt% coated cycled at a rate of C/5.

FUTURE PLANS

Doped Spinels

- Utilizing the knowledge gained with the $LiMn_2O_4$ system, continue an investigation into $Li_4Mn_5O_{12-\eta}F_\eta$ oxyfluorides. The synthesis and processing conditions will be optimized and the performances of the $Li_4Mn_5O_{12-\eta}F_\eta$ oxyfluorides will be evaluated.
- Investigate oxygen deficient spinels to increase the capacity further.
- Compare and evaluate the consequences of metal ion dissolution in various cathodes.

'Layered-Layered' and 'Layered-Spinel' Electrodes

- Optimize integrated 'layered-layered' and 'layered-spinel' electrodes.
- Determine how to optimize capacity (200-250 mAh/g) and power.
- Evaluate low-temperature behavior and electrochemical behavior in full cells.
- Investigate reduction of first-cycle irreversible capacity loss (acid-treatment).
- Investigate the structure – electrochemical property relationships using *in-situ* XRD and XAS, neutron diffraction, NMR, high resolution transmission electron microscopy (HRTEM), etc.

Nanoparticle Coatings and Improved Electrode Stability

- Establish correlation between the microstructure and transport properties for uncoated $LiNi_{1/3}Mn_{1/3}Co_{1/3}O_2$ and $LiMn_2O_4$.
- Complete EIS, GITT and TEM studies of commercially available $LiNi_{1/3}Mn_{1/3}Co_{1/3}O_2$.

IV.A.3 Nickelate Systems: Performance and Limitations

OBJECTIVES

The primary objective of this work is to evaluate alternative Ni-based cathode materials for high power Li-ion batteries. A second objective is to determine the effect of structure on cathode stability, and specifically to explore rate limitations and their relation to structure.

APPROACH

Solid state NMR is used to characterize local structure, and diffraction/TEM for long range structure, as a function of sample preparation method, state of charge, and number of charge cycles for layered nickelate materials. First principles calculations (density functional theory) are used to identify redox-active metals, determine the relative stability of different structures, and the effect of structure on cell voltages and to identify promising cathode materials. The results of this investigation have shown a direct correlation between preparation method, resulting structure, and performance.

Another approach used to characterize nickelate systems is a combination of *in-situ*, *ex-situ* and time resolved synchrotron based x-ray techniques. The surface and bulk of electrodes signatures are identified using *ex-situ* soft XAS through electron yield (EY) and fluorescence yield (FY) detectors, respectively. A time-resolved XRD technique is also used to understand the reactions that occur in charged cathodes at elevated temperatures in the presence of electrolyte. Hard and soft XAS are used to elucidate the charge compensation mechanisms for cathode materials during cycling.

Microwave Plasma Assisted Chemical Vapor Deposition (MPACVD) has been developed and is being used to produce highly conductive graphitic films directly on cathode active material powders. Also, Raman microscopy and ^{13}C carbon additive marker were used to monitor carbon distribution changes within tested cells.

Different ion exchange routes were explored for preparing $LiNi_{1-x}Mn_xO_2$ samples from $NaNi_{1-x}Mn_xO_2$. A sol-gel method based on a complex with citric acid and ethylene glycol was used for the $NaNi_{1-x}Mn_xO_2$ preparation. Two different methods, *i.e.* a molten-salt route with $LiNO_3$ and LiCl as Li sources, and a liquid-flow route with LiBr in alcohol as the Li source, were used for ion exchange.

ACCOMPLISHMENTS

Studies on $LiNi_{1-x}Mn_xO_2$ (Ceder/Grey) – A key milestone has been achieved in understanding the chemical and structural factors that affect the rate capability of layered compounds and that knowledge has been used to develop a $Li(Ni_{0.5}Mn_{0.5})O_2$ material with superior rate performance.

$Li(Ni_{0.5}Mn_{0.5})O_2$ is environmentally friendly, has the potential to be low cost, and has some of the best thermal stability in the classes of Ni-Mn-Co layered materials, but previously was unable to sustain high rates. First principles computations have been used to evaluate the factors that affect this rate performance. The results show that a material with a 50% Ni^{2+} content should have intrinsically high Li mobility as the activation energy for Li migration near Ni^{2+} is lower than near

any other cation tested. But the largest factor to influence the Li mobility is found to be the interslab space (*i.e.* the distance between the oxygen layers that surround the Li layer).

Ab-initio computations of the activation energy as function of the distance between the oxygen layers on each side of the Li planes show that as the layer-to-layer distance grows, the activation energy for Li motion decreases dramatically. This explains why traditional solid state $Li(Ni_{0.5}Mn_{0.5})O_2$ does not have good rate capability: The large amount of Li/Ni exchange between the layers reduces the Li-slab distance (and more importantly, reduces its opening upon delithiation), Figure IV-18.

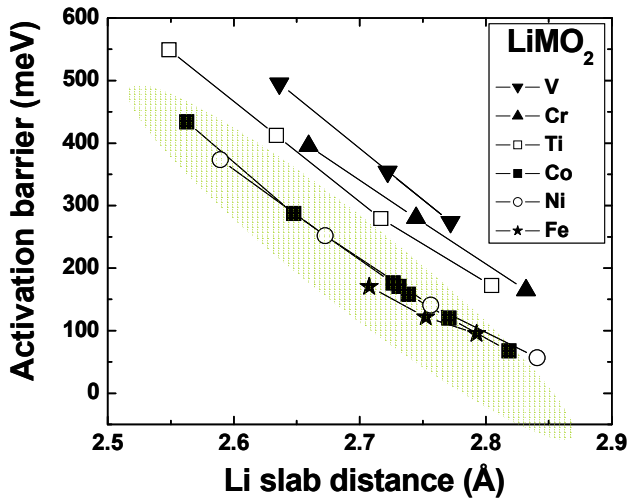

Figure IV-18. Li migration activation energy vs. interlayer spacing for several "M" atoms

To test this hypothesis a well layered material with significantly less Li/Ni ion-exchange was prepared by ion-exchanging it from a $Na(Ni_{0.5}Mn_{0.5})O_2$ precursor. NMR on the ion-exchanged material confirms that very little Li is present in the transition metal layer. Initial rate tests show that this material has excellent rate capability, Figure IV-19. With this proof of concept, the structural and chemical factors that control rate in layered oxides are much better understood.

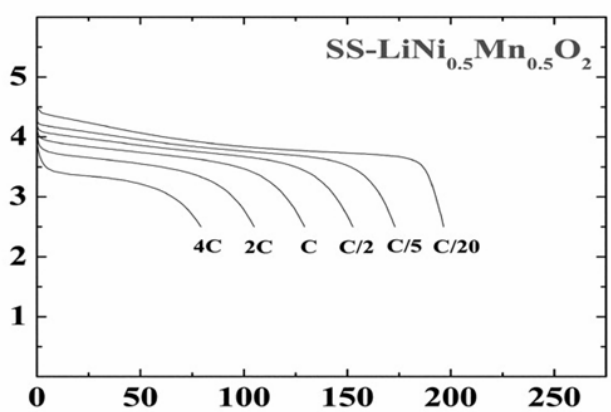

Figure IV-19. Rate capability of well ordered $LiNi_{0.5}Mn_{0.5}O_2$

Preparation Routes for Layered Structures (Goodenough) – Different ion exchange routes were explored for preparing $LiNi_{1-x}Mn_xO_2$ samples from $NaNi_{1-x}Mn_xO_2$. A sol-gel method based on a complex with citric acid and ethylene glycol was used for the $NaNi_{1-x}Mn_xO_2$ preparation. It was found that a single phase could be obtained only with $x \geq 0.5$; otherwise an NiO impurity phase would appear. Two different methods, *i.e.* a molten-salt route with $LiNO_3$ and LiCl as Li sources, and a liquid-flow route with LiBr in alcohol as the Li source, were used for ion exchange. With both methods, a pure $LiNi_{0.5}Mn_{0.5}O_2$ phase was obtained. The capacity of the $LiNi_{0.5}Mn_{0.5}O_2$ sample prepared by ion-exchange with the molten-salt route was 160 mAh/g at C/10.

Next, the effects of stoichiometry in the starting materials and sintering temperature on the structure and electrochemical performance were investigated. Rietveld refinement showed that the sample with a 20% excess Li source in the starting materials sintered in air at 600ºC for 3 h and further at 900ºC for 5 h exhibited a perfectly ordered structure. A discharge capacity as high as 190 mAh/g was obtained at C/20 in the voltage range of 4.5-2.7 V. As shown in Figure IV-20, the ordered $LiNi_{2/3}Mn_{1/3}O_2$ sample exhibits excellent rate capability. Even at 5C, the discharge capacity is higher than 100 mAh/g.

However, the cycle stability is not very good. About 24% fade was observed after 50 cycles. In order to enhance cycle life, this sample was coated with carbon, $LiAlO_2$, Al_2O_3 and SiO_2. It was found that coating with SiO_2 was most effective. The specific capacities vs. cycle number for $LiNi_{2/3}Mn_{1/3}O_2$ and SiO_2 (3wt%)-coated $LiNi_{2/3}Mn_{1/3}O_2$ at a rate of 0.1 C (4.3-2.7V) were compared. Only 5% fade in capacity was observed after 100 cycles for the latter. The improvement in cycle stability by SiO_2 modification can be ascribed to the protection of the $LiNi_{2/3}Mn_{1/3}O_2$ particles from dissolution into the electrolyte.

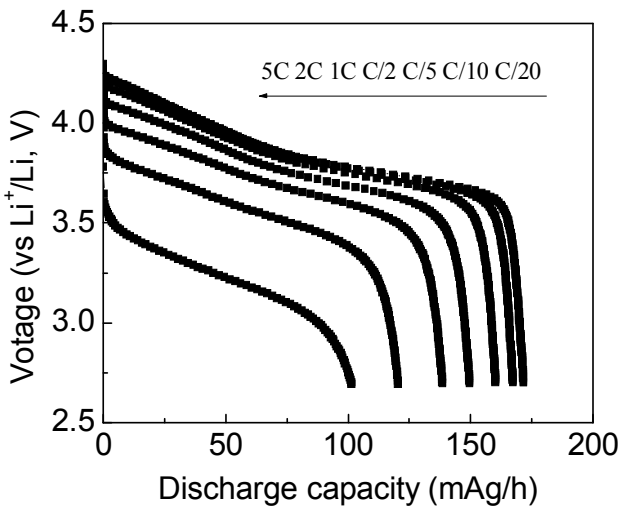

Figure IV-20. Specific discharge capacity at various rates for the ordered $LiNi_{2/3}Mn_{1/3}O_2$ sample (4.3-2.7V).

Layered Mixed Metal Oxides (Whittingham) – This work continues the exploration of the effect of reducing cobalt content in $LiNi_yMn_yCo_{1-2y}O_2$. Recent work concentrated on the effect of the addition of a few per cent excess lithium on the electrochemistry of the phase containing 10% cobalt: $Li_{1.024}(Ni_{0.45}Mn_{0.45}Co_{0.1})_{0.976}O_2$ where Li/TM=1.05.

The synthesis temperature was varied from 700 to 1000°C. It was found that the layered character of the structure is almost temperature independent (constant *c/a* ratio) while the distance between the Li and transition metal layers increases. The temperature was found to have little effect on the Ni disorder; there was ~5% Ni on the Li site. An increase in both crystallinity and particle size was found as the synthesis temperature was increased. The optimum synthesis temperature was found to be 800°C giving the largest cycling capacity combined with the smallest polarization. The capacity was 180 mAh/g at 0.5 mA/cm^2 between 2.5 and 4.6 volts. The 800°C synthesized material held its capacity well over the first 50 cycles.

The cycling behavior of this Li-rich compound was compared with the Li-stoichiometric material. The former shows an enhanced capacity over the first ten cycles, but then decays to a slightly lower capacity by the fiftieth cycle. Thus, there is no clear advantage of the Li-rich sample under the cycling conditions used here. In both of these cases 5% excess Li was added to the reaction media to obtain the desired composition.

MPACVD Carbon Films on Gen 2 and 3 Cathodes (Kostecki) – In a further investigation of the impact of MPACVD of carbon coatings, the effect of MPACVD deposited carbon thin-film coatings on the electrochemical performance of Gen 2 and Gen 3 cathode powders was evaluated. XRD spectra of the cathode materials showed no indication of structural damage or new phase formation due to heating. Low-temperature Ar-plasma, rapid film growth prevented overheating and the consequent reduction of the oxide active material by carbon. Raman spectra of carbon coated powders revealed spectral features typical of the raw materials accompanied by strong D and G bands characteristic of highly graphitized sp2-coordinated carbon. A full electrochemical evaluation of the cathodes vs. Li anode in a button cell configuration showed an improvement of material utilization, power performance and cycle life of the MPA carbon-coated electrodes vs. uncoated materials.

In-situ Diagnostics of Gen 2 and 3 Cathodes (Yang) – Another team has continued to investigate the structural changes in various layered materials, including $Li_{1-x}Co_{1/3}Ni_{1/3}Mn_{1/3}O_2$ (Gen 3) and $Li_{1-x}Ni_{0.8}Co_{0.15}Al_{0.05}O_2$ (Gen 2) using *in-situ* synchrotron XRD techniques. Figure IV-21 shows changes in the unit cell volumes of the Gen 2 and Gen 3 materials as a function of x during first charge. For $0 \leq x \leq 0.8$ in Gen 2, the unit cell volume decreased ~5.9%. For $0 \leq x \leq 1.0$ in Gen 3, the unit cell volume decreased ~3.4%. This smaller relative change in unit cell volume may give the Gen 3 material better structural reversibility for a longer cycling life. In addition, it was observed through *in-situ* time resolved XRD that the Gen 3 material exhibits formation of an NiO phase at higher temperatures than the Gen 2 material (Figure IV-22) again indicative of its greater stability at high temperatures and high states of charge.

Carbon Redistribution and Capacity/Power Fade in Gen 2 Cathodes (Kostecki) – As previously reported, tested commercial and ATD Li-ion cells showed a lower surface concentration of carbon additives as the cells aged. To further study this phenomenon, Raman microscopy and a ^{13}C carbon additive marker were used to monitor carbon distribution changes within tested cells. Specifically, ^{13}C-enriched composite Gen 2 cathodes were manufactured and characterized. These electrodes consisted of 84% active material, 4% ^{12}C graphite, 4% ^{13}C carbon black, and 4% PVDF binder. ^{13}C soft carbon, which emulates physico-chemical properties of acetylene black, was used.

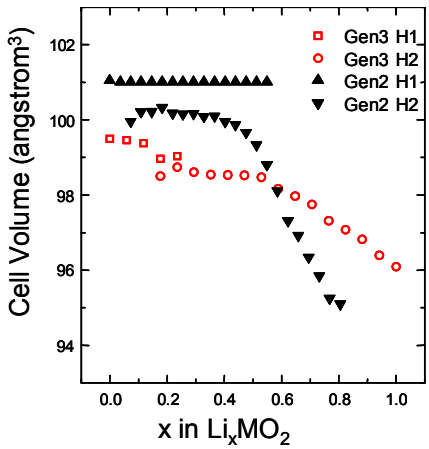

Figure IV-21. Changes in the unit cell volumes of $Li_{1-x}Co_{1/3}Ni_{1/3}Mn_{1/3}O_2$ (Gen 3) and $Li_{1-x}Ni_{0.8}Co_{0.15}5Al_{0.05}O_2$ (Gen 2) as a function of x during first charge.

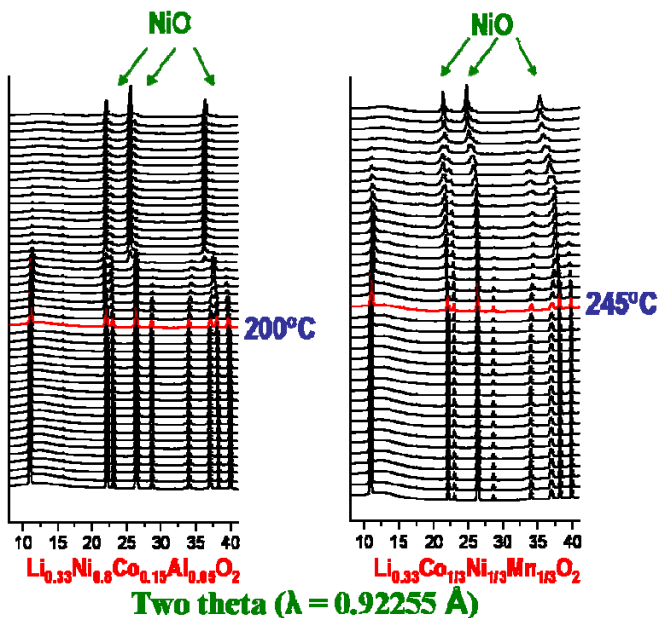

Figure IV-22. Gen 3 cathode shows better thermal stability than the Gen 2 material.

Electrochemical cycle life tests of the cathodes at C/10 and C/5 rates were carried out at room temperature and at 45°C in Swagelok model cells vs. a Li-metal anode with 1.2 M $LiPF_6$ in EC/DEC (3:7 vol. %) electrolyte. The cells lost ~80% of discharge capacity at C/10 and ~30% discharge capacity at C/20 after 180 cycles. ^{13}C -sensitive Raman analysis of the cell components was used to monitor carbon distribution within tested cells. It was found that:

- Post-mortem micro-Raman analysis of the cathodes showed a higher surface concentration of the active material and lower surface concentration of carbon additives.

- Only small amounts of carbon particles are carried away from the cathode. Fine carbon particles were trapped in the separator and traces of carbon additives were found in the electrolyte and at the surface of the Li anode.

- The Raman spectra of the carried-away carbons clearly showed contributions from amorphous ^{12}C and ^{13}C, Figure IV-23.

- The changes in the carbon additive distribution in composite cathodes are mainly responsible for the long-term capacity and high-rate performance loss of composite Li-ion cathodes.

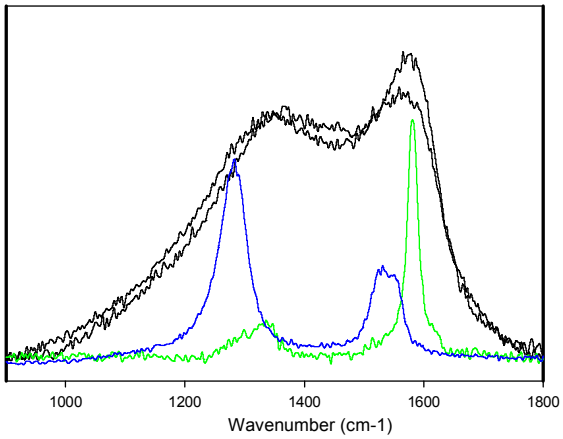

Figure IV-23. Raman spectra of ^{12}C graphite, ^{13}C carbon black, and carbon particles found away from the cathode showing that the carbon is indeed migrating.

FUTURE PLANS

Studies on $LiNi_{1-x}Mn_xO_2$

- Explore alternative routes to synthesize ideal, layered $Li(NiMn)_{0.5}O_2$.
- Investigate long term cycling on structure, rate and Li mobility in $Li(Ni_{0.5}Mn_{0.5})O_2$.
- Understand thermal & cycling stability of mixed transition-metal compounds.

Layered Mixed Metal Oxides

- Studies of $LiNi_{0.5}Mn_{0.5}O_2$ suggest that there might be drastic movement of the Ni ions in the Li layer as soon as cell charging begins, or alternatively that these Ni ions are the first to be charged from Ni(II) to Ni(III). Expand on this study, as it could lead to an understanding of what causes the first cycle capacity loss in these materials.
- Study Li diffusion in the layered materials.

MPACVD Carbon Coating

- Employ industrial MPACVD coater to guarantee uniform and reproducible processing of active materials.

In-situ Diagnostics

- Perform *in-situ* XRD work on Gen 3 cathode materials cycled at low temperatures.

IV.B New Anode Materials

OBJECTIVES

The objectives of the tasks in this area are to replace the presently used carbon anodes with more abuse tolerant materials that, in particular, will be compatible with low-cost manganese oxide and phosphate cathodes and the associated electrolyte. In addition, higher energy anodes are being investigated to permit eventual use of Li-ion batteries in EV or other high energy applications. For example, one project is investigating means to mitigate the growth of dendrites on Li metal anodes.

One project is attempting to improve irreversible capacity losses (ICL) of intermetallic electrodes.

APPROACH

One project identifies candidate electrode compositions by systematic comparison of phase diagrams and literature reports, and is investigating LiMg alloys presently by preparing electrodes and evaluating them in small cells.

Another approach pursed has been to search for inexpensive intermetallic electrodes (powder laminates rather than thin films) that provide 1) an electrochemical potential a few hundred mV above the potential of metallic Li, and 2) a capacity of at least 300 mAh/g (>1000 mAh/ml). This is focused predominantly on Sn-based systems that appear to have a good chance of success in practical cells (*cf.* Sony 'Nexelion' cells). In addition, Sb and Si based systems continue to be studied as these provide valuable information about reaction mechanisms and first-cycle ICL. Promising electrodes are evaluated in full cells against the high capacity metal oxides being studied in the cathode area.

Another team is investigating the SEI layers in a model system, AlSb, using XPS to examine the thickness and composition of the SEI layer. Laminated AlSb electrodes on copper foil and a metallic lithium counter electrode were used in pouch-type cells for the electrochemical tests.

Another project monitors dendrite formation and growth by electrochemical and optical methods as a function of electrolyte composition and applied potential. In an attempt to study the causes of dendrite formation, the impact of pulse plating parameters on dendrite formation is being considered. Furthermore, nucleation and growth of Li deposits are being characterized by electrochemical methods.

ACCOMPLISHMENTS

Li-Mg Alloy Anodes (Richardson): It has been shown that dendrite growth is suppressed in Li-Mg alloy anodes, Figure IV-24. The Li-Mg system has a large solid solution region with an open BCC Li structure, indicating the possibility for good Li diffusion. However, while these materials' capacities are very high, Figure IV-25, they appear to have limited rate capability (~ 0.5 mA/cm^2) during discharge. In addition, Li-Mg alloys are typically difficult to prepare on a laboratory scale. Here, a novel method of preparation of Li-Mg cermets containing inert Mg_3N_2 inclusions has been developed and shown to produce electrodes with performance superior to that of the pure alloys. This ceramic-metallic composite "cermet" can be pressed into discs, rolled into sheets, and cut into any desired shape. The Li_3N/Mg mixture can also be formed prior to reaction. It is believed that

microporous cermet anodes made by this method may cycle at higher rates due to increased wetted areas.

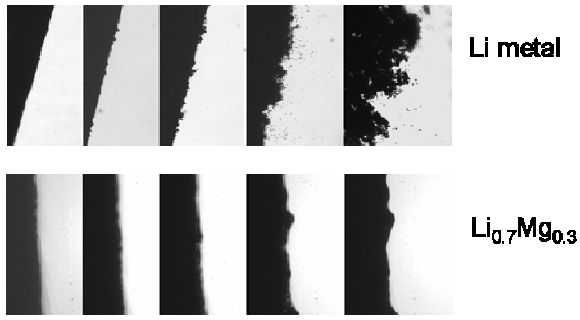

Figure IV-24. Dendrite growth on pure Li vs. LiMg alloys

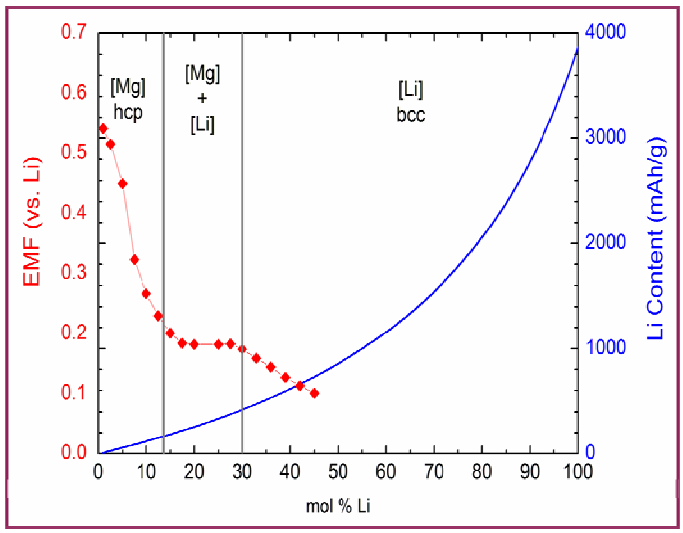

Figure IV-25. Energy density depends upon Li /Mg ratio

AlSb SEI Investigation (Thackeray) – A model system, AlSb, has been used to study SEI layers on intermetallic electrodes. This system was selected because limiting the lower voltage to 0.5 V greatly extended its cycle life[15]. For this work, in collaboration with Dr. Edström's group at Uppsala Sweden, XPS was used to examine the thickness and composition of the SEI layer. Laminated AlSb electrodes on copper foil and a metallic Li counter electrode were used in pouch-type cells for the electrochemical tests. The cells were potentiostatically equilibrated at 0.9, 0.75, 0.5 and 0.01 V during the initial discharge. Cells were also galvanostatically cycled at room temperature from either 0.5 or 0.01 V to 1.2 V at 3.0 mA/g. XPS data were collected, *ex-situ*, from the electrodes at these potentials, as shown by points A-F in Figure IV- 26 left.

C1s XPS data indicate that when cells are discharged to 0.5 V, the SEI layer is relatively thin. But the thickness of the SEI layer, monitored as a function of the concentration of reaction products, increases significantly on further discharge to 0.01 V (Figure IV- 26 right). XPS data indicate that at 0.01 V the SEI layer is comprised largely of Li-alkyl carbonates and electrolyte salt degradation products. On charge, the SEI layer reverts nearly to its original thickness. This dynamic process,

[15] Vaughey et al., J. Power Sources 97-8, 194 (2001).

in which the deposition of the Li-alkyl carbonates in the SEI appears to be reversible whereas the depositing of salt degradation products is not, continues on cycling.

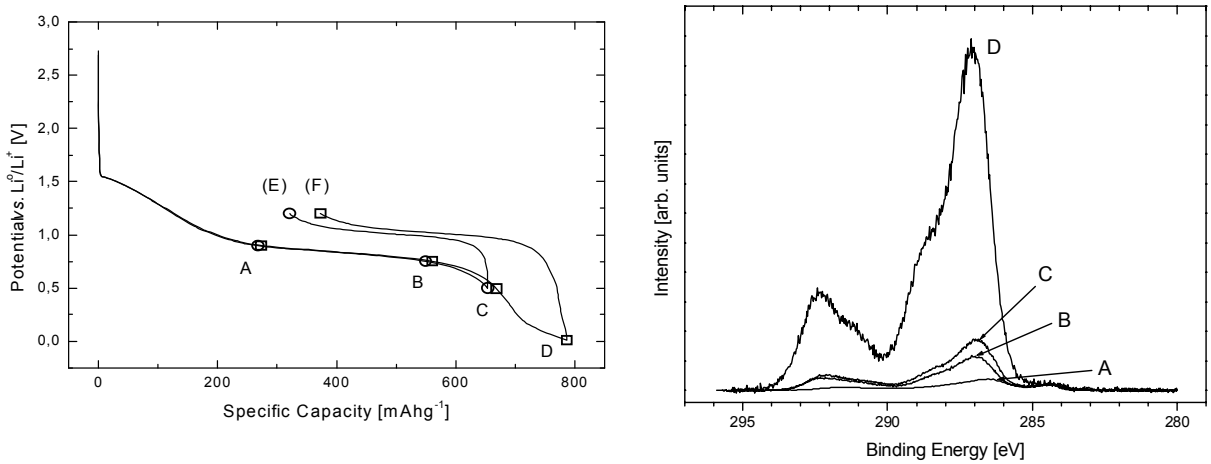

Figure IV-26. Voltage profiles of Li/AlSb cells showing the points at which electrodes were sampled for XPS data collection (left), C1s XPS spectra, showing the relative increase in the SEI layer from 0.5 V (A) to 0.01 V (D) (right).

Intermetallics and Li Coating (Thackeray) – This project studies the mechanisms that limit the cycle life of intermetallic anodes. This includes detailed examinations of the SEI layer, the effect of various surface coatings, roles of electrolyte and salt, the effect of particle size and morphology, and the limitations imposed by the electrochemical cycling routine. The recent introduction of the amorphous Co-Sn-C anode in Sony's 'Nexelion' product has provided additional motivation for work on intermetallic electrodes. In particular, researchers have initiated investigations of ternary cobalt-tin alloys. Preliminary studies have revealed some interesting new compounds whose capacity and stability appear promising, Figure IV-27.

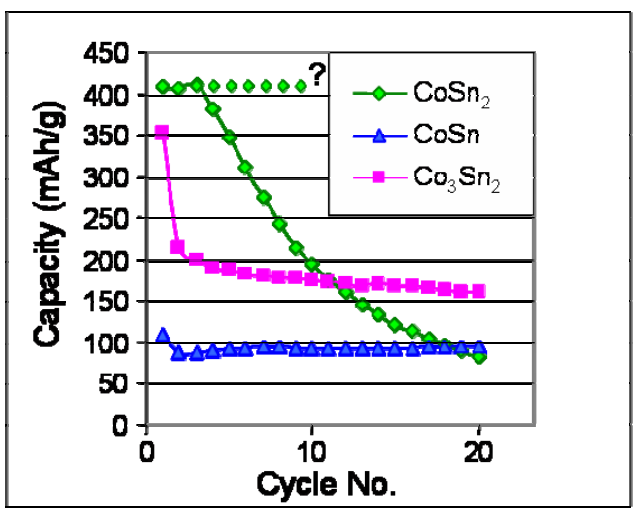

Figure IV-27. Electrochemical Behavior of Co-Sn alloys

In addition, this group is developing methods to prepare nanosized intermetallic electrode particles. Recent work has focused on synthesizing materials using high-energy ball milling (HEBM) of metal elements, direct synthesis at elevated temperature with subsequent mechanical particle size

reduction, and a molten spray pyrolysis method. The intermetallic particles in the 'Nexelion' anode were found to be 5-10 nm in size and approximately spherical in shape. These features indicate a solution-based synthesis method. Therefore, such techniques are being reinvestigated to prepare intermetallic materials.

A solution method that this group employed several years ago was based on the zinc reduction of metal salts dissolved in organic solvents at elevated temperatures, e.g., 200ºC, with subsequent annealing. For the Cu-Sn system, typical products included the desired product Cu_6Sn_5, as well as $Cu_{41}Sn_{11}$ and metal oxide impurities. Using this technique, the Cu_6Sn_5 particles prior to annealing exhibited a dendritic morphology and did not provide satisfactory electrochemical properties, exhibiting fade on cycling possibly due to loss of active material.

The use of various alternative reductants in organic solvents is being explored in an attempt to synthesize compositionally homogenous intermetallic materials. Common alcohols, such as ethanol and isopropanol, although leading to increased metal salt solubility, also tended to yield more metal oxide by-products. Potassium borohydride (KBH_4) used instead of zinc has been more successful, due to the solubility of KBH_4 in the host solvent, although notably with alcohols there was evidence of solvent reactivity. Best results, to date, have been obtained using the high boiling point solvent tetra-ethylene glycol as it dissolved adequate amounts of the metal salts and was stable to KBH_4. For the Cu-Sn system, a stoichiometric mixture of salts was added to the solvent system and reduced to form suspended copper and tin particles. Heating the sample to 130ºC resulted in near single phase Cu_6Sn_5. SEM images revealed 100-200 nm primary particles, agglomerated into larger 2-5μm grains, in contrast to 0.5-35μm sized primary particles obtained by HEBM and 10-2 μm by spray pyrolysis. Using this method, the Cu_6Sn_5 particle morphology after annealing was similar to that obtained from melts.

Nano-sized Tin Based Anode Materials (Whittingham) – It was previously reported that tin foil had a higher initial capacity than graphite but rapidly decayed after 10 to 15 cycles to values comparable to that of graphite. This investigation is evaluating the impact of using nano-particle/ amorphous tin to determine if more emphasis should be placed on amorphous vs. crystalline anode materials. It was recently demonstrated that amorphous materials cycled much better than the crystalline tin or tin-cobalt compounds. A commercial tin anode showed a large cobalt content plus carbon with some titanium; TEM analysis showed grain sizes <10 nm (Figure IV-28).

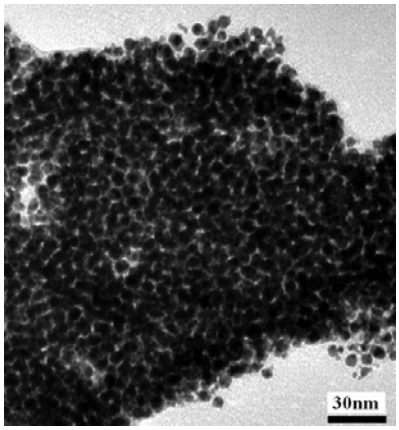

Figure IV-28. Characterization of amorphous nano tin-cobalt anode nanoparticles of anode.

A collaboration has been initiated with Dr. Chupas at the APS facility at ANL to determine the local structure of this new anode material, as regular XRD showed no long range order. A Pair Distribution Function (PDF) study has been undertaken to determine the local bonding and to understand some critical parameters of this material in both the charged and discharged state. This may then let one understand the role of the cobalt, and replace it with other lower cost materials such as manganese or iron, which form related bulk materials to the cobalt compound.

Oxide Based Anodes (Whittingham) – Work has continued on manganese oxides that might react reversibly with lithium. Although the behavior of CoO as an anode has been described, MnO is notable for its absence from prior studies. Nanofibers of this material have been made that readily react with lithium in cells, but the capacity is much higher than expected suggesting that the nano-sized manganese might be catalyzing the decomposition of the electrolyte.

The strategy was to form nanosized particles of the MnO in the hope that they would not decrepitate on reaction during cycling. To give these particles some strength, fibers were used, which should form an interwoven mat. The desired Mn oxide nanofibers were made by using a polymer-templated electrospinning process followed by heat treatment to remove the polymer. This resulted in 200-300 nm diameter oxide fibers, which were found to be electrochemically active. The major phase present is Mn_3O_4. The electrochemical behavior of these manganese oxide nanofibers is shown in Figure IV-29, at 0.5mA/cm^2. The discharge and charge curves indicate a single-phase reaction. It appears that the reversible reaction is: $Mn_3O_4 + 8Li \leftrightarrow 3Mn + 4LiO_2$. This large Li insertion leads to a high theoretical capacity > 900 mAh/g. After the first cycle the capacity decays steadily reaching a plateau between 400 and 500 mAh/g by the 50th cycle. The absence of a catastrophic capacity loss after a few cycles signals that electrospun oxides have promise for anodic use in lithium batteries, and maybe even for cathodes.

There cause of fade is now being investigated, and the team is trying to understand a larger than theoretical Li insertion capacity in the first cycle.

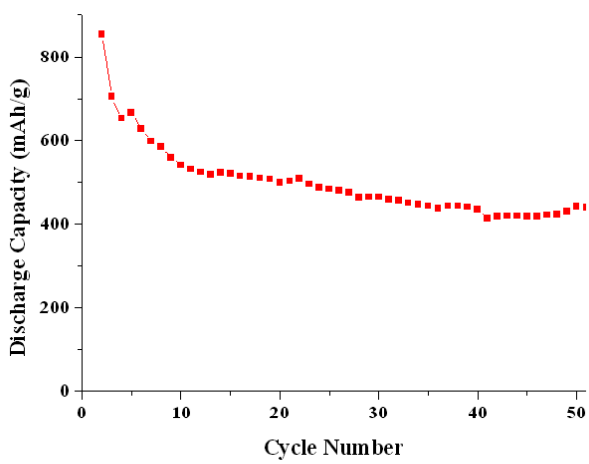

Figure IV-29. Electrochemical behavior of electrospun Mn_3O_4

Li Dendrite Growth and Diagnostics (West) – This project aims to understand the mechanism of dendrite formation during charging of a secondary lithium battery. The mechanism for dendrite formation during the deposition of other metals (e.g., copper) is well understood, they propagate

rapidly as the deposition current approaches the limiting current. However, dendrites form at currents well below the limiting current during lithium deposition, and the exact mechanism is unclear. In particular, why do dendrites form at rates of 10-20% of the limiting current?

This works is addressing this question by studying the deposition of lithium on a nickel substrate. Currently, potentiostatic and galvanostatic lithium deposition experiments using a Ni/$LiPF_6$ in PC/DMC/Li system are being conducted.

Data from cyclic voltammetry and cell cycling experiments match well with published results. Surface profiles obtained using simple profilometry show an increase in surface roughness with increased cycling, shown in Figure IV-30. However, these early experimental attempts to quantify Li dendrite growth gave unreliable data. Li was deposited, the Li substrate was then rinsed and allowed to dry. *Ex-situ* surface profiles were then measured to determine the surface roughness. However, the surface roughness increased with increasing air exposure time. This indicates the need for *in-situ* methods to measure dendrite growth to avoid reaction of Li with atmospheric oxygen and humidity. Recently, an *in-situ* optical microscopy station was installed.

Also, microfluidic test cells are being used to obtain a reproducible view of the electrode/ electrolyte interface. The cell consists of two similar PDMS molds into which working, counter, and reference electrodes are inserted. In between the electrodes, there is an electrode/electrolyte interface area that is connected to a reference electrode and an electrolyte reservoir to prevent electrolyte depletion and minimize any effect of the counter electrode. The flow channels are approximate 150μm in height. The cell will provide a working electrode area of ~0.15 mm^2.

Experiments to determine the effect of varying the PC to DMC ratio in the electrolyte are planned. Since PC is a cyclic molecule and DMC is a linear molecule, these experiments should help to explain the effect of the solvent molecules on lithium deposition.

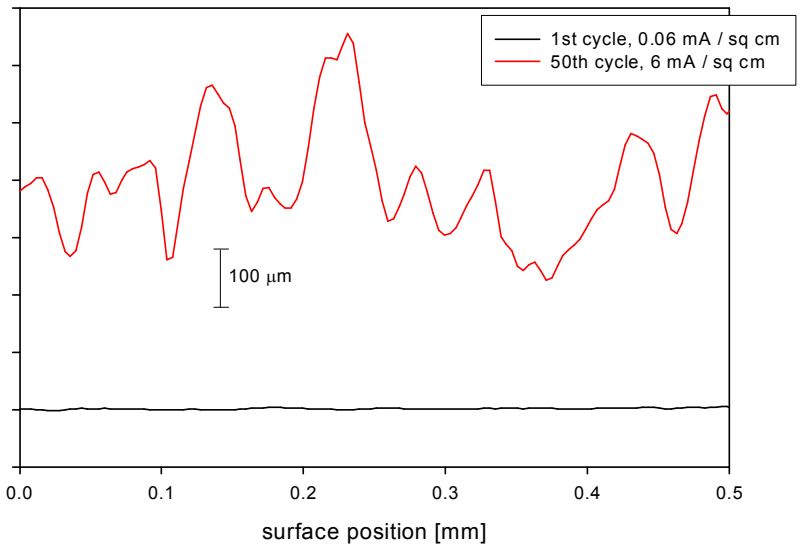

Figure IV-30. Surface profiles showing an increase in surface roughness with increased cycling.

FUTURE PLANS

Intermetallics and SEI Investigation

- Extend work to other binary and ternary intermetallic compounds, notably those containing cobalt and tin.
- Exploit and optimize Cu-based intermetallic systems.
- Undertake SEI studies of Li-Cu-M-Sn electrodes.
- Evaluate intermetallic anodes in full cells.
- Extend NMR studies of InSb to Cu-M-Sn systems.
- Use NMR to study anode lithiation reactions with Dr. Grey's team.

Nano-sized Tin-Based Anode Materials

- Understanding solid tin system, is capacity loss due to the SEI layer?
- Further investigate nano particulate tin anodes.
- Is role of cobalt and carbon in Sony anode to accept expansion?
- Is cobalt unique? Why not manganese? Role of titanium?
- Emphasize amorphous materials, enhance collaborations to characterize materials.

Dendrite investigation

- Continue to study the relationship between electrolyte composition, deposition rate, and applied potential on interfacial stability in nonaqueous liquid electrolytes.
- Relate experiments to theoretical stability analysis.
- Begin to transition to the use of polymer electrolytes.
- Use *in-situ* XRD and XAS to study new alloyed anode systems and functional electrolytes.

IV.C Novel Electrolytes and Their Characterization

OBJECTIVES

The objectives of this task area are to

- Determine and quantify the improvement (if any) in abuse tolerance of polymer gel electrolytes over liquid electrolytes.
- Determine the limitations on Li-ion transport in polymer gel electrolytes and develop materials capable of high-power operation at ambient temperature.
- Evaluate ionic melts and their ability to function as high power Li-ion electrolytes.
- Develop and evaluate composite polymer electrolytes that offer the possibility of dendrite free cycling with Li metal.
- Gain a fundamental understanding of the transport mechanism in ionic liquids and develop new electrolytes with improved transport and mechanical properties.

APPROACH

Synthesize and characterize robust nanostructured dry polymer electrolytes with high conductivity and high shear modulus that resist dendrite growth during cell cycling. Synthesize polymers and characterize salt/polymer mixtures using AC impedance spectroscopy. Test promising candidates for stability against Li electrodes and in Li cells. Fully characterize the materials of interest using methods such as neutron and light scattering, rheology, and transmission electron microscopy.

Using molecular dynamics, gain molecular level understanding of the cation transport mechanism in liquid electrolytes, single ion conductor gel electrolytes, and ionic liquids. Investigate transport properties of novel gel electrolytes and ionic liquids with improved lithium transference number.

Use surface-functionalized fumed silica fillers in BATT-baseline systems to determine the effects of filler type and concentration on interfacial stability and cell capacity upon cycling. Attempt to correlate electrochemical characteristics with mechanical properties and materials chemistry (e.g., silica-type, salt, or PEO-type,) with novel materials.

ACCOMPLISHMENTS

Liquid* vs. *Gel Type Electrolytes and Abuse Tolerance (Kerr) – TGA measurements of gel polymer electrolytes (EC/EMC-$LiPF_6$ with cross-linked polyethers (PEO-type)) and PVDF (phase separating) show that the presence of the polymer does little, if anything, to suppress the volatility of the liquid electrolyte components, Figure IV-31. Flammable vapors are produced even at room temperature resulting in an abuse event if the cell is breached. Polymer gels prepared with typical electrolytes therefore offer no significant safety improvement over liquid electrolytes. By contrast, ionic liquid gels prepared using pyrrolidinium and TFSI salts are completely stable to 200ºC and it is the polymer that generates the volatile vapors not the electrolyte. Ionic liquid electrolytes therefore show better thermal behavior. This also includes stability towards reaction with nascent oxygen evolving from decomposing cathode materials. DSC measurements show reaction of Gen 2 and Gen 3 cathodes with EC/EMC-$LiPF_6$ electrolytes at ~150ºC whereas ionic liquid electrolytes do not react until ~300ºC.

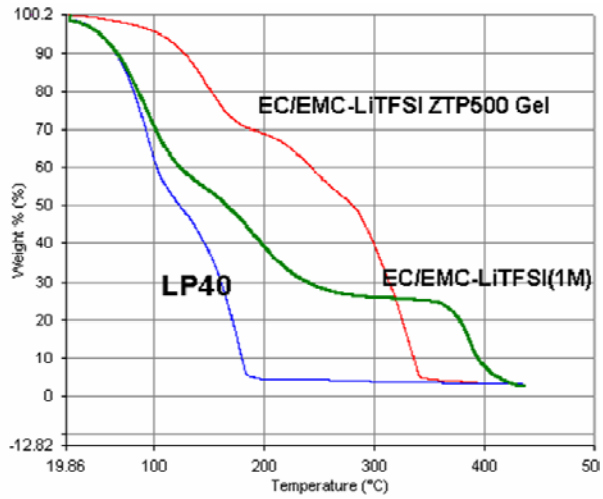

Figure IV-31. TGA measurement of weight loss vs. T for a gel electrolyte and two standard liquid electrolytes.

Effects of Impurities, Particularly Water, on Interfacial Behavior of Electrolytes (Kerr) – It is widely believed that water contamination can severely impact Li-ion cell life, and water can be introduced in a variety of cell formation steps. For example, carbon black, often used as a conductive additive, contains up to 3000 ppm water if not dried prior to use. Karl-Fischer (KF) titration measurements and other methods are being used to measure the water content of cells and electrode components. Solid components up to $10cm^3$ in size are heated in an oven that is purged with dry gas, which picks up the moisture contained in the sample and carries it to the titrator cell.

Measurements made by A. Weber of Energizer have been confirmed that show that any water present in the original solvent is converted to HF over time. Thus, KF titration is insufficient (by itself) for quality control of electrolytes and a measure of the HF must be included. The HF initiates polymerization reactions of the electrolyte and produces side reactions during cell formation and cycling. These polymerization reactions are suppressed if the electrolyte is kept sealed in a container where CO_2 cannot be removed.

Chemical reactivity experiments with EC/EMC electrolyte components show that PF_5 reacts at sub-zero temperatures to initiate polymerization reactions. PF_5 reacts more rapidly in a sealed reaction flask with polyethers than with the carbonate solvents to form fluorophosphates and phosphate anions. This then determines what the polymerization reaction produces. When LiF is added to the solvent components it completely suppresses these reactions by preferentially reacting with the PF_5. This suggests a method to produce very pure electrolytes by reaction of pure gaseous PF_5 with thoroughly dried and purified EC/EMC-LiF solution. This electrolyte contains no protic species and cannot form HF.

Nanostructured Polymer Electrolytes (Balsara) – This project is using composite polymer electrolytes comprised of an extremely hard (but non-conducting) polystyrene (PS) based portion (to block dendrite formation), interwoven with a conducing PEO based portion (to permit Li diffusion), Figure IV-32.

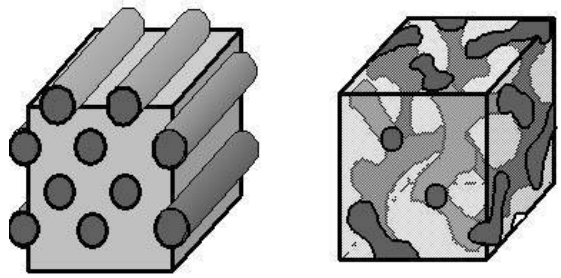

Figure IV-32. Schematic of a nanostructured polymer electrolyte

In the past, this group has reported that the ionic conductivities for a variety of PS-b-PEO copolymers (SEO) increase with the molecular weight (MW) of the PEO block. Recently, they have attempted to understand the origin of this trend. The PEO volume fraction in the composite electrolyte, ϕ_{PEO}, varies from 0.38 to 0.55. If all of the PEO channels in the nanostructured electrolyte provided conducting pathways for the ions, and if the conductivity of the PEO channels was identical to that of PEO homopolymer/salt mixtures, then the expected value of the conductivity of the doped sample, σ_{max}, would be the product $\phi_{PEO}\sigma_{PEO}$. The ratio σ / σ_{max} thus normalizes the measured conductivity data for differences in ϕ_{PEO}. In Figure IV-33 is plotted σ/σ_{max} versus M_{PEO}, the average MW of the PEO block. A systematic increase in conductivity with M_{PEO} is observed. It is evident that the ionic conductivity of the electrolytes is mainly affected by M_{PEO}, and not by block copolymer composition.

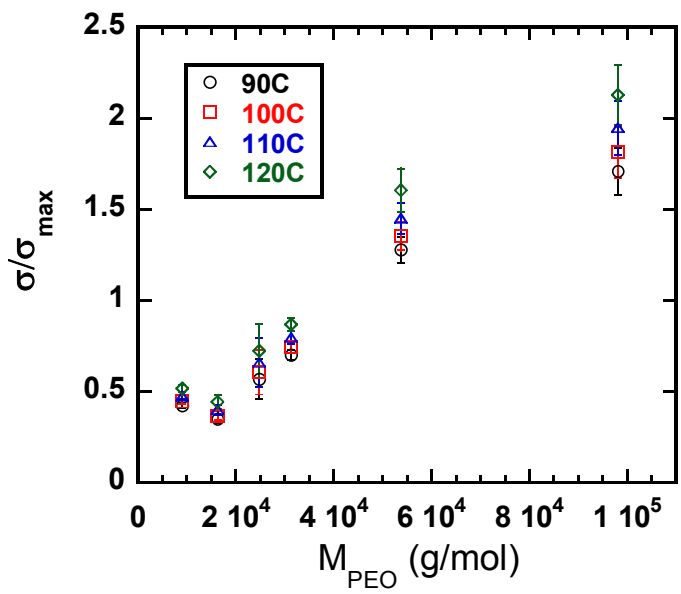

Figure IV-33. Ionic conductivity of electrolytes based on PEO containing copolymers vs. the molecular weight of PEO block in the copolymer. The [LiTFSI]/[EO] ratio is approximately 0.02 for all the electrolytes.

The fact that σ/σ_{max} is greater than unity indicates that the conductivity in the nanoscale PEO channels must be greater than in bulk PEO. It has been argued that dissociated Li ions are tightly coordinated with the ether linkages in PEO and thus disruption of this coordination could lead to faster ion transport. Block copolymer chains stretch when they form ordered phases. This is evident in the scaling of the periodic length scale, d, with N, the degree of polymerization. A least

squares power law fit through the *d* (nm) versus *N* data yields $d = 0.41 * N^{0.68}$, which is the expected result in the strong segregation limit. It is proposed that the stretched PEO chains in these high MW block copolymers are not as tightly coordinated with Li ions as PEO random coils, and this leads to enhanced conductivity.

Recently, dendrite free cycling has been found at currents approximately 50% of the limiting current. The interface between Li metal and these polymer electrolytes was studied by constructing Li/polymer/Li cells. The Li metal was evaporated onto the electrolyte in a vacuum chamber. Preliminary results of reversing a DC current of 76 $\mu A/cm^2$ through a copolymer electrolyte with r=0.02 (1/2 the estimated limiting current density for this system) are shown in Figure IV-34. The constancy in the cycling data indicates stability of the polymer/Li interface.

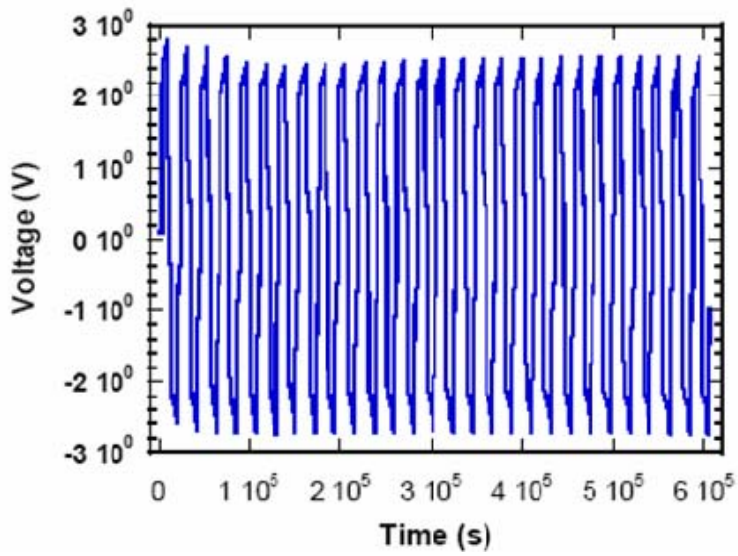

Figure IV-34. Results of cycling experiments on Li/polymer/Li cells.

Single Ionic Conductors and Ionic Liquids (DesMarteau) – The purpose of this research is to create and characterize new ionic melts that promise safer more stable behavior in Li-ion cells. Galvanostatic DC polarization studies were performed to address the question of whether salt concentration polarization occurs when DC current is passed through ionic melt electrolytes. Figure IV-35 presents representative data.

For salt-in-solvent electrolytes the applied potential shifts up following application of a DC current, whereas for the ionic melts the potential remains nearly invariant with time. This behavior strongly indicates a lack of salt concentration polarization in the ionic melt electrolyte. These measurements put to rest earlier concerns regarding the possible presence of trace nonionic impurities in samples.

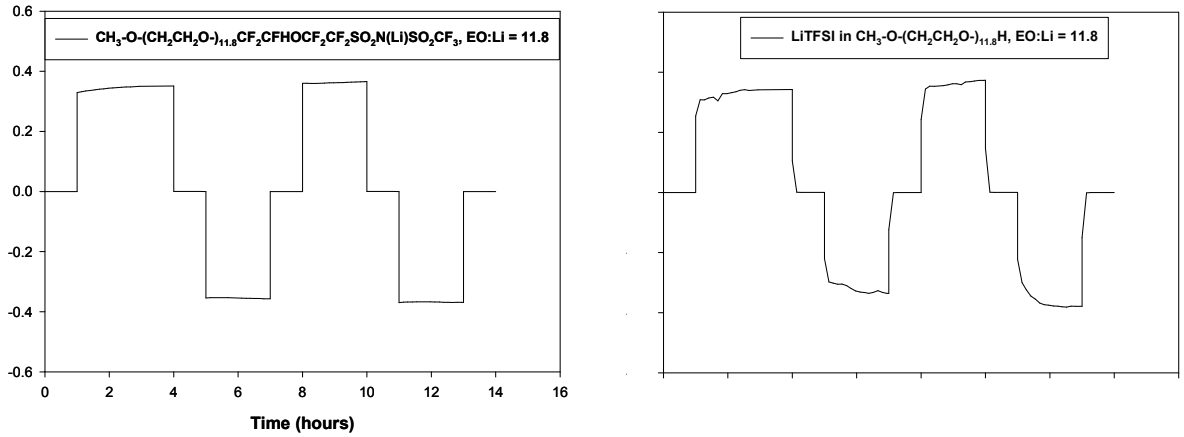

Figure IV-35. Current-time plots for a DC galvanostatic polarization program applied to electrolytes poised between dual lithium titanate electrodes. Right, LiTFSI dissolved in PEGME550 at a EO:Li ratio of 11.8:1. Left, lithium fluorosulfonimide ionic melt electrolyte.

Rheological studies on IM550 samples in the presence and absence of added polyethylene glycol (PEG) plasticizer were performed. Results from dynamic cone-and-plate rheology measurements on IM550 alone at ambient temperature are shown in Figure IV-36. The near-zero value for the elastic modulus over the full frequency range confirms the viscous liquid character of the electrolyte. Steady-state viscosity measurements of PEG-plasticized IM550 samples revealed a strong plasticization effect of the PEG. At ambient temperature and 1.0 s^{-1} rotation rate, the viscosity decreased from 117 Pa s without plasticizer to 4.8 Pa s with 20% plasticizer added. Even larger effects were seen with more plasticizer present. These findings are consistent with observations that the low-temperature ionic conductivity of IM550 is strongly increased by addition of PEG plasticizer.

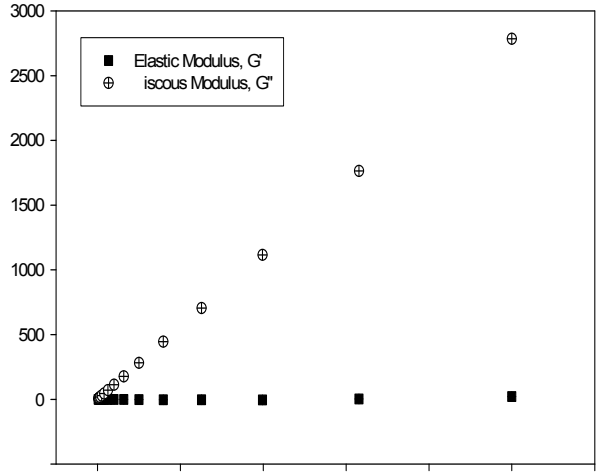

Figure IV-36. Dynamic rheology data for a sample of IM550 acquired at ambient temperature using a ARES-LS type rheometer in a cone-and-plate geometry.

Molecular Dynamics of Li^+ Transport in Ionic Liquids and Plasticized Ionic Liquids (Smith) – MD studies of N-methyl-N-propylpyrrolidinium bis(trifluoromethanesulfonyl)imide (mppy+TFSI-) and N,N-dimethyl- pyrrolidinium bis(trifluoromethanesulfonyl)imide (mmpy+TFSI+) ionic liquids (IL) doped with 0.25 mol LiTFSI salt at 303 K – 500 K have been performed. The predicted liquid density, ion self-diffusion coefficients, and conductivity were found to be in good agreement with experimental data, where available, Figure IV-37. MD simulations reveal that the Li^+ environment was similar in mppy+TFSI- and mmpy+TFSI+ ILs doped with LiTFSI. The Li^+ cations were found to be coordinated on average by slightly less than four oxygen atoms with each oxygen atom provided by a different TFSI- anion. Li^+ transport was found to occur primarily by exchange of TFSI- anions in the first solvation shell with a smaller (~30%) contribution due to Li^+ cations diffusing together with their first solvation shell. Conductivity due to the Li^+ cation in LiTFSI doped mppy+TFSI- IL was found to be greater than that for a model PEO/LiTFSI polymer electrolyte but significantly lower than that for EC/LiTFSI liquid electrolyte.

In an effort to design ILs with improved Li^+ transport, additional simulations have been performed on the EO_{12}TFSI-/Li+ IL that have the Li^+ /EO interactions decreased such that 90% of Li^+ are in contact with TFSI- anions. One can achieve this in actual materials by fluorination or introduction of ethylene units, *etc.* Note, that the original (unmodified) EO_{12}TFSI-/Li+ has about 10-20 % of Li^+ in contact with the TFSI- groups. At 393 K the simulations of the modified IL yield only 20% faster ion transport in comparison with a original, however, at 333 K ion transport is almost twice as fast, indicating improved low-temperature performance for the modified ILs.

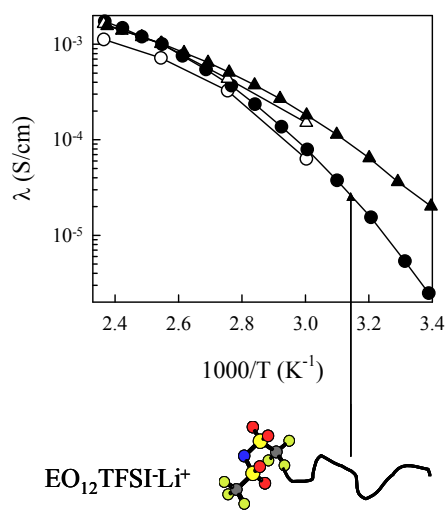

Figure IV-37. Comparison between theoretical and experimental (Creager et al) conductivity values

Characterization of Ils (Doeff) – Li/P14TFSI, 0.5m LiTFSI/Li_xMnO_2 or $Li_xTi_{0.11}Mn_{0.89}O_2$ cells were built and compared to cells with conventional electrolytes. The room temperature performance of the ionic liquid (P14TFSI) cells is poor, due to the high interfacial impedance at the Li electrode, but is improved considerably at 55ºC. Advantages to the ionic liquid system include better thermal and oxidative stability and decreased dissolution of manganese oxide electrodes at 55ºC compared to $LiPF_6$-containing electrolyte systems (Figure IV-38). A new ionic

liquid P14FSI has been received from CSIRO in Australia, and is expected to result in better room temperature performance.

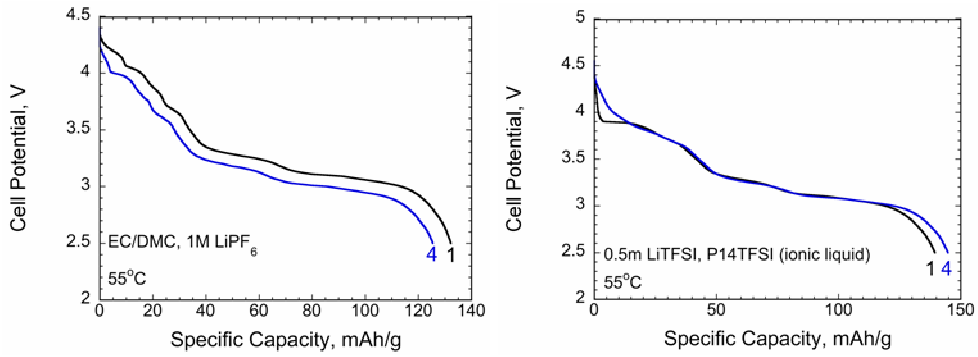

Figure IV-38. Capacity retention after four cycles

Gel Electrolytes (Zaghib) – Many researchers believe that better binders may provide one solution to power fade in cells and this project is focused on a water soluble binder (WSB) paired with $LiFePO_4$. A new generation of $LiFePO_4$ cathode electrodes and WSB were evaluated in laminated lithium and Li-ion cells. Li-ion laminated cells with a new higher rate $LiFePO_4$ cathode and graphite anode were made, both prepared with WSB. Figure IV-39 shows the high rate capability of Li-ion cell at 25°C. The evaluation was based on two successive Ragone tests by fixing the charging rate at C/6. About 100% of the reversible capacity was obtained at 2C and more than 80% at 10C. The second Ragone test shows the same performance even after the cell was operated at 40C peak rate.

Next, the effect of gel polymer formation on cell performance was studied. The high-power capability of the Li-ion laminated cell in the gel configuration showed comparable results to a liquid cell up to the 4C rate. At >4C, a noticeable difference is observed between liquid and gel cells. The capacity in the gel cells was 20% lower than the liquid cells at 10C.

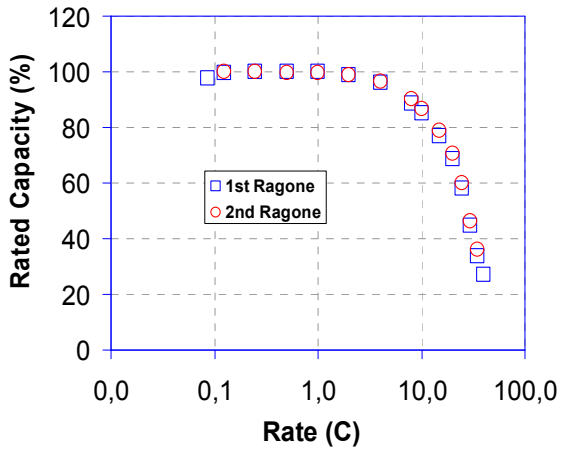

Figure IV-39. Ragone test on Li-Ion laminated cell in EC/DEC-$LiPF_6$ at 25°C

This team has continued this work in an attempt to optimize the cathode by introducing mixed $LiFePO_4$ from different synthesis routes. Cathodes based on mixed $LiFePO_4$ produced by

hydrothermal (HD) and solid state (SSR) reactions were coated with carbon. Different (HD)/(SSR) ratios were evaluated, and the optimum performance was found with (HD)/(SSR) = 80/20. The capacity of the cell was 161 mAh/g at C/8. At 10C rate, the cell delivered 104 mAh/g, and at 20C the cell still delivered 49% of the capacity at the C/8 rate.

The addition of vapor-grown carbon fiber (VGCF) in the cathode greatly improves the performance at high rate. In the PVDF-based cathode, the VGCF improved the capacity at 5C to 126 mAh/g from 98 mAh/g. At high rate (12C), the cathode with VGCF delivers 92 mAh/g compared to 49 mAh/g, see Figure IV-40.

When WSB is used in the cathode instead of PVDF binder, the high-rate performance improved. At 5C, the PVDF-cell delivers 126 mAh/g compared to the WSB-containing cell which yields 133 mAh/g. The cell with WSB still showed better performance (15% better discharge capacity) when the rate was increased to 12C.

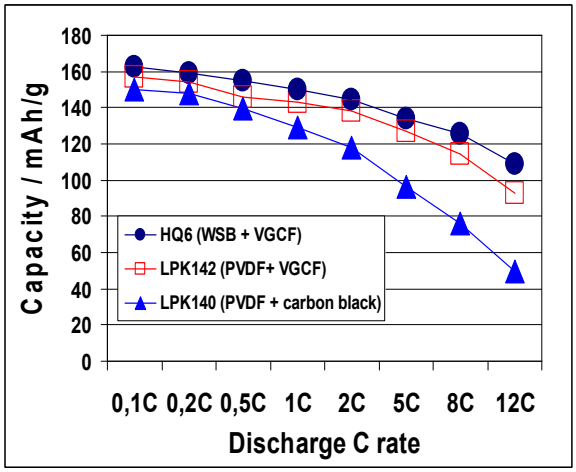

Figure IV-40. Ragone plot of Li-LiFePO_4 cell in EC/DEC-LiPF_6 with different cathode composition at 25°C

Fumed Silica and other Gel Electrolytes (Khan) – This research is developing composite-gel electrolytes with fumed silica additives. Two types of fumed silica have been used, hydrophilic A200 and hydrophobic R805. The conductivity results show that silica nanoparticles have complicated effects on transport properties compared with oligomer PEO. At the low salt concentration of 0.2 M LiBOB/γBL:EA (1:1), 10 wt% R805 has a negligible effect on conductivity; at the intermediate salt concentration of 0.7 M LiBOB/ γBL:EA (1:1), 10 wt% R805 decreases the conductivity; at the high salt concentration 1.2 M LiBOB/γBL:EA (1:1), 10 wt% R805 decreases the conductivity significantly, especially in the low-temperature range (< 10 ºC). Work on these composite gel electrolytes was ended in 2007.

FUTURE PLANS

Effects of Impurities on Interfacial Behavior of Electrolytes

- Accurately measure H_2O content and determine effects on electrolyte reactivity rates.
- Measure interfacial properties of liquid and gel electrolytes with carbon anodes and cathodes from cell development task and other sources as available.

- Determine the role of electrolyte reactivity in interfacial impedance growth.
- Test radical polymers with ILs for thermal abuse resistance and high rate cycling ability.

Nanostructured Polymer Electrolytes

- Study dendrite growth in Li/PE/Li cells. Establish the performance of the polymer electrolyte as a dendrite inhibitor
- Synthesize higher molecular weight samples.
- Understand the origin of improved conductivity using e.g., NMR, neutron scattering, electron tomography.

SIC and Ionic Liquids

- Test reactivity using charged electrodes / cells filled with electrolyte.
- Study interfacial impedance in various cells and address the generality and cause of the unexpectedly low impedance of ionic melt/electrode interfaces.
- Fabricate new electrolytes based on: partially fluorinated polyethers; ionic melt / inorganic support composites; electrolytes with plasticizers.
- Characterize electrolytes with respect to structure, purity, transport properties, reactivity, and especially, charge-discharge behavior in Graphite / Electrolyte / $LiFePO_4$ cells.

MD Simulations

- Expand investigation of the SEI-electrolyte interfaces for mixed solvent electrolytes and ILs.
- Simulate novel ionic liquids and polymeric electrolytes
    - ILs with non–PEO solvating groups (siloxane oligomers with attached TFSI-, carbonate solvating groups, etc)
    - Siloxane-oligoether-TFSI-ionic liquids
    - Siloxane/oligoether-combs with attached TFSI- (dry and gel)
- Based on promising initial results, investigate non-EO-based ionic liquids and single ion conductors, zwitterionic electrolytes and siloxane-oligoether-TFSI electrolytes.

Characterization of ILs

- Determine if Li/ionic liquid/tunnel compounds can make a high energy cell.

Gel Electrolytes

- Demonstrate batch-to-batch repeatability.
- Determine rate capability of WSB based anode (Hard carbon vs. graphite).

IV.D Li-Ion Modeling, Diagnostics, and Cell Analysis

OBJECTIVES

The primary objectives of the modeling and diagnostics tasks are to establish correlations between electrode materials, engineering choices, interfacial phenomena, and cell performance. The objective of the cell development task is to establish a test vehicle for the evaluation of new materials for high-power or high-energy, low-cost Li-ion cells. In addition, researchers are determining the influence of corrosion and passivation of Al current collectors on the capacity loss of Li-ion batteries.

APPROACH

One diagnostic approach is to use *ex-situ* and *in-situ* Fourier transform infrared (FTIR) spectroscopy to study the interfacial chemistry in model electrode/electrolyte systems, particularly at low temperature. The spectrometer optics and spectro-electrochemical cell have a special design that enables any electrode material to be studied. The FTIR spectroscopy is accompanied by classical electroanalytical methods such as cyclic voltammetry and ac impedance.

Another focus area that continued in 2006 was to develop experimental methods for measuring transport and thermodynamic properties.

The modeling teams develop mathematical models for various Li-ion chemistries to optimize performance, identify limiting factors, and mitigate failure mechanisms. They also design experiments to test theoretical predictions and to estimate properties needed for the models.

The research tasks into Al current corrosion include: (1) determine the mechanism of underdeposit corrosion (udc) of Al current collectors, in particular determine role of cathodes and temperature; (2) evaluate remedial actions, such as modifying the Al surface and adding inhibitors to the electrolyte; (3) develop a short-time laboratory test of udc; (4) microscopically inspect Al current collectors of ~50 additional coin cells cycle life tested to test earlier conclusions regarding importance of corrosion and to confirm that corrosion occurs by udc.

The cell development team tests novel materials in standard cells with preset protocols to provide the necessary link between battery components and the diagnostic evaluation of failure modes. They also incorporate new components into standardized cells and test them using a consistent protocol to determine cell capacity, energy, power, and lifetime characteristics. Finally, they deliver tested cell components to investigators involved with BATT Program diagnostic projects.

ACCOMPLISHMENTS

Interfacial Chemistry at Low Temperature (Ross) – This work focused on creating novel SEI layers outside of a cell, then characterizing those films and comparing their diagnostic signatures with those seen in actual Li-ion interfaces. The FTIR signature of the SEI on a graphite anode in 1.2 M $LiPF_6$/EC:EMC(3:7) was compared against the model compounds mentioned above, typical results are shown Figure IV-41. The impedance characteristics of SEI-related compounds were also measured, specifically Li oxalate, Li ethylene carbonate, and Li ethylene dicarbonate. Qualitatively the characteristics of all three compounds were very similar, and characteristic of that for pure Li-ion conductors. The DC conductivity (1 Hz to 1 kHz) was measured as a function

of temperature by placing the Swagelok cells in an environmental chamber with controlled temperature. Arrhenius plots of log σ vs. T^{-1} were reasonably linear with an activation energy for conduction that is relatively high, e.g. 50 - 60 kJ/mol, compared to that for glass electrolytes, e.g. 25 - 30 kJ/mol (Abe et al, JECS 152, 2005, A2151). The activation energy for transport through the SEI is thus quite close to the activation energy for Li ion transfer at the SEI-solution interface as reported by Abe et al, making it very difficult to separate these two resistances. They may, in fact, be fundamentally related.

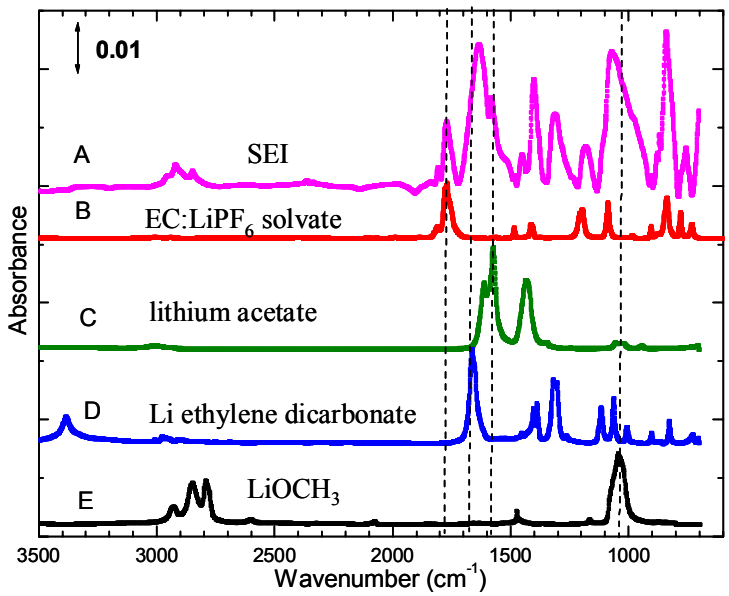

Figure IV-41. Deciphering the Anode SEI Composition

Molecular Dynamics Simulations of Li^+ at EC – Graphite Interface (Smith) – The structure of the electrolyte – graphite interface is highly relevant to battery operation. MD simulations of EC/LiTFSI (EC:Li=10) next to a stack of graphene sheets were performed at 313 K to understand interfacial electrolyte structure and the free energy barrier for Li intercalation into graphite (without an additional SEI layer). The ability of the force field to predict Li^+-graphite interactions was checked by comparing Li^+ interactions with a benzene dimer from molecular mechanics calculations with the developed force field and from quantum chemistry calculations.

MD simulations predict that Li^+ transport between the electrolyte and graphite occurs at timescales longer than a few nanoseconds, even without the SEI, a typical time of MD simulations. Therefore, a free energy barrier for the Li intercalation cannot be studied in conventional equilibrium MD simulations. Thus, a "constraint-force" method was used that yields a force on a Li^+ fixed at a certain separation from the graphite surface. Li positions ranging from inside the graphite to ~1nm from the graphite were studied. A potential of mean force ("free energy") acting on a Li^+ was obtained as a function of Li position. The free energy barrier was found to be ~10 kcal/mol (41 kJ/mol), which is an order of magnitude smaller that the hydration free energy of a Li cation in EC but an order of magnitude larger than the thermal energy (k_BT), Figure IV-42. In addition, it was found that Li^+ is complexed to one EC or TFSI- anion while being intercalated (~2 Å) into graphite.

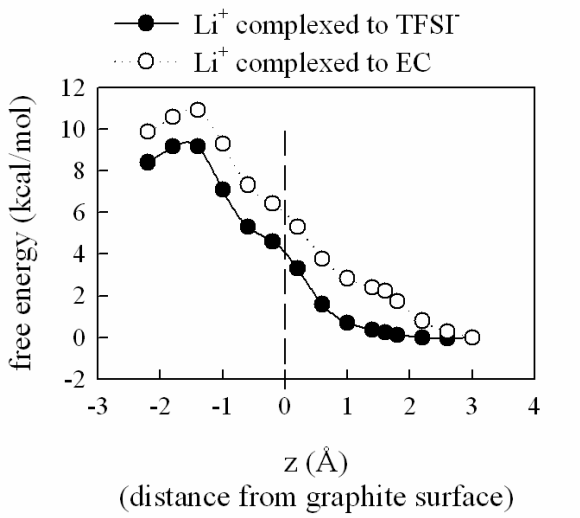

Figure IV-42. Graphite‖EC/LiTFSI Interface Simulation

Recently, MD simulations of the lithium alkyl monocarbonate (LiMC) were finalized and contrasted with the previous results for the lithium alkyl dicarbonate SEI components (Li_2EDC), Figure IV-43. Conductivity of Li_2EDC extrapolated to -30°C was ~10^{-10}S/cm indicating a significant resistance of this SEI layer component at low temperatures, while conductivity of LiMC was an order of magnitude higher.

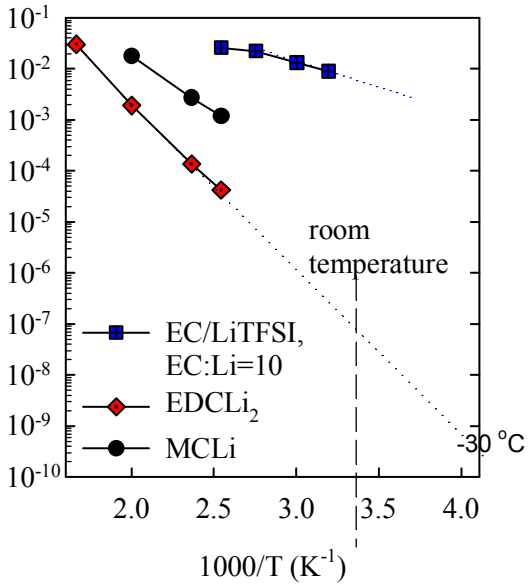

Figure IV-43. Lithium transport in molten alkyl carbonates

Conclusions from this work include that the temperature dependence of the SEI materials' conductivity is significantly stronger than for liquid electrolytes, that LiMC has higher conductivity than $EDCLi_2$, and that the resistance of a thin SEI layer could well exceed resistance of bulk electrolyte.

Modeling Electrochemical Performance (Sastry): Engineering of electrode materials, including particle size, particle size distribution, particle shapes, and conductive additives and binders, have a very large impact on the resulting material's performance. The same active material can be made into a relatively high energy or high power electrode.

One aspect of this project is to investigate the various packing geometries that might be achieved in Li-ion cathode materials and the resulting impact on the conductivity. The ultimate goal of this type of investigation is to provide guidelines to manufacturers.

The packing architectures of composite electrodes, including polydisperse arrangements, were studied, using particle geometries and sizes obtained from LBNL. A dynamic collision model developed previously by this group[16] was used to generate composite electrodes. Higher densities result from poly-disperse arrays. Because contact strongly affects conduction, heterogeneous coatings (*i.e.* pvdf+carbon black) produce different results than coatings + particles. Manufacturing should rely on use of polymer coatings to prevent settling, if both high porosity and minimum thickness, are desired.

The packing analysis was then extended to study conductivity, by converting the architecture of particulate networks to finite element models, and assigning material properties to different particles. Four systems ($LiMn_2O_4$, $LiFePO_4$, Gen 2, and Gen 3) were studied, with two different conductive additives (carbon black and graphite) and binder (PVdF). The conductivities were obtained experimentally and/or from literature values.

Conductive coatings result in low contact resistance, which is necessary to create conductive networks. Thus, using carbon black/ PVdF composite coatings is more advantageous than addition of conductors (e.g. graphite) to composite cathodes in improving conductivity for all materials investigated. Initial studies show that the contact resistance strongly affects total resistive losses in these porous electrodes.

Intercalation and Compressive Stresses in Cathode Particles: Cracking and fracture due to the stresses induced by packing, intercalation, or thermal expansion, have been implicated in limiting the lifetime of Li-ion cathodes. The purpose of this work is to investigate this phenomenon. An analogy to thermal stress was used to calculate intercalation stress inside a single particle, representative results are shown in Figure IV-44 left. Finite element analysis was used to determine the pressure require to compress a $LiMn_2O_4$ electrode. Compressive stress and maximum stresses were estimated by finite element models of particulate networks.

Maximum stresses within particulate networks varied from 1.5 to 2.5 GPa as the volume fraction was reduced to 20% from 60%, Figure IV-44 right. Reactive compression pressures of 0.2 - 1.6MPa were required for the same reduction. Intercalation stresses are on the order of MPa, *via two independent estimates*. Maximum stresses from compression of electrodes may be ~ three orders of magnitude larger than induced intercalation stresses; reaction stresses during compression are of the same order. Thus, compressed cathode particles may undergo more damage during initial compressions, than induced by any single cycle of operation, due to intercalation.

---

[16] C.W. Wang, K.A. Cook and A.M. Sastry, *JECS*, **150,** 3, A385-A397 (2003); Y.-B Yi, C.-W. Wang and A.M. Sastry, *JECS*, **151,** 8, A1292-A1300 (2004).

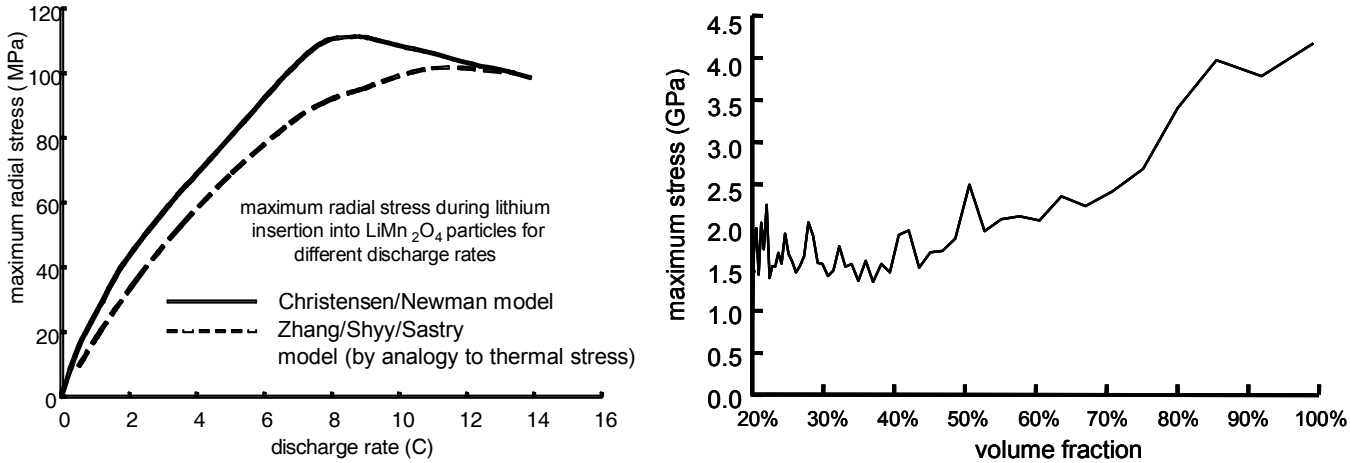

Figure IV-44. Radial stress during Li insertion into Mn spinel for different discharge rates (left), maximum stresses within packed active material particles ($LiMn_2O_4$) during compression (right).

Microscopic Model of Conduction in Oxides (Srinivasan) – The previous models for oxide cathodes have neglected specific details on the microscopic speciation in the particles. In other words, a simple diffusion equation was solved to account for transport limitations in the solid phase with no consideration given to how the charged species interact. In order to incorporate this feature, a speciation model is being developed where the Li^+ ions and e^- hop on specific lattice sites. While the lattice sites are considered to be uncharged, one could easily incorporate additional charged species to account for, say, electron-hole pair generation in low-band gap oxides. Equations for transport within the oxide have been developed using this concept that accounts for both diffusion and migration of ions and the impact of both the concentration of ions and sites in the lattice. The impact of non-idealities is also being considered.

This model has allowed estimation of the conductivity change in the particle due to the insertion of charge carriers within the single-phase region in $LiFePO_4$ and $FePO_4$. While results show that the changes can be significant, it has been suggested that dissociation of charge carriers can be low in $LiFePO_4$ (so-called quasiparticle formation). This low dissociation can result in much lower conductivity change compared to complete dissociation, Figure IV-45. Thin-film experiments are being planned that, when combined with the model, should allow quantification of these issues.

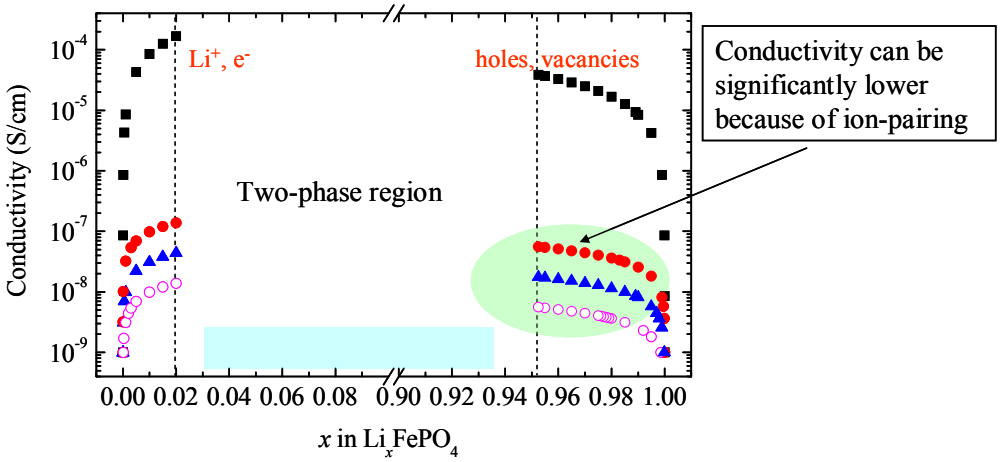

Figure IV-45. Conductivity with and without pairing, black points are without, colored points are with varying degrees of ion pairing in Li_xFePO_4

Cell Optimization Modeling (Srinivasan) – The model graphite used in previous simulations had less than idea performance, exhibiting an ASI=40Ωcm^2. That has since been replaced by ASI values associated with currently available high power graphites, ~15Ωcm^2. Results are shown in Figure IV-46. The implication being that excellent high-power capability is possible from presently-available $LiFePO_4$ materials

In addition, this modeling effort is being used to estimate the applicability of various Li-ion chemistries for HEV applications. Specifically, an analysis has begun of the correlation between the ASI and the maximum power, at a power to energy ratio defined by the published battery goals. The methodology involves using the mathematical model to perform the HPPC pulse test on a battery of specified design (*i.e.*, thickness, porosity, and anode to cathode ratio), evaluating the ASI as a function of DOD, and subsequently, the discharge and regen power vs. DOD. This information is then used to calculate the DOD range of operation and obtain a plot of the maximum power vs. the available energy from which the DOD range which satisfies the goal is identified. This procedure is repeated for various values of the pulse current and cell designs.

Results suggest that for the spinel-graphite cell, the ASI deceases with increasing pulse current until 30C. This decrease can be attributed to the kinetic resistance in the system. In addition, increasing the thickness of the cathode decreases the ASI until a point where liquid-phase limitations dominate. However, interestingly, the model suggests that the optimum design is not at the minimum ASI value, but a thickness that is smaller than that value. In other words, choosing a battery design based on a minimum in the ASI does not allow one to capture the maximum performance of the chemistry. This result occurs because as the electrode is made thicker, the ASI does not decrease at the same rate as the increase in the weight of the cell. The study suggests that care should be taken when comparing different chemistries with each other only based on ASI data.

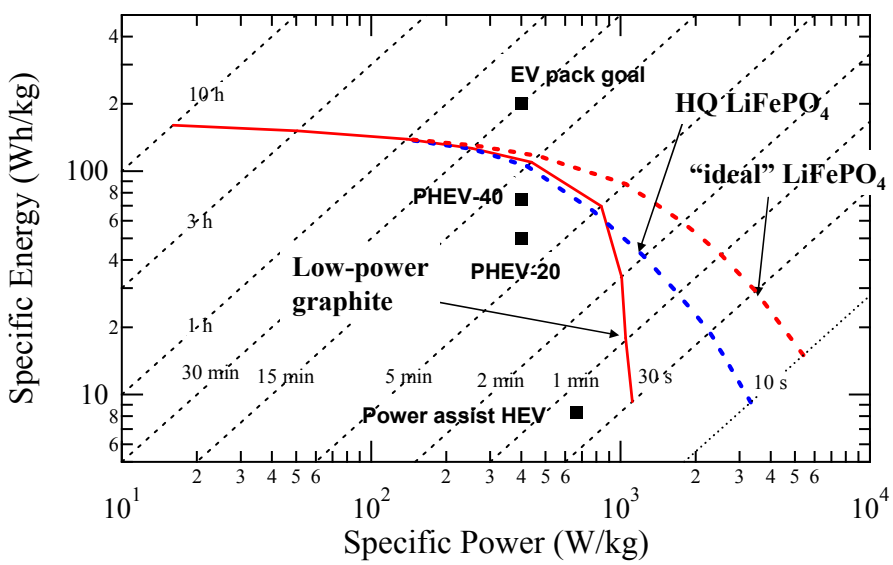

Figure IV-46. Maximum power and energy densities with improved graphite

Thermodynamic and Transport Property Measurements (Newman) - Full characterization of transport in a binary electrolyte entails measurement of the conductivity, diffusion coefficient, and

the transference number. The accurate measurement of the diffusion coefficient has been extremely difficult and time intensive. Recently, a relatively inexpensive, simple, and reproducible technique for measuring diffusion coefficients in Li-ion battery electrolytes has been developed.

The new method for diffusion-coefficient measurement avoids the effects of side reactions. This method is a modification of the technique of restricted diffusion and does not require the use of electrodes. The experimental setup allows for temperature control in ACN as well as the Gen 2 electrolyte. Results indicate that the diffusion coefficient for $LiPF_6$ is one order of magnitude higher in ACN than in baseline electrolytes, Figure IV-47. The technique has shown reproducible results that compare well with literature values.

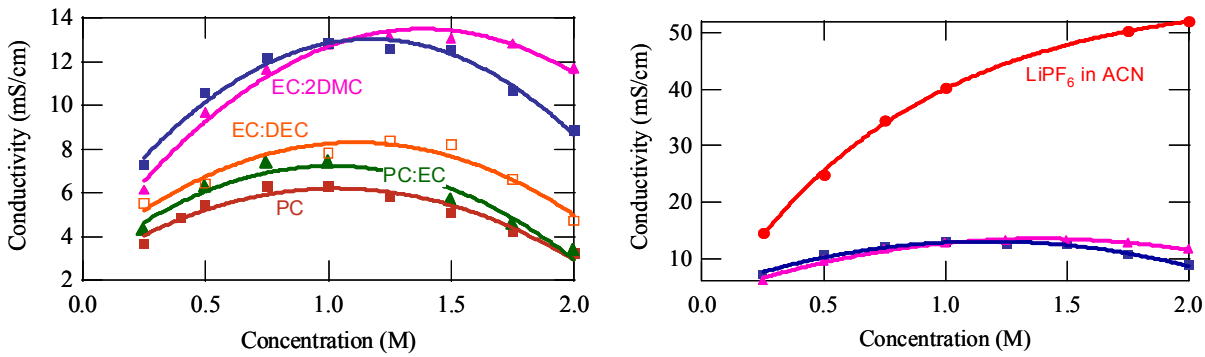

Figure IV-47. $LiPF_6$ Conductivity Measurements

Cell Construction (Battaglia) – The objective of this task is to make repeatable and high quality lab sized cells and to supply them to the program's researchers. Towards this end, the team has identified limitations with their current equipment and procedures, re-configured the laboratory and purchased equipment to address them, assessed reproducibility, identified a technique for identifying the highest quality cells, and begun to iterate through this process, incorporating improvements at each step.

Recently, this group showed that it could repeatably make cells from batch-to-batch. Four new cells were fabricated that showed the same impedance and the same capacity as cells made nine months earlier. However, the previously fabricated cells were tested at three and four months and found to have lost a significant amount of their capacity, shown in Figure IV-48, perhaps due to water intrusion. To test this theory, two of the four cells built recently were encapsulated in glass and tested side-by-side to two cells without the glass encasement. After aging the cells for four weeks at 45ºC, all four cells performed similarly, suffering a 50% loss of capacity. The next step is to determine if the water is introduced during the fabrication process. This concept has been supported by trips to Mine Safety Appliances, Yardney, and Quallion where the need to keep water out of the cells during fabrication was emphasized.

Test Vessel Optimization (Battaglia) – New pouches were acquired from NEC, a Japanese company working to develop a pouch-cell battery. The pouches were tested for leaks by filling them with a gram of electrolyte and aging them at 45ºC. Weight measurements were taken every two weeks, which only gives an indication of the difference between electrolyte leaving the pouch and water entering the pouch. None-the-less, the weight loss for these pouches was approximately

0.12% per month. This was far superior to pouches from Sumitomo Electric Industries (SEI) that showed a weight loss of ~2% per month, Figure IV-49.

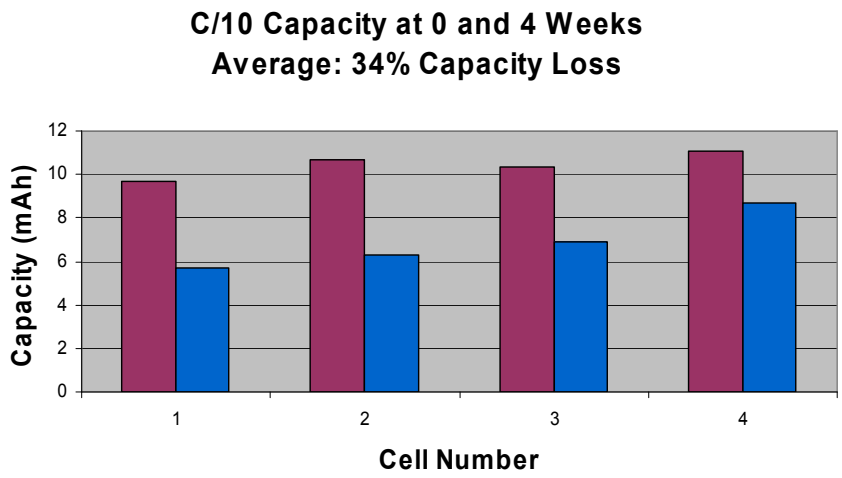

Figure IV-48. Initial capacity of four test cells and their capacity after four weeks.

Al Current Collector Corrosion (Devine) – In 2006, work was focused on inspecting Al current collectors in life-tested ATD batteries for evidence of corrosion, and determining the mechanism of Al current collector corrosion in Li-ion batteries. 19 Gen 2 ATD batteries that were previously cycle life tested from ~25-60ºC were studied. Both laboratory corrosion tests and inspections of the cells' current collectors indicated aluminum current collectors were susceptible to crevice corrosion.

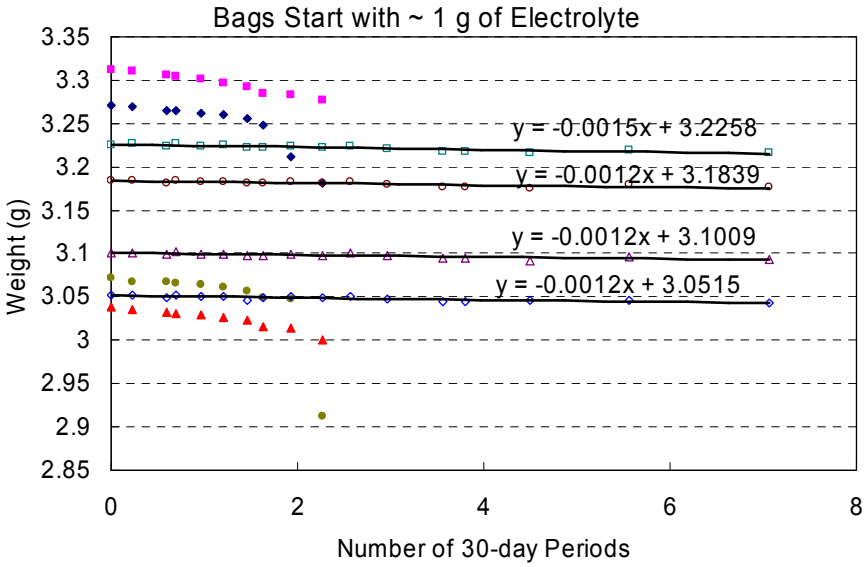

Figure IV-49. Electrolyte losses from pouch cells (solid points, SEI pouches, open points, NEC pouches).

Initial results show extensive localized corrosion in all 19 cells, even in those tested at 25ºC for a short time (4 weeks). A statistical analysis of the severity of corrosion has begun, with initial results shown in Figure IV-50. Microscopic investigation of the surfaces of Al current collectors

in life tested cells shows the formation of a large number of pits under the cathode. The pits are distributed over the entire cathode, and are ~10μm in diameter. In addition, ICP measurements detected traces of Al in the electrolyte of three of the ATD cells. In cells tested at 25ºC for 52 and 68 weeks 2528 and 2668 ppm were measured, respectively; and in another cell tested at 45ºC for 16 weeks 2793 ppm Al was measured.

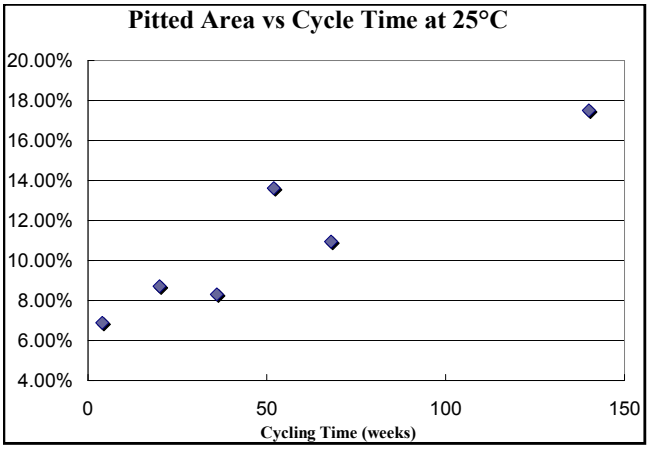

Figure IV-50. Pitted Area vs. Cycling Time

FUTURE PLANS

Modeling Electrochemical Performance

- Study the cumulative effect of intercalation stresses as part of lifetime modeling, including multiscale modeling (with Grey/Ceder).
- Incorporate electrochemical and atomistic simulations with existing codes, to design materials for longer life and higher power.
- Particle size, orientation, and interface conditions impact kinetic performance of the cell, especially the particle interface conditions with other particles or the current collector. Fibers work well and will be studied (with Doeff).
- Test electrodes prepared at LBNL to identify superior designs, by which electrodes can achieve minimum resistivity, mass density, and maximum strength. Prior modeling approaches and codes will be used to handle the experimental systems.

Thermodynamic and Transport Property Measurement

- Complete development of method of independent f_{+-} and t_{+}^{0} determination.
- Investigate optimization of asymmetric-hybrid supercapacitor.

Cell Construction

- Investigate cell making variables.
- Investigate methods and sequences of mixing.
- Complete characterization of baseline chemistries.
- Complete thermal and chemical stability analysis.

Cell Optimization

- Examine how two-phase behavior impacts transport (with Richardson).
- Examine impact of quasi-particle formation on particle transport (with Ceder).

- Link microscopic transport to performance (with Battaglia, Sastry).
- Repeat simulations with high power graphite for additional cathode chemistries.

Selected Publications

1. A. Salah, M. Mauger, K. Zaghib, N. Ravet, J. Goodenough and J. Julien; "Fe^{3+} impurity reduction by carbon coating process in $LiFePO_4$," JECS 153, A1692 (2006).
2. G. Chen, X. Song, and T. J. Richardson, "Electron Microscopy Study of the $LiFePO_4$ to $FePO_4$ Phase Transition," ESSL, 9, A295 (2006).
3. H Gabrisch, J. Wilcox, and M. Doeff, "Carbon Surface Layers on a High-Rate $LiFePO_4$," ESSL 9, A360 (2006).
4. J. Chen and M. S. Whittingham, "Hydrothermal Synthesis of Lithium Iron Phosphate", Electrochem. Commun., 8, 855 (2006).
5. J. Christensen and J. Newman, "A mathematical model of stress generation and fracture in lithium manganese oxide," JECS, 153 A1019 (2006)
6. K Chung, H Lee, W-S Yoon, J McBreen, X-Q Yang "Studies of $LiMn_2O_4$ Capacity Fading at Elevated Temperature Using *In-situ* Synchrotron XRD" JECS, Vol. 153, A774 (2006).
7. K. Kang, Y.S. Meng, J. Breger, C.P. Grey and G. Ceder, "Electrodes with High Power and High Capacity for Rechargeable Li Batteries," Science, 311, 977 (2006).
8. K. S. Park, S. B. Schougaard, J. B. Goodenough, "Composite conducting-polymer/iron-redox-couple cathodes for lithium secondary batteries", Adv. Mater. (submitted).
9. K.A. Cook, F. Albano, P. E. Nevius, and A.M. Sastry., "POWER (Power Optimization for Wireless Energy Requirements): A MatLab Based Algorithm for Design of Hybrid Energy Systems," JPS, in press (2006).
10. O. Borodin; G. Smith, "Development of the Many-Body Polarizable Force Fields For Li-Battery Applications: 1. Ether, Alkane and Carbonate-Based Solvents" J. Phys. Chem. B., 110, 6279 (2006).
11. O. Borodin; G. Smith,. "Development of the Many-Body Polarizable Force Fields For Li-Battery Applications: 2. LiTFSI-Doped Oligoether, Polyether, And Carbonate-Based Electrolytes" J. Phys. Chem. B., 110, 6293 (2006).
12. O. Borodin; G. Smith, "LiTFSI Structure and Transport in Ethylene Carbonate from Molecular Dynamics Simulations" J. Phys. Chem. B, 110, 4971 (2006).
13. O. Borodin; G. Smith, "Mechanism Of Ion Transport In Amorphous Poly(Ethylene Oxide)/LiTFSI From Molecular Dynamics Simulations" Macromolecules, , 39, 1620 (2006).
14. S. B. Schougaard, J. Bréger, M. Jiang, C. P. Grey, J. B. Goodenough, "$LiNi_{0.5+x}Mn_{0.5-x}O_2$ (A high-rate, high-capacity cathode for lithium rechargeable batteries", Adv. Mater., 18, 905 (2006).
15. W. Choi and A. Manthiram, Electrochem. Solid State Lett., 9, A245 (2006).
16. W-S Yoon, J Hanson, J McBreen, and X-Q Yang "A Study on the Newly Observed Intermediate Structures during the Thermal Decomposition of Nickel-Based Layered Cathode Materials Using Time Resolved XRD" Electrochemistry Communications, 8, 859 (2006).
17. WS Yoon, KY Chung, J McBreen, K Zaghib, and XQ Yang "Electronic Structure of the Electrochemically Delithiated $Li_{1-x}FePO_4$ Electrodes Investigated by P K-edge X-ray Absorption Spectroscopy" ESSL, 9, A415 (2006)
18. X. Sun, & JB Kerr, "Synthesis and characterization of network single ion conductors based on comb-branched polyepoxide ethers and lithium bis(allylmalonato)borate", Macromolecules 39, 362 (2006).
19. Y Park and M. Doeff, "Synthesis and Electrochemical Characterization of $M_2Mn_3O_8$ (M=Ca, Cu) Compounds and Derivatives" Sol. State Ionics, 177, 893 (2006).
20. Y. Wu and A. Manthiram, "High Capacity, Surface-Modified Layered $Li[Li_{(1-x)/3}Mn_{(2-x)/3}Ni_{x/3}Co_{x/3}]O_2$ Cathodes with Low Irreversible Capacity Loss," ESSL 9, A221 (2006).
21. Y.J. Park and M. Doeff, "Effect of Structure on the Storage Characteristics of Manganese Oxide Electrode Materials", JPS, in press.

22. YB Yi, CW Wang, and AM Sastry, "Compression of Packed Particulate Systems: Simulations and Experiments in Graphitic Li-ion Anodes," ASME Journal of Engineering Materials and Technology, 128 73 (2006).

Appendix A

Contributors

Battery Technology Development	
J. Barnes	Naval Surface Warfare Center West Bethesda, MD 20817-5700
J. Deppe[17]	Deppe Consulting Services, LLC PO Box 366 Davidsonville MD 21035 jbdeppe@lbl.gov
A. Pesaran	National Renewable Energy Laboratory 1617 Cole Boulevard Golden, CO 80401-3393
I. Weinstock	Sentech Corp 7475 Wisconsin Ave. Bethesda, MD 20814

Applied Battery Research	
DOE Program Manager	**David Howell** U.S. Department of Energy Office of FreedomCar & Vehicle Technologies 1000 Independence Avenue, SW Washington, DC 20585
National Laboratory Program Manager	**Gary Henriksen** Argonne National Laboratory Chemical Engineering Division, Bldg 205 9700 South Cass Avenue Argonne, IL 60439
Understand and Enhance Low-Temperature Performance	
Focus area Point of Contact	**D. Dees** Chemical Engineering Division Argonne National Laboratory, Building 205 9700 South Cass Avenue Argonne, IL 60439 Phone: 630.252.7349, E-mail: dees@cmt.anl.gov

[17] Preparer of this report.

Applied Battery Research	
D. Abraham, K. Amine, I. Bloom, S. Busking, J. Heaton, G. Henriksen, A. Jansen, S.H. Kang, J. Liu, W. Lu, Q. Wang	Argonne National Laboratory Argonne, IL 60439
J. Allen, W. Behl, T. R. Jow. K. Xu, S. Zhang	Army Research Laboratory 2800 Powder Mill Rd Adelphi, MD 20783-1197
K. Y. Chung, H. S. Lee, J. McBreen, X. Q. Yang, W. S. Yoon	Brookhaven National Laboratory P.O. Box 5000, MSD Bldg. 555, Upton, NY 11973-5000
K. Gering, T. Murphy	Idaho National Engineering and Environmental Laboratory Idaho Falls, ID 83415-3830
S. Kawauchi, J. Prakash	Illinois Institute of Technology Department of Chemical and Environmental Engineering, Chicago, IL 60616
R. Spotnitz	Battery Design Inc. 2277 Delucchi Dr Pleasanton, CA 94588
Understand Life-Limiting Mechanisms and Enhance Life	
Focus area point of contact	**Gary Henriksen** Chemical Engineering Division Argonne National Laboratory, Building 205 9700 South Cass Avenue Argonne, IL 60439 Phone: 630.252.4591, E-mail: henriksen@cmt.anl.gov
D. Abraham, K. Amine, I. Bloom, Z. Chen, D. Dees, A. Escalona, J. Heaton, A. Jansen, C. Johnson, S.H. Kang, J. Lui, W. Lu, P. Nelson, L. Walker	Argonne National Laboratory Argonne, IL 60439
C Ashton, J. Belt, J. Christophersen, G. Cole, J. Einerson, K. Gering, C. Ho, G. Hunt, D. Jamison, T. Murphy	Idaho National Engineering and Environmental Laboratory Idaho Falls, ID 83415-3830
S. Kawauchi, J. Prakash	Illinois Institute of Technology Department of Chemical and Environmental Engineering, Chicago, IL 60616
V. Battaglia, G. Chen, M. Kerlau, J. Kerr, R. Kostecki, M. Marcinek, K. McCarthy, J. Newman, T. Richardson, P. Ross, A S. VanDyke, X. Song, V. Srinivasan, H. Yang, S. Zhang, V. Zhuang	Lawrence Berkeley National Laboratory Berkeley CA 94720-8168

Applied Battery Research	
E. Thomas	Sandia National Laboratories Albuquerque, NM 87185-0613
R. Haasch, C. Lei, S. MacLaren, I. Petrov, E. Sammann, T. Spila	University of Illinois at Urbana Champaign Center for Microanalysis of Materials 368 Frederick Seitz Materials Research Laboratory 104 S. Goodwin Avenue Urbana, IL 61801 USA
Understand and Enhance Abuse Tolerance	
Focus area point of contact	**E. P. Roth** Advanced Power Sources R&D Sandia National Laboratories, MS: 0613 P.O. Box 5800 Albuquerque, NM 87185 Phone: 505.844.3949, E-mail: eproth@sandia.gov
K. Amine, I. Belharouak, G. Henriksen A. Jansen, W. Lu, D. Vissers	Argonne National Laboratory Argonne, IL 60439
J. Prakash	Illinois Institute of Technology Department of Chemical and Environmental Engineering, Chicago, IL 60616
H. Case, L. Davis, D. Doughty, B. Hance, D. Johnson, J. Langendorf, G. Nagasubramanian, D. Pile, B. Sanchez	Sandia National Laboratory Mail Stop 0613 Albuquerque, NM 87185
R. Spotnitz	Battery Design Inc. 2277 Delucchi Dr Pleasanton, CA 94588
Cell-Level Cost Reduction	
Focus area point of contact	**K. Amine** Chemical Engineering Division Argonne National Laboratory, Building 205 9700 South Cass Avenue Argonne, IL 60439 Phone: 630.252.3838, E-mail: amine@cmt.anl.gov
I. Belharouak, S. Busking, Z. Chen, G. Henriksen, A. Jansen, J. Lui, W. Lu, P. Nelson, S. H. Park, D. Vissers, L. Wenquan	Argonne National Laboratory Argonne, IL 60439
J. Prakash	Illinois Institute of Technology Department of Chemical and Environmental Engineering, Chicago, IL 60616

Long-Term Battery Research	
DOE Program Manager	**David Howell** U.S. Department of Energy Office of FreedomCAR & Vehicle Technologies 1000 Independence Avenue, SW Washington, DC 20585
National Laboratory Program Manager	**Venkat Srinivasan** Lawrence Berkeley National Laboratory MS 70R-0108B One Cyclotron Road Berkeley, CA 94720
New Cathode Systems, Performance and Limitations	
$LiFePO_4$ System	
J. Harb and D. Wheeler	Brigham Young University Chemical Engineering Department, 350 CB Provo, UT 84602
K.-Y. Chung, J. Hanson, H. S. Lee, J. McBreen, X.-Q. Yang, and W.-S. Yoon	Brookhaven National Laboratory Upton, NY 11973
K. Zaghib	Hydro Quebec Varennes, J3X 1S1 Quebec Canada
G. Chen, M. Doeff , M. Kerlau, R. Kostecki, M. Marcinek, K. McCarthy, T. Richardson, P. Ross, V. Srinivasan	Lawrence Berkeley National Laboratory Berkeley CA 94720-8168
G. Ceder	Massachusetts Institute of Technology Cambridge, MA 02139-4307
J. Chen, N. Chernova, S. Whittingham and J. Xiao	State University of New York at Binghamton Chemistry and Materials Research Center Binghamton, NY 13902-6000
C. P. Grey	State University of New York at Stony Brook, Department of Chemistry Stony Brook, NY
A.M. Sastry	University of Michigan Dept of Mechanical Engineering and Applied Mechanics Ann Arbor, MI 48109-2125
Y. Huang, J. Goodenough,	University of Texas at Austin 1 University Station C2200 Mechanical Engineering Dept. Austin, TX 78712-0292

Long-Term Battery Research	
$LiMn_2O_4$ Spinel System	
C. Johnson, S-H Kang, M. Thackeray, J. Vaughey	Argonne National Laboratory Chemical Technology Division Argonne IL 60439
K.-Y. Chung, J. Hanson, H. S. Lee, J. McBreen, X.-Q. Yang, and W.-S. Yoon	Brookhaven National Laboratory Upton, NY 11973
K. Zaghib	Hydro Quebec Varennes, J3X 1S1 Quebec Canada
Y.S. Horn	Massachusetts Inst of Technology Mechanical Engineering, 3-158 77 Massachusetts Avenue Cambridge, MA 02139
C. P. Grey	State University of New York at Stony Brook, Department of Chemistry Stony Brook, NY
J. Choi, W. Choi, A. Manthiram, and Y. Wu	Univ of Texas Texas Materials Institute , ETC 9-104 Austin TX 78712-0292
$LiNi_{1/3}Co_{1/3}Mn_{1/3}O_2$ System	
M. Thackeray, C. Johnson	Argonne National Laboratory Chemical Technology Division Argonne IL 60439
K.-Y. Chung, J. Hanson, H. S. Lee, J. McBreen, X.-Q. Yang, and W.-S. Yoon	Brookhaven National Laboratory Upton, NY 11973
M. Doeff , M. Kerlau, R. Kostecki, M. Marcinek, K. McCarthy	Lawrence Berkeley National Laboratory Berkeley CA 94720-8168
G. Ceder, Y.S. Meng, Y. Hinuma, K. Kang, F. Zhou, T. Maxisch and L. Wang , Y.S. Horn	Massachusetts Institute of Technology Cambridge, MA 02139-4307
S. Whittingham, Jiajun Chen, Jie Xiao, Natasha A. Chernova,	State University of New York at Binghamton Chemistry and Materials Research Center Binghamton, NY 13902-6000
C. P. Grey, Julien Breger, Dongli Zeng, Jordi Cabana	State University of New York at Stony Brook, Department of Chemistry Stony Brook, NY
A.M. Sastry	University of Michigan Dept of Mechanical Engineering and Applied Mechanics Ann Arbor, MI 48109-2125

Long-Term Battery Research	
Y. Huang, J. Goodenough, K-S. Park	University of Texas at Austin 1 University Station C2200 Mechanical Engineering Dept. Austin, TX 78712-0292
New Anode Materials	
S. Busking, P. Chupas, A. Jansen, C. Johnson, M. Thackeray, J. Vaughey	Argonne National Laboratory Chemical Technology Division Argonne IL 60439
O. Crowther, A. West	Columbia University Chemical Engineering 812 Mudd Bldg New York, NY 10027-0000
G. Chen , R. Kostecki, T. Richardson, P. Ross	Lawrence Berkeley National Laboratory Berkeley CA 94720-8168
Q. Fan, S. Whittingham	State University of New York at Binghamton Chemistry and Materials Research Center Binghamton, NY 13902-6000
C. P. Grey	State University of New York at Stony Brook Department of Chemistry Stony Brook, NY
Novel Electrolytes and their Characterization	
W.-S. Yoon	Brookhaven National Laboratory Upton, NY 11973
S. Creager, D. DesMarteau, P. Hallac, O. Geiculescu, R. Rajagopal, M. Herath	Clemson University Department of Chemistry Clemson, SC 29634-0973.
K. Zaghib, P. Charest, M. Dontigny, A. Guerfi, P. Hovington, M. Petitclerc and R. Veillete	Hydro Quebec Varennes, J3X 1S1 Quebec Canada
V. Battaglia, N. Balsara, T. Cohen-Hyams, T. Devine, M. Doeff, J. Kerr, R. Kostecki, G. Liu, L. Odusanya, M.J. Park, P. Ross, M. Singh, S. Stewart, V. Srinivasan	Lawrence Berkeley National Laboratory Berkeley CA 94720-8168
J. Goodenough	University of Texas at Austin 1 University Station C2200 Mechanical Engineering Dept. Austin, TX 78712-0292

Long-Term Battery Research	
P. S. Fedkiw, S. A. Khan	North Carolina State University Department of Chemical Engineering Raleigh, NC 27695
O. Borodin, G. D. Smith	University of Utah Department of Materials Science and Engineering Salt Lake City, UT
Li-Ion Modeling, Diagnostics, and Cell Analysis	
T.R. Jow, K. Xu , S.S. Zhang	Army Research Laboratory 2800 Powder Mill Rd Adelphi, MD 20783-1197
K. Zaghib	Hydro Quebec Varennes, J3X 1S1 Quebec Canada
P. Albertus, A. Avecilla, V. Battaglia, J. Couts, T. Cowen-Hyams, T. Devine, M. Doeff, J. Go, M. Kerlau, R. Kostecki, G. Liu, F. McLarnon, J. Newman, T. Richardson, P. Ross, A. Sierra-VanDyke, S. Stewart, V. Srinivasan, X. Song, J. Wilcox, H. Yang, V. Zhuang	Lawrence Berkeley National Laboratory Berkeley CA 94720-8168
A. M. Sastry, C-W. Wang	University of Michigan Dept of Mechanical Engineering and Applied Mechanics Ann Arbor, MI 48109-2125
O. Borodin, G. D. Smith	University of Utah Department of Materials Science and Engineering Salt Lake City, UT

Appendix B

List of Acronyms

ACN	Acetonitrile
AEM	Advanced electrolyte model
ANL	Argonne National Laboratory
ARC	Accelerated rate calorimetry
ARL	Army Research Laboratory
ASI	Area specific impedance
ATD	Advanced Technology Development
BATT	Batteries for Advanced Transportation Technologies
BCF	Binder and carbon free
BET	Brunauer, Emmett, and Teller surface area
BNL	Brookhaven National Laboratory
CC	Current collector
CPI	Compact Power Inc.
DEC	Diethyl carbonate
DMC	Dimethylcarbonate
DOD	Depth-of-discharge
DOE	Department of Energy
DSC	Differential scanning calorimetry
E_a	Activation energy
EA	Ethylene acetate
EC	Ethylene carbonate
EIS	Electrochemical impedance spectroscopy
EMC	Ethyl methyl carbonate
EP	Ethyl proprionate
EV	Electric vehicle
EXAFS	Extended x-ray absorption fine structure
EY	Electron yield
FCV	Fuel cell vehicle
FCVT	FreedomCAR and Vehicle Technology
FTIR	Fourier transform infrared
FY	Fluorescence yield
□BL	γ-butyrolactone
GITT	Galvanostatic intermittent titration technique
HEBM	High-energy ball milling
HEV	Hybrid electric vehicle

HPPC	Hybrid pulse power characterization
HRTEM	High resolution transmission electron microscopy
ICL	Irreversible capacity loss
IL	Ionic liquids
IMC	Isothermal Microcalorimeter
INL	Idaho National Laboratory
JCS	Johnson Controls/Saft
KF	Karl-Fischer
LBNL	Lawrence Berkeley National Laboratory
LCL	Lower confidence limit
LiBOB	Lithium bis(oxolato)borate
LiDFOB	Lithium difluoro(oxalate)borate
LiTFSI	Lithium bis(trifluoromethane-sulfonyl)imide
LiTO	Lithium titanate, $Li_4Ti_5O_{12}$
MCMB	Meso carbon micro beads
MD	Molecular dynamics
M-HEV	Minimum HEV battery requirements
mFEC	Mono-fluoroethylene carbonate
MPA	Microwave plasma assisted
MPACVD	Microwave assisted chemical vapor deposition
MPPC	Minimum pulse power characterization
MW	Molecular weight
NCA	$LiNi_{0.8}Co_{0.15}Al_{0.05}O_2$
ND	Neutron diffraction
NiMH	Nickel metal hydride
NMC	$LiNi_{1/3}Co_{1/3}Mn_{1/3}O_2$
NMR	Nuclear magnetic resonance
NREL	National Renewable Energy Laboratory
OCV	Open circuit voltage
PC	Propylene carbonate
PEG	Polyethylene glycol
PEO	Poly(ethylene oxide)
PHEV	Plug in Hybrid Electric Vehicle
PPY	Polypyrrole
PS	Polystyrene
PVdF	Poly(vinylidene fluoride)

RE	Reference electrode
RPT	Reference performance test
SBIR	Small Business Innovative Research
SEI	Solid electrolyte interphase
SEM	Scanning electron microscopy
SEO	PS-b-PEO copolymers
SOC	State of charge
SNL	Sandia National Laboratory
STTR	Small Business Technology Transfer Program
TEM	Transmission electron microscopy
TGA	Thermal gravimetric analysis
TLVT	Technology Life Verification Test
TMO	Transition metal oxide
TOF-SIMS	Time of flight secondary ion mass spectrometry
UCV	Upper cutoff voltage
UDC	Under deposit corrosion
USABC	United States Advanced Battery Consortium
USCAR	United States Council for Automotive Research
VC	Vinylene carbonate
VEC	Vinyl ethylene carbonate
VGCF	Vapor grown carbon fibers
VP	Vinyl propionate
WSB	Water soluble binder
XANES	X-Ray Absorption Near Edge Structure
XAS	X-ray absorption spectroscopy
XPS	X-ray photoelectron spectroscopy
XRD	X-ray diffraction

This document highlights work sponsored by agencies of the U.S. Government. Neither the U.S. Government nor any agency thereof, nor any of their employees, makes any warranty, express or implied, or assumes any legal liability or responsibility for the accuracy, completeness, or usefulness of any information, apparatus, product, or process disclosed, or represents that its use would not infringe privately owned rights. Reference herein to any specific commercial product, process, or service by trade name, trademark, manufacturer, or otherwise does not necessarily constitute or imply its endorsement, recommendation, or favoring by the U.S. Government or any agency thereof. The views and opinions of authors expressed herein do not necessarily state or reflect those of the U.S. Government or any agency thereof.

Printed on
recycled
paper

A Strong Energy Portfolio for a Strong America

Energy efficiency and clean, renewable energy will mean a stronger economy, a cleaner environment, and greater energy independence for America. Working with a wide array of state, community, industry, and university partners, the U.S. Department of Energy's Office of Energy Efficiency and Renewable Energy invests in a diverse portfolio of energy technologies.

For more information contact:
EERE Information Center
1-877-EERE-INF (1-877-337-3463)
www.eere.energy.gov